



Dipl.-Ing. Thomas Schlegl

# **Open Environment Capacitive Sensing for Safety Applications**

## **DOCTORAL THESIS**

to achieve the university degree of  
Doktor der technischen Wissenschaften  
submitted to

**Graz University of Technology**

Tutor

Univ.-Prof. Dipl.-Ing. Dr.techn. Hubert Zangl

Institute of Electrical Measurement and  
Measurement Signal Processing

## **AFFIDAVIT**

I declare that I have authored this thesis independently, that I have not used other than the declared sources/resources, and that I have explicitly indicated all material which has been quoted either literally or by content from the sources used. The text document uploaded to TUGRAZonline is identical to the present doctoral dissertation.

---

Date

---

Signature

*to Eva*





# Abstract

Keeping humans safe while they interact with machinery (e.g. robots, cars, elevators, etc.), is a growing issue in all areas of industry and science. Due to the rapidly increasing amount of robotic assistance in various kinds of work environments, methods for detecting and avoiding dangerous situations are investigated. A solution would, for example, have a high impact on an industry where humans share their workplace with machinery.

Capacitive sensing has proven to be a mature and reliable measurement principle for a high number of applications ranging from chemical sensing, acceleration, pressure, force and position measurement all the way to human-machine interfaces found in billions of consumer electronics. However, as of yet, no general capacitive measurement system exists that can be used in a wide field of applications and that can measure longer distances (for example  $> 10$  mm) in an unknown and undefined open environment. Nevertheless, this thesis shows that capacitive sensing has the ability to close the existing gap between vision sensors (with which it is difficult to measure short distances) and haptic (i.e. touch) sensors.

First, this thesis will investigate the steps that are necessary in order to develop such a safety measurement device using international standards. The second step describes, simulates and reconstructs the effects of using capacitive sensing for measuring in an unknown open environment. Known reconstruction techniques from electrical capacitance tomography (ECT) are adopted and a method for reconstructing 3D effects in a 2.5D simulation (i.e. two 2D simulations) instead of a 3D simulation is presented. Since no tested measurement system was able to cope with the requirements arising from open environment applications, the third step in this thesis discusses the development of a novel capacitance measurement system. This measurement system can be used for highly reactive applications and is able to deal with various parasitic effects. Both the developed algorithm and the measurement system were successfully tested and used in real-world (safety) applications, such as in protecting humans and sensitive objects from collisions with robots.

# Kurzfassung

Die Vermeidung von Unfällen während der Interaktion von Personen mit Maschinen (z.B. mit Robotern, Autos, Aufzügen etc.) erlangt einen immer größeren Stellenwert. Sowohl in der Industrie als auch in vielfältigen Anwendungsbereichen im privaten Umfeld wird eine rapide steigende Anzahl maschineller Unterstützungen durch z. B. Roboter verzeichnet. Aus diesem Grund werden Lösungen gesucht, die für Menschen gefährliche Situationen besser erkennen und vermeiden können. Eine ubiquitäre Lösung würde zum Beispiel die Unfallwahrscheinlichkeit auf mit Maschinen geteilten Arbeitsplätzen signifikant reduzieren.

Kapazitive Messtechnik wird seit über 20 Jahren zuverlässig in einer Vielzahl verschiedener Anwendungen eingesetzt. Beispiele dafür sind chemische Sensoren, Beschleunigungssensoren sowie Druck-, Kraft- und Positionssensoren. Ein breitgefächertes Anwendungsgebiet finden kapazitive Sensoren auch im Bereich der Mensch-Maschinen-Kommunikation (z. B. Berührungssensoren in Milliarden verschiedener Unterhaltungs- und Kommunikationsgeräte). Trotz dieser etablierten Technik ist dem Autor bis heute kein kapazitives Messsystem bekannt, das in verschiedenen Anwendungen zuverlässig zur Objektdetektion und Objektklassifizierung für höhere Distanzen (d. h.  $> 10$  mm) in unbekanntem und undefinierten Umgebungen verwendet werden kann. In dieser Dissertation wird gezeigt, dass kapazitive Messtechnik das Potential besitzt, die beschriebene Lücke zwischen kamera-basierten Sensoren für größere Distanzen und haptischen Sensoren zu schließen.

Im ersten Schritt wird das Vorgehen erläutert, welches nötig ist, um gemäß internationaler Normen ein wie oben beschriebenes Sicherheitssystem herzustellen. Danach werden auftretende (parasitäre) Effekte der kapazitiven Messung in unbekanntem Umgebungen beschrieben, simuliert und rekonstruiert. Eine neuartige 2.5D-Simulation zur Rekonstruktion der beschriebenen 3D-Effekte mithilfe von nur zwei 2D-Simulationen anstatt einer 3D-Simulation wird vorgestellt. Da kein kapazitives Messsystem mit der nötigen Performance gefunden werden konnte, wurde in einem weiteren Schritt ein neues Messsystem entwickelt. Dieses System kann sowohl zur Rekonstruktion verschiedener parasitärer Effekte als auch für hochreaktive Robotik-Anwendungen verwendet werden. Sowohl der Algorithmus als auch das Messsystem wurden erfolgreich in verschiedenen Anwendungen wie z. B. dem Schutz vor Kollisionen von Menschen mit Robotern getestet.

# Contents

<b>Abstract</b>	<b>v</b>
<b>Kurzfassung</b>	<b>vi</b>
<b>1. Introduction</b>	<b>1</b>
1.1. Motivation and Aims . . . . .	1
1.2. Problem Statement . . . . .	2
1.3. Proposed Solution . . . . .	5
1.4. Original Knowledge Contribution . . . . .	5
1.4.1. Sensor Design and Fusion . . . . .	6
1.4.2. Capacitive Sensor Applications . . . . .	6
1.4.3. Patent Application . . . . .	7
1.5. Thesis Overview . . . . .	7
<b>2. Safety Standards for a Safe Human Environment</b>	<b>9</b>
2.1. History of Safety Standards . . . . .	9
2.2. Terms and Definitions . . . . .	13
2.3. Functional Safety and IEC 61508 . . . . .	15
2.3.1. Safety Integrity Level (SIL) . . . . .	16
2.3.2. Life Cycle Approach . . . . .	17
2.3.3. Overview of IEC 61508 . . . . .	20
2.4. Application of IEC 61508 through Design Patterns . . . . .	22
2.4.1. What are Design Patterns and Examples . . . . .	22
2.4.2. Design Patterns in Terms of International Electrotechnical Commission (IEC) 61508 . . . . .	23
2.4.3. Example of a Safety Device Realized . . . . .	26
2.5. Application for Pretouch Systems . . . . .	27
2.5.1. Risk Assessment . . . . .	28
2.5.2. Specification of Function Blocks . . . . .	30
2.5.3. Safety Requirements for each Subsystem in a FB . . . . .	31
2.5.4. Evaluation of Safety Requirements . . . . .	31
2.5.5. Verification and Validation . . . . .	33
2.5.6. Result and Consequences . . . . .	33

<b>3. Survey of Measurement Systems for Safety Applications</b>	<b>34</b>
3.1. State-of-the-Art Sensor Technology . . . . .	35
3.1.1. Vision . . . . .	35
3.1.2. Radio frequency identification (RFID) . . . . .	38
3.1.3. Time-of-flight Sensors . . . . .	38
3.1.4. Seashell Effect . . . . .	39
3.1.5. Magnetic Sensing . . . . .	39
3.1.6. Tactile Sensing . . . . .	41
3.1.7. Proprioceptive Sensing . . . . .	41
3.1.8. Comparison of State-of-the-Art Sensor Technology . . . . .	42
3.2. Safety Through Capacitive Sensing . . . . .	42
3.2.1. Car Bumper . . . . .	43
3.2.2. Icing . . . . .	44
3.2.3. Protection of Power Line Contacts . . . . .	45
3.2.4. Chainsaw . . . . .	46
3.2.5. Object Ranging and Material Type Identification . . . . .	47
3.2.6. Pretouch for Robot Grasping . . . . .	47
3.3. Comparison of (Safety) Sensor Systems . . . . .	51
<b>4. Capacitive Sensing and the Open Environment</b>	<b>53</b>
4.1. Capacitive Sensing in a Nutshell . . . . .	53
4.1.1. The First Capacitive Sensor . . . . .	53
4.1.2. Physics Behind Capacitive Sensing and Simulation . . . . .	54
4.2. State-of-the-Art Capacitive Sensing . . . . .	58
4.2.1. Well-Known Objects . . . . .	59
4.2.2. Well-Known Environment . . . . .	60
4.3. Capacitive Sensing in the Open Environment . . . . .	62
4.3.1. Not Well-known Environment and Objects . . . . .	63
4.3.2. Parasitic Effects . . . . .	63
4.3.3. Shielding and Coupling . . . . .	64
4.3.4. Leakage . . . . .	66
4.3.5. Geometric Effects for Elongated Capacitance Sensors . . . . .	81
4.4. The ECT Approach . . . . .	84
4.4.1. A Mobile and Wireless ECT System . . . . .	84
4.4.2. ECT and Leakage . . . . .	88
4.4.3. From ECT to Open Environment Sensing . . . . .	93
4.5. Measurement System for Open Environment Applications . . . . .	95
4.5.1. Measurement Circuitries and Modes . . . . .	95
4.5.2. Capacitance Measurement System . . . . .	97

---

<b>5. Object Detection and Classification</b>	<b>102</b>
5.1. Reconstruction in the Open Environment . . . . .	102
5.1.1. Calibration for Open Environment Sensing . . . . .	102
5.1.2. Reconstruction Results for Dielectric and Leakage Objects . .	104
5.2. Realisation Example - Robot Collision Avoidance . . . . .	114
5.2.1. Highly Reactive Robot Motion Generation and Control . . . .	114
5.2.2. Experiments and Results . . . . .	116
<b>6. Conclusion and Outlook</b>	<b>120</b>
<b>Appendix</b>	<b>122</b>
<b>A. Leakage Approach for Quadratic Triangular Shape Functions</b>	<b>123</b>
<b>B. Circuitry</b>	<b>126</b>
B.1. Front-End Circuitry . . . . .	126
B.2. Signal Generation and Data Acquisition Circuitry . . . . .	130
<b>List of Figures</b>	<b>133</b>
<b>List of Tables</b>	<b>136</b>
<b>Acronyms</b>	<b>137</b>
<b>Bibliography</b>	<b>138</b>

# 1. Introduction

## 1.1. Motivation and Aims

Every year a high number of people get injured or even die because they are in areas they just should not be in [Eur13]. This is not an application-specific problem but happens in all areas ranging from industry (e.g. people controlling machinery) to leisure time or working at home (for example housework).

A lot of these injuries could be prevented if there were a sensor system detecting and classifying objects (e.g. humans) in those dangerous areas. If such a detection and classification system could identify a dangerous situation, special actions could be taken to prevent an accident (for example in an industrial environment: stop a machine).

In the future, such detection and classification systems (safety devices) will become more important as we can expect that an increasing number of autonomous devices and robots will become part of our lives. Robots, for example will operate in fairly undefined environments, where little prior knowledge is available. Thus, it is very important to have safety devices that can, for example, help to prevent machinery from colliding with humans.

Although special sensor systems exist for certain applications (see section 3), only a few measurement principles exist that can cope with the requirements of such applications. These requirements include:

- Limitations with respect to spatial dimensions
- Weight
- Power consumption
- No line of sight
- Detection failure and false alarms
- Response time

In the next section an example will be that explains the possible impacts of these requirements.

As will be shown in this thesis, capacitive sensing has the potential to cope with most of the requirements arising in the presented safety applications. Although

capacitance measurement is a well-known measurement principle several unsolved challenges exist for open-environment sensing and object classification. They will be presented in chapter 4.

The aims of this thesis can be divided into following objectives:

1. Defining safety systems and what is necessary to build a system for safety-related functions.
2. Using capacitance measurement hardware and algorithms (for example: adopted algorithms from ECT), safety functions (for example: object detection or object classification).
3. Ensuring that the developed capacitance measurement system is able to deal with the arising (parasitic) effects occurring in open-environment measurements. Furthermore, it should be possible to use the system for different applications with different requirements.

## 1.2. Problem Statement

For the stated aims no general measurement system exists that can deal with the different arising requirements for different applications. Several measurement systems can be used for specific safety tasks but have drawbacks were they to be used for a different task. An overview of possible measurement principles including their benefits and drawbacks is given in Chapter 3.

A simple example will be used for the problem statement. This example gives an understanding of the stated requirements for a collision- detection measurement system and the challenges that arise when a capacitance measurement system is used.

A robot arm should be attached with a collision detection system. Fig. 1.1(a) to (c) present pictures of such a robot arm. It can be assumed, that the robot arm works in a defined region indicated by black arrows. In the case of an approaching object the robot arm should stop or avoid a collision with this object (for example, the human hand in Fig. 1.1(a) to (c)). With this example it is easy to understand the presented requirements in section 1.1:

**Size and weight** A measurement system mounted on this robot arm must not extend certain spatial dimensions and weight due to the size and maximum allowed payload of the robot arm.

**Power consumption** In the case of a static robot arm, power consumption is not a big issue. At the same time, the issue could be of interest for applications on mobile robots.

**Response time** As stated in section 1.1 the response time of the measurement system is also an important requirement. If the robot arm moves, for example, at a velocity of 5 m/s and the measurement system has a response time of 10 ms, the robot arm will move 50 mm before an alarm can be sounded from the measurement system. Extra time has to be allowed for the robot motion controller. Additionally, this calculation is only valid, if the object of interest is not moving. Thus, a response time shorter than 5 ms is necessary for this simple example (see Fig. 1.1).

**False alarms** Obviously the measurement system used has to be reliable (i.e. low number of “false negatives”). This reliability is covered in chapter 2. At the same time, a high number of false alarms (i.e. “false positives”), will reduce the acceptability of the measurement system. For example, if the robot arm often stops without an object in the vicinity it would not be as productive as without the safety device. Thus, the user would eventually turn off the safety feature.

In this thesis, capacitive sensing is used for open environment sensing and to bring about a proximity- and classification system that can be used in the stated aims. As shown in Fig. 1.1, the capacitance measurement front end consists of simple copper stripes attached to the robot arm. Fig. 1.1(d) and Fig. 1.1(e) show simulated measurement results for the stated example. The measurement principle is described in chapter 4. With the copper stripes, the size and weight objectives are met. However, several effects occur when capacitive sensing is used in a moderately undefined open environment (see chapter 4). For example, a capacitance measurement system is faced with:

- Very high offset capacitance and low measurement capacitance (differ by several orders of magnitude, see Fig. 1.1(d) and (e)).
- Disturbers and noise (see [Bra03]).
- Shielding and coupling effects (see section 4.3.3).
- Leakage effects (see section 4.3.2).

As shown in [Zano5] capacitive sensing is able to deal with these effects if it is used in a defined environment. However, for open environment sensing in different applications, the environment is fairly undefined and thus different (sometimes competing) effects can occur (see chapter 4). Thus, the used measurement hardware has to be able to deal with these uncertainties.

With a measurement hardware capable of dealing with the above-mentioned requirements, software algorithms are necessary for interpreting or transferring the measurements to proximity and classification data (also called reconstruction). Additionally, the software algorithm used has to deliver results within a certain time to be able to implement real-time systems (there are different levels of real time for different applications).



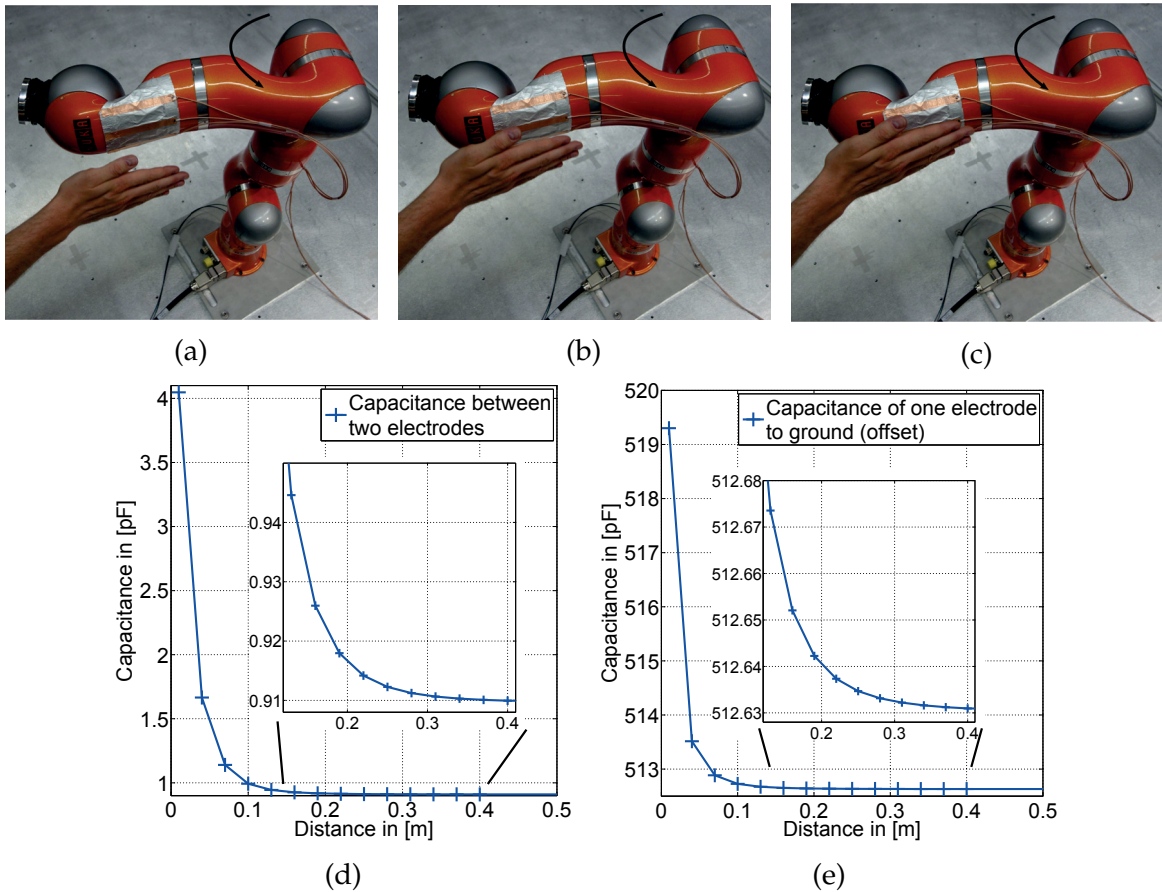


Figure 1.1.: Example of a collision detection system and simulated measurement results. On the basis of this example an understanding of the requirements for a collision detection system and the challenges with a capacitance measurement system can be presented. (a) to (c) Pictures of a robot arm moving in a work region (indicated by a black arrow). If an object (for example a human hand) gets into the work region, the robot should stop or avoid collision with the object. (d) and (e) Simulated measurement results for a capacitance measurement system.

### 1.3. Proposed Solution

A review of capacitance measurement systems for open environment sensing within this thesis aims to show potential candidates for usage. Since no satisfying system was found, a capacitance measurement system for open environment sensing was developed by the author at the Institute of Electrical Measurement and Measurement Signal Processing. This thesis presents investigations towards the use of this measurement system for different applications and in different environments. Details on the measurement system can be found in section 4.5 and the appendix.

A software framework originally used in ECT was adopted with respect to different requirements in open environment sensing. This includes the incorporation of parasitic effects (leakage) and additionally available measurements due to the developed measurement system. This enables the reconstruction of not only the proximity of approaching objects but also the classification of approaching objects based on their electric properties.

The following aspects are described in this work:

- Safety aspects for pretouch and collision avoidance sensing
- Capacitance measurement effects in the open environment
- Reconstruction algorithms
- Capacitance measurement hardware aspects

The results achieved in this work were proved in several applications. One application for example was a pretouch sensor on a robot arm at the Stanford University's Robotics Group. The results of these applications are also described in this thesis (see chapter 5).

### 1.4. Original Knowledge Contribution

Investigations that led to the creation of this thesis were conducted during the author's research work in the Sensors and Instrumentation Group in the Institute of Electrical Measurement and Measurement Signal Processing at the Graz University of Technology and during a research stay at the Stanford University's Robotics Group. During this time, several conference proceedings, journal articles, one book chapter and one patent application were published. A summary of the publications with a contribution leading to this thesis is given below.

### 1.4.1. Sensor Design and Fusion

- **T. Schlegl**, T. Bretterklieber, and H. Zangl. "Curvature Effects on Elongated Capacitive Proximity Sensors." In: Sensor+Test Conference. June 7–9, 2011. [SBZ11]'
- **T. Schlegl** and H. Zangl. "Simulation and Verification of a Capacitive Proximity Sensor." In: COMSOL Conference. Oct. 26–28, 2011. [SZ11]'
- **T. Schlegl**, S. Mühlbacher-Karrer, M. Neumayer, and H. Zangl. "A GMR Based Magnetic Pretouch Sensing System for a Robot Grasper." In: 2012 IEEE International Instrumentation and Measurement Technology Conference (I2MTC). IEEE. 2012, pp. 1506–1510. [Sch+12]'
- **T. Schlegl**, M. Neumayer, S. Mühlbacher-Karrer, and H. Zangl. "A Pretouch Sensing System for a Robot Grasper Using Magnetic and Capacitive Sensors." In: Instrumentation and Measurement, IEEE Transactions on 62.5 (2013), pp. 1299–1307. [Sch+13b]'
- **T. Schlegl** and H. Zangl. "Sensor Interface for Multimodal Evaluation of Capacitive Sensors." In: Journal of Physics: Conference Series. 2013. [SZ13]'

### 1.4.2. Capacitive Sensor Applications

- **T. Schlegl**, T. Bretterklieber, M. Neumayer, and H. Zangl. "A novel sensor fusion concept for distance measurement in automotive applications." In: IEEE Sensors. 2010, pp. 775–778. [Sch+10]'
- **T. Schlegl**, T. Bretterklieber, M. Neumayer, and H. Zangl. "Combined Capacitive and Ultrasonic Distance Measurement for Automotive Applications." In: Sensors Journal, IEEE 11.11 (Nov. 2011), pp. 2636–2642. [Sch+11]'
- **T. Schlegl**, M.J. Moser, and H. Zangl. "Directional human approach and touch detection for nets based on capacitive measurement." In: Instrumentation and Measurement Technology Conference (I2MTC), 2012 IEEE International. 2012, pp. 81–85. [SMZ12]'
- **T. Schlegl**, M. Neumayer, and H. Zangl. "A Mobile and Wireless Measurement System for Electrical Capacitance Tomography." In: Mikroelektroniktagung ME12. Apr. 2012. [SNZ12]'
- **T. Schlegl**, T. Kröger, A. Gaschler, O. Khatib, and H. Zangl. "Virtual Whiskers - Highly Responsive Robot Collision Avoidance." In: Intelligent Robots and Systems, 2013. IROS 2013. IEEE/RSJ International Conference on. [Sch+13a]'
- **T. Schlegl** and H. Zangl. Chapter: "Capacitive Sensing for Safety Applications." In: Technologies for Smart Sensors and Sensor Fusion. Ed. by Kevin Yallup and Kris Iniewski, 2014. [SMZ13]'

### 1.4.3. Patent Application

- T. Schlegl, M. Moser, and H. Zangl. „Vorrichtung zur Erkennung eines Naheverhältnisses und Erfassung von Eigenschaften von Objekten.“ Austrian patent application, 2013.

Some of the results published in above documents make up parts of this thesis. Sections containing content already published are marked by footnotes and corresponding citations. Publications by the author are additionally marked with an apostrophe ([Ref']) to indicate work already presented to the scientific community.

## 1.5. Thesis Overview

This section presents an outline of the thesis and lists the main parts of each chapter.

In chapter 2 the term “safety” as it relates to international standards is discussed and insight into existing safety standards is given. A simple example explains the requirements that a collision avoidance measurement system must fulfil in order to be allowed to be used for “safety related functions”.

Chapter 3 is divided into two parts. The first part discusses state-of-the-art sensor technologies for safety applications. At the end of the first part the different technologies are compared to one another and evaluated for the use in safety applications in the context of this thesis. The second part discusses capacitive sensing for safety applications. Different applications where capacitive sensing is intended to be used for certain safety-related functions are compared and evaluated.

The use of capacitive sensing in the open environment is discussed in Chapter 4. It starts with a brief introduction into capacitive sensing and state-of-the-art systems. Effects on the measurement system when used in the open environment are discussed and counter measures are presented. An ECT system is presented and used to develop a measurement system for open environment applications. The developed measurement system is described and used for the applications in Chapter 5.

Chapter 5 presents two applications where the developed measurement system is used to detect and classify objects in the open environment.

Finally, Chapter 6 concludes the thesis and offers a perspective on ongoing research. The interested reader will find additional information in the appendix.

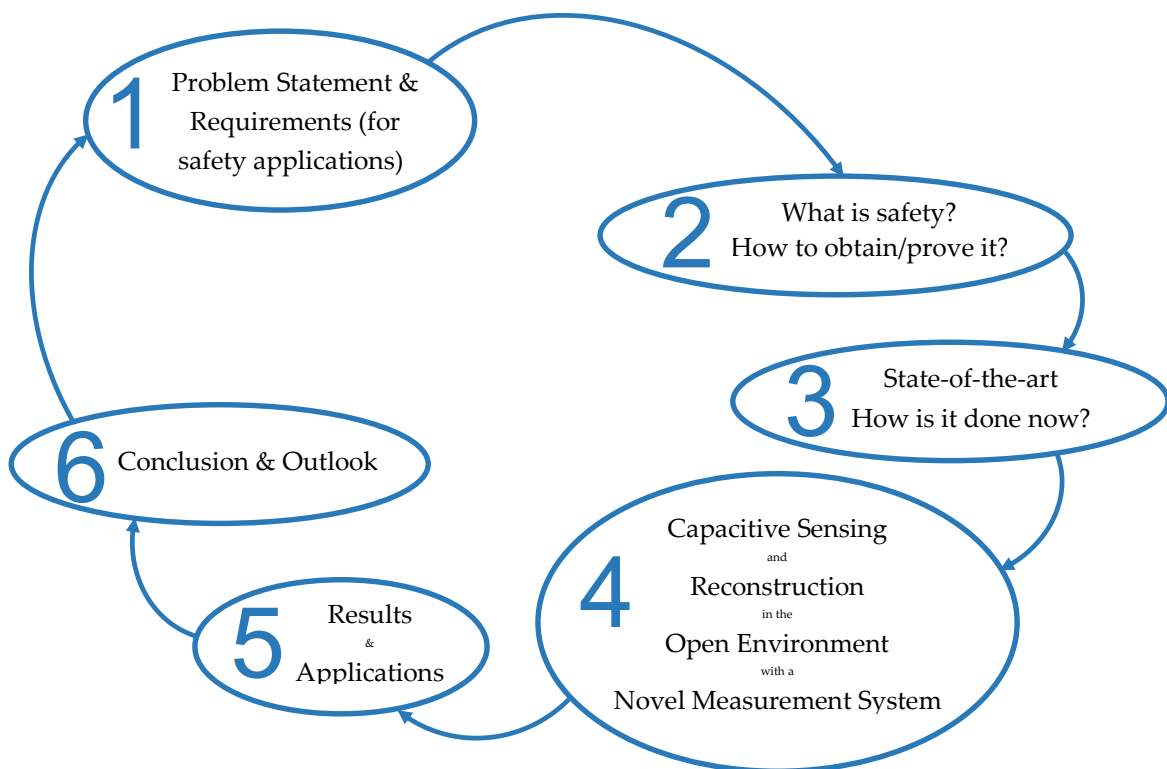


Figure 1.2.: Overview and common thread of this thesis.

## 2. Safety Standards for a Safe Human Environment

Below, an introduction to the topic of “safety” based on international standards is given. The goal is to explain the necessary steps needed to build a measurement system for “safety related” functions. This “safety related” design is especially required were a system ever to be used outside of scientific work. Since the malfunction of a safety-related function can lead to serious impacts, it is necessary to deliberately take all possible safety measures when designing, building and maintaining such parts. This can be verified by sticking to one of the presented standards (and the presented methods shown in the standards) in this section.

First, an overview of safety standards is provided. The most relevant terms and definitions used in the standards are explained and aim to clarify ambiguities in the second subsection. More detailed insight into functional safety and the IEC61508 standard ([IEC10b]) is given afterwards. Safety patterns are presented in order to provide a method for easier implementation of safety standards. The section closes with an application example. The necessities to consider when building a collision detection system will also be presented (i.e. the “safety related function”) in terms of safety standards and how safe (in terms of safety integrity level (SIL)s) such a system must be.

### 2.1. History of Safety Standards

With the foundation of the IEC in 1906, international standards started to be developed. Early on, the IEC focused on standards for units of measurement and in 1930 the following electrical units were established (taken from [IEC13a]):

- Hertz, the unit of frequency
- Oersted, the unit of magnetic field strength
- Gauss, the unit of magnetic flux density
- Maxwell and Weber, the units of magnetic flux ( $1 \text{ Wb} = 10^8 \text{ Mx}$ )
- Gilbert, the unit of magnetomotive force
- Var, designating the unit of reactive power

Consequentially, the Giorgi System was proposed, which was the first comprehensive system of physical units. It later became known as the International System of Units (SI).

In 1946 the International Organization for Standardization (ISO), which is now the world's largest developer of voluntary International Standards ([ISO13a]) was founded in London. Five years later in 1951 its first standard was published: "ISO/R 1:1951 Standard reference temperature for industrial length measurements" [Sta97]. For more information about the history of (safety) standards, the reader is referred to [SS11].

Today, International Organization for Standardization (ISO) and IEC cooperate closely and standards published together carry both acronyms (e.g. "ISO/IEC 27001 Information technology – Security techniques – Information security management systems – Requirements"). Since "safety" is a concern in nearly all fields where standards are used, both organizations publish them as they relate to different safety aspects both together and on their own (shown in Fig. 2.1). The ISO and IEC published a technical report entitled "Guidance on the application of ISO 13849-1 & IEC 62061 in the design of safety-related control systems for machinery". This report was created by members of both the ISO and IEC organisations and shows the close relationship between the standards. A drawback can be the difficulty in deciding which standard applies for which product or system. Fig. 2.1 from [Fuk11] presents an overview of different ISO and IEC safety standards and the standard types in which they belong (it makes no claim to be complete).

It is stated in [ISO12b]: "Close coordination within and among committees responsible for preparing standards on different products, processes or services is necessary in order to achieve a coherent approach to the treatment of risk". This results in different types of safety standards. As referenced in Fig. 2.1 the different types of standards are [ISO12b]:

- Basic safety standards: For general concepts and requirements regarding a wide range of products and systems
- Group safety standards: For a family of products or systems (dealt with by more than one committee). It should reference basic safety standards.
- Product safety standards: For one product or system dealt with by one committee. It should reference basic safety standards and group safety standards.
- Safety standards containing safety aspects (not shown in Fig. 2.1) but that do not only address safety aspects. They should reference basic safety standards or group safety standards.

Guides to a structured approach in other fields can be found e.g. in the IEC Guide 104 [IEC10a] (fields of electrical and electronic engineering), ISO Guide 78 [ISO12a]



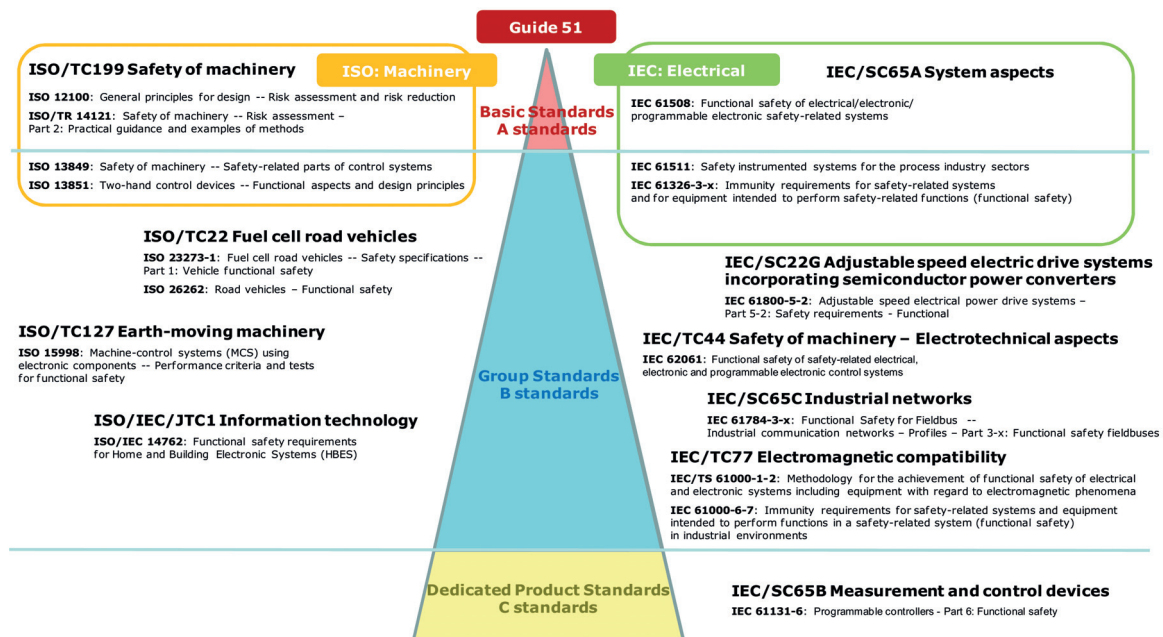


Figure 2.1.: Overview of safety standard groups by different standardization organisations [Fuk11].

(field of machinery) and ISO/IEC Guide 50 and 70 [ISO02; ISO01] (safety of children and vulnerable consumers).

Fig. 2.2 [SS11] shows the relation of the IEC 61508 to other industry-specific standards. As can be seen from Fig. 2.2, the measurement system presented in this work relates to different standards, depending on where it is used and which function or task it has in the final product or system. The standard IEC 61508 [IEC10b] is a generic standard. It is a basis for industry, product or system-specific standards but can also be used on its own for products or systems, where specific standards do not (yet) exist. Thus, section 2.3 gives an introduction to the IEC 61508 and some insight into IEC 62061. The standard IEC 62061 (Functional safety of safety-related electrical, electronic, and programmable electronic control systems) is an example of a system-specific standard in which the presented measurement system could be used. The complementary ISO 13849 (Safety of machinery - Safety-related parts of control systems) can also be used instead of IEC 62061. A detailed understanding of both standards and the product or system is necessary to decide which standard will deliver the best result for each product or system.



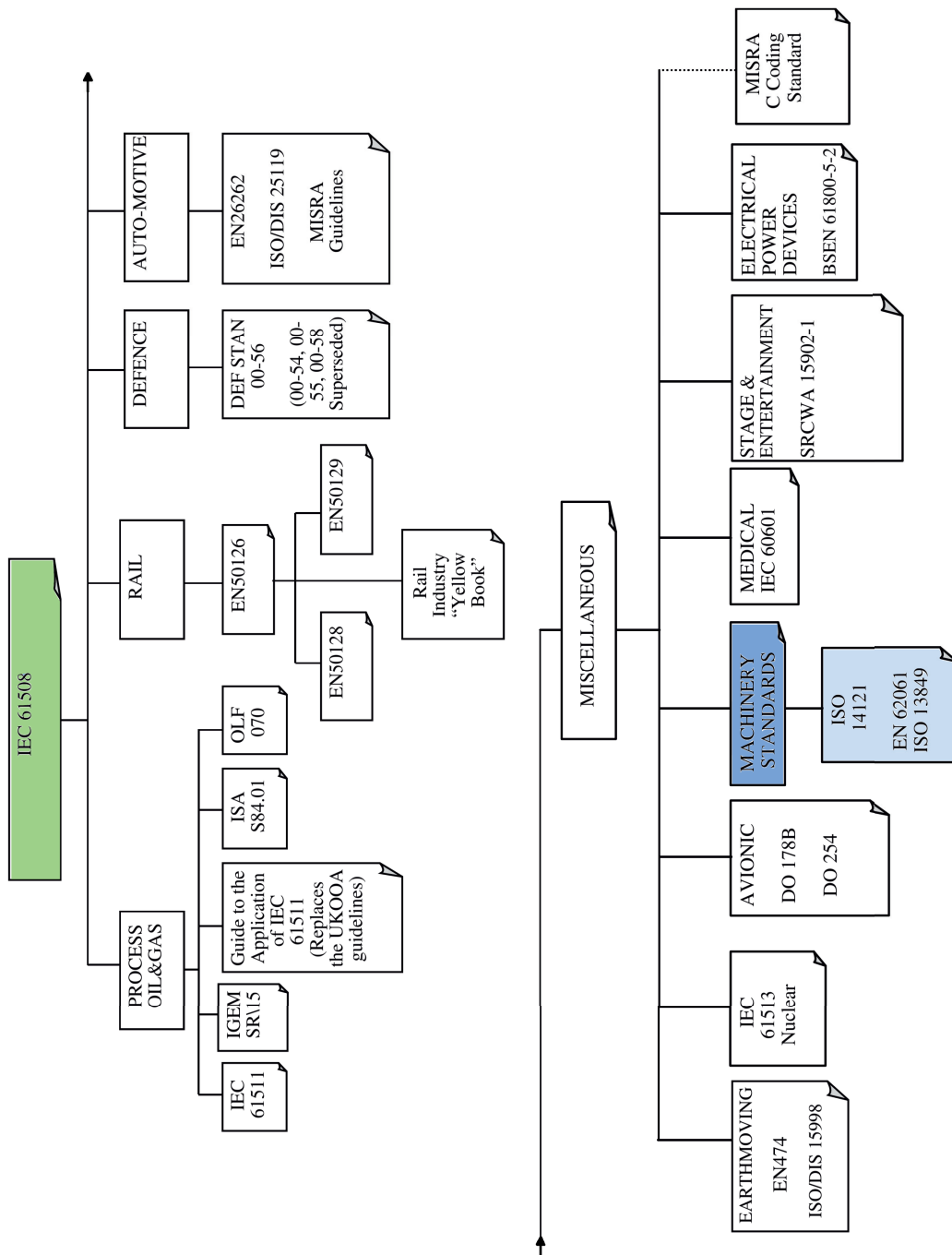


Figure 2.2.: Relation of the IEC 61508 standard to other industry-specific standards (from [SS11]). The presented measurement system in this thesis will most likely be used in the machinery sector. Thus, the standards shaded in light blue would apply.

## 2.2. Terms and Definitions

For the goal of making a product or system “safe”, the state “safety” has to be defined. According to [ISO12b], being in a state of “safety” means “being protected from recognized hazards that are likely to cause harm”. Thus, there is no alternative to being absolutely safe or having a complete absence of risk. Table 2.1 shows the probability of every day risk of death from different causes (from [SS11]).

Table 2.1.: Probability of everyday risk of death from different causes from [SS11].

Cause	Probability per year
Natural disaster (per individual)	$2 \times 10^{-6}$
Road traffic accident	$6 \times 10^{-5}$
Accident in the home	$4 \times 10^{-4}$
All accidents (per Individual)	$5 \times 10^{-4}$
All causes (mid-life including medical)	$1 \times 10^{-3}$

Additional standards, necessary to paint a complete picture and to apply the presented safety standards are:

- ISO3864, all parts, “Graphical symbols - Safety colours and safety signs”
- ISO7000, “Graphical symbols for use on equipment – Index and synopsis”
- ISO7001, “Graphical symbols – Public information symbols”
- IEC60417, all parts, “Graphical symbols for use on equipment”

Therefore it can be argued that every product or system includes some risk. The different elements of risk are shown in Fig. 2.3.

A more detailed explanation about risk assessment, SIL, etc. is given in the following section.

The presented terms and definitions in table 2.2 are taken from [ISO12b]. Although, slightly different definitions may apply for the same terms in other standards (e.g. [ISO10; IEC13b]) the broad concepts are the same and thus are used in this work.

Table 2.2.: Terms and definitions used in safety standards from [ISO12b].

Terms	Definition
Safety	Freedom from unacceptable risk
Risk	Combination of the probability that harm occurs and the severity of that harm
Harm	Injury or damage to the health of people, or damage to property or the environment
Hazard	Potential source of harm
Hazardous event	Event in which a situation may result in harm
Hazardous situation	Circumstance in which people, property or the environment are exposed to one or more hazards
Tolerable risk	Risk which is accepted in a given context based on the current values of society
Risk reduction measure (protective measure)	Any action or means to eliminate hazards or reduce risks
Residual risk	Risk remaining after risk reduction measures (protective measures) have been taken
Risk analysis	Systemic use of available information to identify hazards and to estimate the risk
Risk evaluation	Procedure based on the risk analysis to determine whether a tolerable risk has been achieved
Risk assessment	Overall process comprised of a risk analysis and a risk evaluation
Intended use	Use of a product or system in accordance with information provided by the supplier
Reasonably foreseeable misuse	use of a product or system in a way not intended by the supplier, but which may result from readily predictable human behaviour (see [ISO13b])

In [ISO12b] and in this work the terms “acceptable risk” and “tolerable risk” are considered to be equal. In the context of consumer safety the terms “reasonably foreseeable use” and “intended use” are used as synonyms.

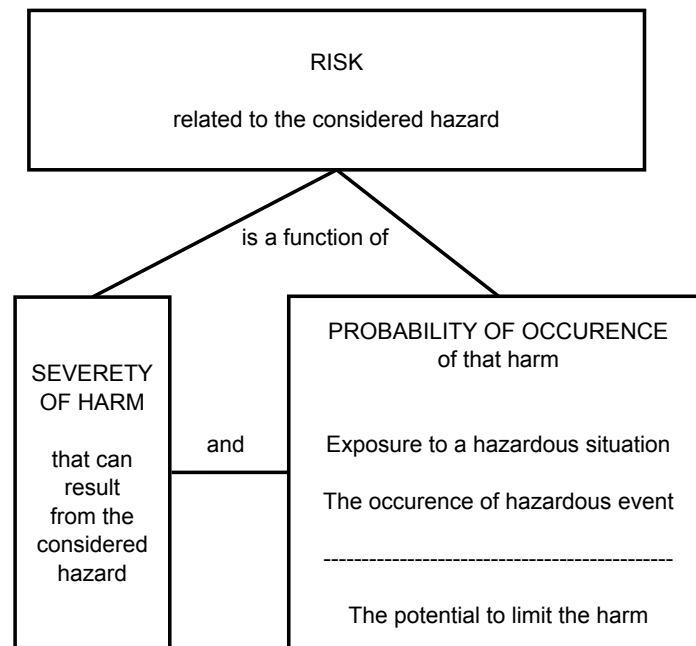


Figure 2.3.: Elements of risk (adopted from [ISO12b]).

### 2.3. Functional Safety and IEC 61508

This section describes the term functional safety, the targets that apply (e.g. SILs) and the according standard IEC 61508. As shown in Fig. 2.2 many industry-specific (also called “second-tier”) documents exist. These documents are derived from IEC 61508, but compliance with one of the industry-specific documents does not imply compliance with IEC 61508. Thus, an introduction to IEC 61508 is given and the interested reader can refer to [SS11] and its references for more information.

Functional safety is the ability of an electrical/electronic/programmable electronic (E/E/PE) system to remain in a safe state or go to a safe state if random (hardware) failures or systematic failures apply. According to [SS11] random failures can be quantified in terms of e.g. failure rates but systematic failures cannot. Thus, it is necessary to introduce integrity levels to address systematic failures in the design and operating activities. Additionally, a life cycle approach is needed to achieve functional safety, since systematic failures can happen in the design and operating life of a piece of equipment. The IEC 61508 is based on such a safety life cycle approach.

### 2.3.1. Safety Integrity Level (SIL)

A short description and the impacts of the four existing SILs according to IEC 61508 [IEC10b] is shown below.

- SIL 4** This is the highest target to achieve. According to [SS11] it should be avoided and other or additional protection levels should be used. The reason for this suggestion is the extremely high costs resulting from using state-of-the-art-practices (e.g. “formal methods” in design) and the required competencies for all techniques (and also not easy to find).
- SIL 3** Sophisticated design techniques are still needed for SIL 3 but it is not as onerous as SIL 4. There will still, however, be a limited number of vendors who can provide SIL 3. Time and costs are also not negligible.
- SIL 2** To achieve this level good design techniques and good operating practice are needed at a level matching what would be found in “ISO 9001:2008 - Quality management systems - Requirements”. SIL 2 is much easier to achieve than SIL 3 and is not very different from SIL 1 in terms of life cycle activities.
- SIL 1** This is the lowest level that still implies good design techniques. According to IEC 61508 SIL 1 is referred to as “not safety related”.

The reason for having SILs arises from the emergence of two different kinds of failures:

- Random hardware failures and
- Systematic failures

As mentioned, random hardware failures can be expressed quantitatively through e.g. failure rates. The frequency of hardware failures is predicted and compared to a maximum tolerable risk. Table 2.3 shows the maximum tolerable risk rate for each SIL according to IEC 61508 (and most other standards using SILs). Additionally, the so called “demand rate” also has to be taken into account. A system or product is called to have a “high demand rate” if the demand on the safety function is higher than once a year [IEC10b]. If it is less frequent it is called “low demand rate”.

At the same time, systematic failures cannot be quantified by e.g. failures rates. These failures are unique to a given product or system and the environment in which the product or system is used. According to [SS11], systematic failures can arise from

- Design tolerances
- Inadequately assessed modifications
- Software

Thus, systematic failures have to be taken into account by also addressing qualitative and not only quantitative safety targets. This is done by applying different

Table 2.3.: Definition of SILs according to IEC 61508 [IEC10b].

SIL	High demand rate (dangerous failures / hour)	Low demand rate (probability of failure on demand)
4	$\geq 10^{-9}t_0 < 10^{-8}$	$\geq 10^{-5}t_0 < 10^{-4}$
3	$\geq 10^{-8}t_0 < 10^{-7}$	$\geq 10^{-4}t_0 < 10^{-3}$
2	$\geq 10^{-7}t_0 < 10^{-6}$	$\geq 10^{-3}t_0 < 10^{-2}$
1	$\geq 10^{-6}t_0 < 10^{-5}$	$\geq 10^{-2}t_0 < 10^{-1}$

defences and design disciplines appropriate to the strictness of the tolerable risk target [SS11]. Therefore, SILs address safety targets quantitatively (e.g. through failure rates) and qualitatively (e.g. through design rules). One cannot assume that quantitative (failure rates) targets will be automatically achieved by applying the right qualitative requirements according to a certain SIL level. These two issues are quite separate [SS11]. Since a product or system's qualitative requirements apply throughout their whole life, IEC 61508 includes a so-called life cycle approach, which will be presented in the following section.

### 2.3.2. Life Cycle Approach

IEC 61508 defines, describes and is based on a safety life cycle. It is necessary to reduce systematic failures in order to achieve functional safety. According to the standard, this process must happen at different stages of design and during the operation of a product or system.

Fig. 2.4 shows a simplified version of the life cycle presented in IEC 61508, which is adopted from [SS11].

The different stages of this safety life cycle are [SS11]:

**Concept and scope** Defines the specific product, which parts are controlled, its boundaries and the safety requirements. Defines the hazard and how it is identified (e.g. hazard and operability study). A safety plan for all life cycle activities is needed.

**Hazard and risk analysis** It is a quantified risk analysis including the consequences of failure.

**Safety requirements and allocation** A maximum tolerable risk target is set for the whole system. Each safety function is defined and each gets its own SIL.

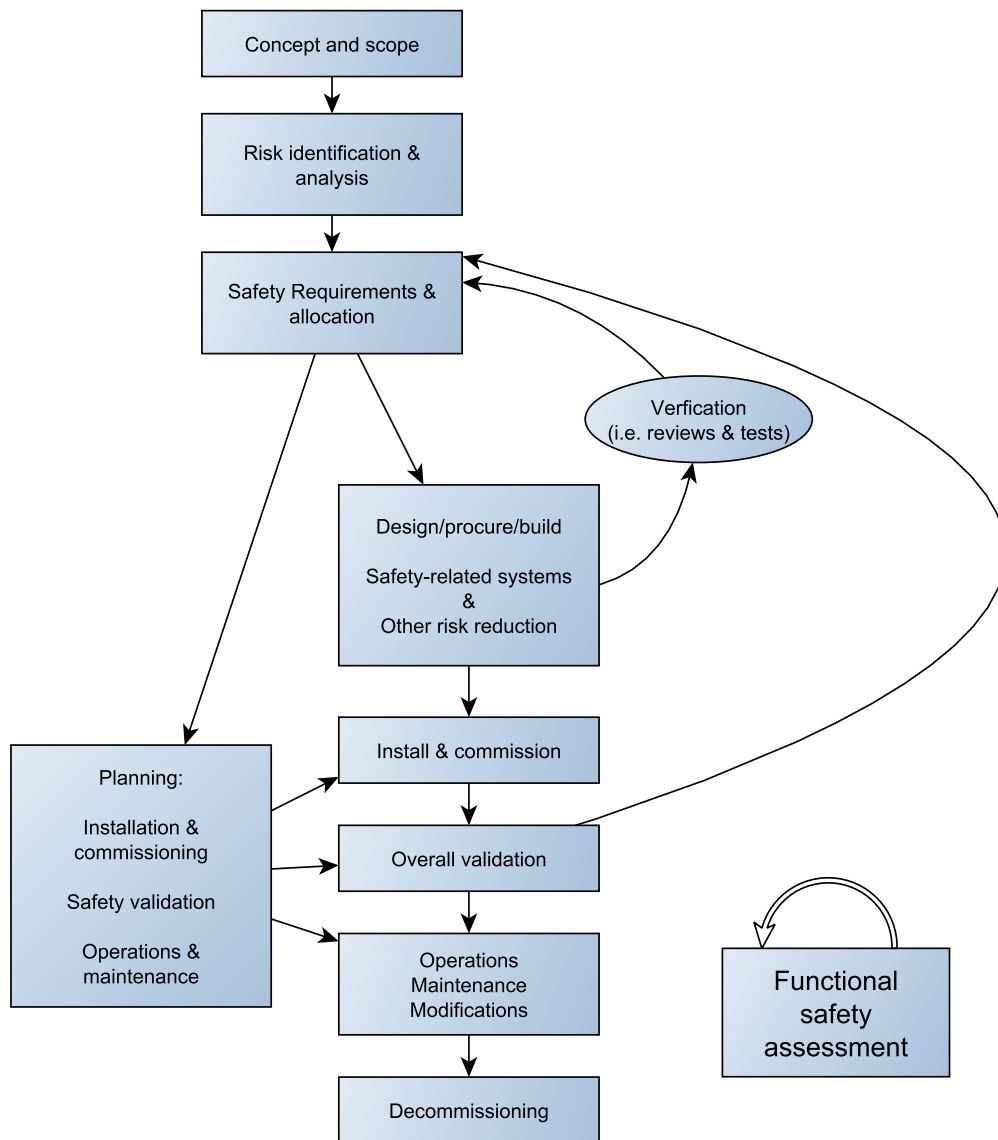


Figure 2.4.: Safety life cycle of a product or system according to IEC 61508 [SS11].

**Plan operations and maintenance** The definition of the effects on functional safety during operation or maintenance is done here. Human error is an important factor.

**Plan the validation** The validation of all functions has to be planned (e.g. putting together evidence from the verifications).

**Plan installation and commissioning** Everything (including human error) that can affect functional safety during the installation has to be planned here.

**The safety requirements specification** A description of all safety functions in detail.

**Design and build the system** The realization of the safety system.

**Install and commission** Implementation of the product or system including documentation of all events especially failures.

**Validate that the safety systems meet the requirements** The allocated targets have to be checked through predictions, reviews and tests. The product or system has to be validated several times during its life.

**Operate, maintain, and repair** Again, documentation is important, especially documentation of failures.

**Control modifications** A modification is a kind of re-design and thus, life cycle activities have to be taken into account.

**Disposal** Decommissioning can also be accompanied by safety hazards which have to be monitored.

**Verification** The demonstration of the implementation of all life cycle activities.

**Function safety assessments** An assessor demonstrates compliance with the according SIL (see table 2.4)

For the assessment process, which is part of the safety life cycle, following steps have to be taken (from [SS11]):

1. Establish functional safety capability (of the assessor and the design organization)
2. Establish a risk target (through e.g. formal hazard identification)
3. Identify the safety-related functions
4. Establish SILs for the safety-related elements
5. Quantitative assessment of the safety-related product or system
6. Qualitative assessment against the respective SIL
7. Establish as low as reasonably practicable (ALARP)

The assessor has to be independent from the assessed product or company. The minimum amount of independence depends on the target SIL. Table 2.4 shows the different levels of minimum independence.



Table 2.4.: Minimum independence of the assessor according to the SILs [IEC10b].

SIL	Consequence	Assessed by
4	Many deaths	Independent organization
3	More than one death	Independent department
2	Severe injury or one death	Independent person
1	Minor injury	Independent person

### 2.3.3. Overview of IEC 61508

The standard IEC 61508 [IEC10b] is divided into 7 parts. Parts 1 to 3 are the main parts and parts 4 to 7 provide additional material. As can be seen from Fig. 2.5 the general process is to establish SIL targets through different methods and then design the product or system. This design phase has to realize a targeted integrity level including random failures and systematic failures.

Below, the 7 parts of the standard are briefly described:

- Part 1 - General Requirements** Including topics like the definition of SILs, the life cycle approach, etc.
- Part 2 - Requirements for E/E/PES safety-related systems** This part covers the hardware aspects of the safety-related system.
- Part 3 - Software requirements** Everything concerning software design.
- Part 4 - Definitions and abbreviations** Terms and definitions used in the standard.
- Part 5 - Examples of methods for the determination of safety-integrity levels** General concepts and methods for information (e.g. methods for determining SIL targets, application of ALARP, qualitative methods of establishing the SILs, etc.)
- Part 6 - Guidelines on the application of part 2 and part 3** Provides material for e.g. calculating probability of hardware failures, common cause failures, etc.
- Part 7 - Overview of techniques and measures** Reference guide to measures and techniques.

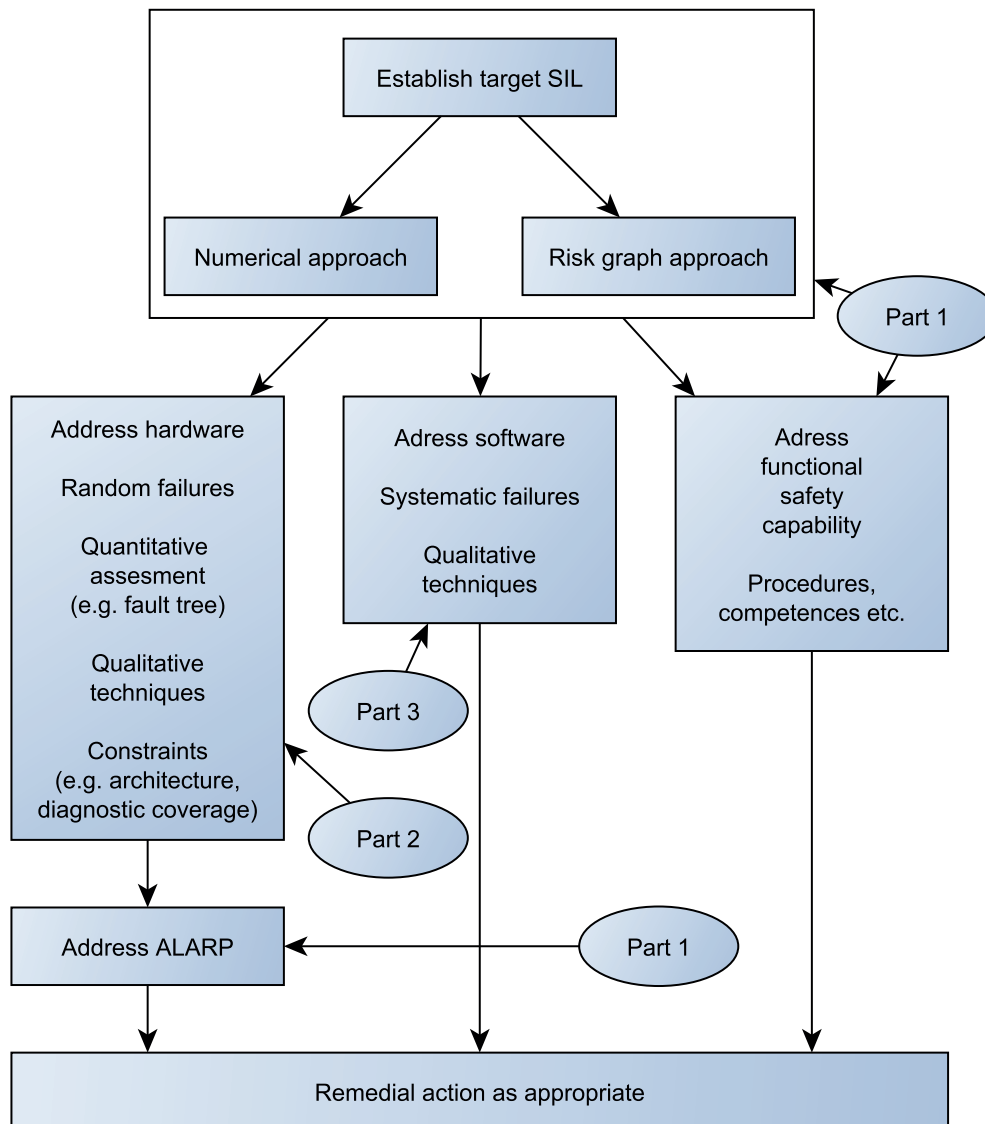


Figure 2.5.: Description of the main parts (parts 1 to 3) of the standard IEC 61508 [SS11].

## 2.4. Application of IEC 61508 through Design Patterns

First introduced in 1977 in the book “A Pattern Language - Towns, Buildings, Construction” [AIS77], design patterns these days are often used by architects and software designers. Design patterns help to solve periodic problems by using a pattern related to that problem. Below, the benefits and purpose of design patterns are described briefly. The basis of their usefulness is also described in terms of safety devices using IEC 61508. A simple example concludes this section and aims to give insight into how useful design patterns can be.

### 2.4.1. What are Design Patterns and Examples

“A pattern describes an optimal solution to a common problem within a specific context” [Yah13]. Most often design patterns consist of four primary components [Yah13]:

1. title
2. problem
3. context
4. solution

Design patterns were introduced the first time in [AIS77] wherein patterns are used for building homes, neighbourhoods, towns, etc. For example, patterns exist for different rooms and different types of houses; patterns exist for the arrangement of houses in neighbourhoods and so on. One pattern will lead to several “smaller” patterns which can be part of it and the pattern itself can be a part of one or more “bigger” patterns. An example is the design pattern “76 House for a Small Family” which states that “In a house for a small family, it is the relationship between children and adults which is most critical” [AIS77]. Thus, the pattern 76 provides three distinct areas necessary for a house for a small family:

- a couple’s realm, which is reserved for the adults
- a children’s realm, which is ruled by the children
- a common area, which is between the first two and connected to both

Smaller patterns then deal with e.g. “the couple’s realm (136)” or “the children’s realm (137)”. The pattern itself is part of the bigger patterns “house cluster (37)” and “row Houses (38)”. Thus, if one has the task of building a house for a small family, these patterns can be used. The patterns allows one to build individual houses without running into problems that have already been solved.

Especially in software architecture (for example in web page design) design patterns are used very often. One example is the “Yahoo! Design Pattern Library” [Yah13],

which consists of 59 design patterns to solve common web design problems. But also in the field of “safety” and the related standardization processes design patterns are used extensively. How this approach can help in terms of the IEC 61508 will be shown in the next two sections.

### 2.4.2. Design Patterns in Terms of IEC 61508

The first step in developing a safety critical system in terms of the IEC 61508 is the design of the system’s architecture. A rich set of high-level architecture is provided by the IEC 61508. The system designer has to choose the architecture most most appropriated for the case. It is also left to the designer of the system to choose which methods to use for refining the architecture and to achieve and prove the necessary safety goals for the system. Many methods are shown in part 7 of the IEC 61508. Since IEC 61508 is a very generic standard it can be difficult to choose the appropriate methods and arguments for system safety [PKK13a]. Thus, in [PKK13b] design patterns are presented to address this problem.

[PKK13b] links the presented patterns with architectural design decisions called safety tactics [PKK13c]. To make this link Goal Structuring Notation (GSN) diagrams [GSN11] are used. At the end, safety patterns are presented which are then linked to IEC 61508 techniques and measures with the help of GSN diagrams. These GSN diagrams can additionally be used to argue for the safety of the system architecture [PKK13a].

One example is the “Homogenous Duplex Pattern” shown in Fig. 2.6 from [PKK13b]. As stated in the beginning of this section, each pattern has a title, a context, a problem and a solution. Additionally, these patterns have other fields for explanation and also to make a link to IEC 61508 (e.g. the field called “GSN Diagram”).

As can be seen in Fig. 2.6 the pattern uses three safety tactics:

- Replication redundancy
- Override
- Condition monitoring

[PKK13c] links these safety tactics to IEC 61508 measures and methods. Table 2.5 shows the related measures and methods for the three safety tactics used by the Homogenous Duplex Pattern [PKK13a; PKK13c].

This tactic enables the system architect to design the safety system and use the methods from IEC 61508 which are most appropriate (i.e. necessary to achieve the required level of system safety).

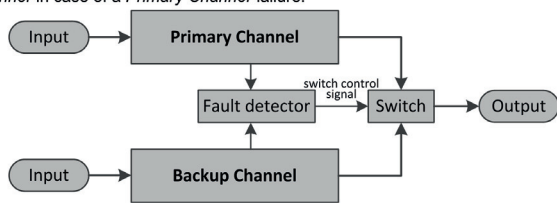
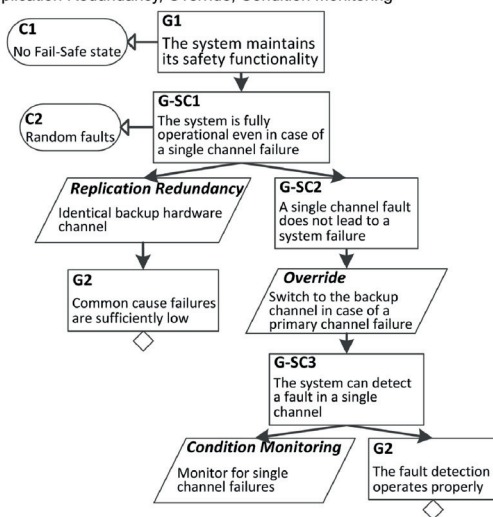
<b>Pattern Name</b>	HOMOGENOUS DUPLEX PATTERN	<b>Pattern Type</b>	hardware, fail-over						
<b>Also Known As</b>	Homogeneous Redundancy Pattern, Standby-Spare Pattern, Dynamic Redundancy Pattern, Two-Channel Redundancy Pattern, 1oo2D Pattern								
<b>Context</b>	A safety-critical application without a fail-safe state has a high random error rate and a low systematic error rate.								
<b>Problem</b>	How to design a system which continues operating even in the presence of a fault in one of the system components								
<b>Forces</b>	<ul style="list-style-type: none"> <li>- the system cannot shut down because it has no safe state</li> <li>- development costs should not increase</li> <li>- the safety standard requires high fault coverage for single-point of failure components</li> <li>- high availability requires hardware platforms to be maintained at the runtime</li> </ul>								
<b>Solution</b>	<p>The system consists of a <i>Primary Channel</i> (active) and a <i>Secondary Channel</i> (backup) which are two identical hardware modules. A <i>Fault detector</i> monitors the channels and controls a <i>Switch</i> to select the <i>Backup Channel</i> in case of a <i>Primary Channel</i> failure.</p> 								
<b>GSN Diagram</b>	<p>Used Tactics: Replication Redundancy, Override, Condition Monitoring</p> 								
<b>Consequences</b>	<p>Systematic and random faults in a single channel are detected and masked. System reliability strongly depends on the fault coverage of the fault detection unit and on the proper functionality of the switch.</p> <table border="1" style="width: 100%; border-collapse: collapse;"> <thead> <tr> <th colspan="2" style="text-align: center;">Affected Attributes</th> </tr> <tr> <th style="width: 50%;">Positively</th> <th style="width: 50%;">Negatively</th> </tr> </thead> <tbody> <tr> <td> <i>Safety:</i> Random Errors in a single channel are handled  <i>Availability:</i> The full system functionality is still available in case of a single random fault  <i>Maintenance:</i> Hardware channels can be maintained at runtime                 </td> <td>Double hardware costs for system replication</td> </tr> </tbody> </table>			Affected Attributes		Positively	Negatively	<i>Safety:</i> Random Errors in a single channel are handled <i>Availability:</i> The full system functionality is still available in case of a single random fault <i>Maintenance:</i> Hardware channels can be maintained at runtime	Double hardware costs for system replication
Affected Attributes									
Positively	Negatively								
<i>Safety:</i> Random Errors in a single channel are handled <i>Availability:</i> The full system functionality is still available in case of a single random fault <i>Maintenance:</i> Hardware channels can be maintained at runtime	Double hardware costs for system replication								
<b>General Scenarios</b>	<b>SC1</b>	The system is fully operational even in case of a single channel failure.							
	<b>SC2</b>	A single channel random fault does not lead to a system failure.							
	<b>SC3</b>	The system can detect a fault in a single channel.							
<b>Usage Examples</b>	<ul style="list-style-type: none"> <li>- TOYOPUC-PCS PLC [Miyawaki, 2008]</li> <li>- Navigation system safety [Ljosland, 2006]</li> <li>- Gebhardt GA DUPLEX-S 1oo2D PLC - <a href="http://www.gebhardt-automation.com">http://www.gebhardt-automation.com</a></li> </ul>								
<b>Credits</b>	[Douglass, 2002] introduces the pattern. [Grunske, 2003] presents a more general version of this pattern and [Armoush, 2010] adds detailed information about quality attribute related consequences.								

Figure 2.6.: Example of a safety pattern (Homogenous Duplex Pattern) from [PKK13b].

Table 2.5.: Link between safety tactics used from the Homogenous Duplex Pattern and IEC 61508 measures and methods from [PKK13a].

Tactics	Linked IEC 61508 measures and methods	Contained in frequency converter from [BM07]
Replication Redundancy	A.2.1 Test by redundant hardware	Redundant electronic subsystem
	A.2.5 Monitored redundancy	Monitored redundant processing units
	A.3.5 Reciprocal comparison by software	Processing units - comparison by software
	A.4.5 Block replication	Processing units - ROM memory replication
	A.6.3 Multi-channel output	-
	A.6.5 Input comparison/Voting	Input comparison for sensors
	A.7.3 Complete hardware redundancy	-
	A.7.5 Transmission redundancy	-
	A.1.3 Comparator	Processing unit result comparator
Override	A.1.5 Idle current principle	Idle current principle for actuators
	A.8.1 Over voltage protection with safety shut-off	Power supply unit
	A.8.3 Power-down with safety shut-off	Safety shut-off for power supply unit
	A.1.1 Failure detection by online monitoring	Online monitoring of the sensors
	A.6.4 Monitored output	-
	A.8.2 Voltage control	Safety shut-off for power supply
	A.9.1 Watchdog with separate time base with-out time-window	Timeout monitored by a watchdog element
	A.9.2 Watchdog with separate time base and time-window	-
	A.9.3 Logical monitoring of program sequence	Watchdog checks correct program sequence
Condition Monitoring	A.9.4 Combination of temporal and logical monitoring of program sequences	Watchdog system checks
	A.9.5 Temporal monitoring with on-line check	-
	A.12.1 Reference sensor	-
	A.13.1 Monitoring	Monitoring of the actuators

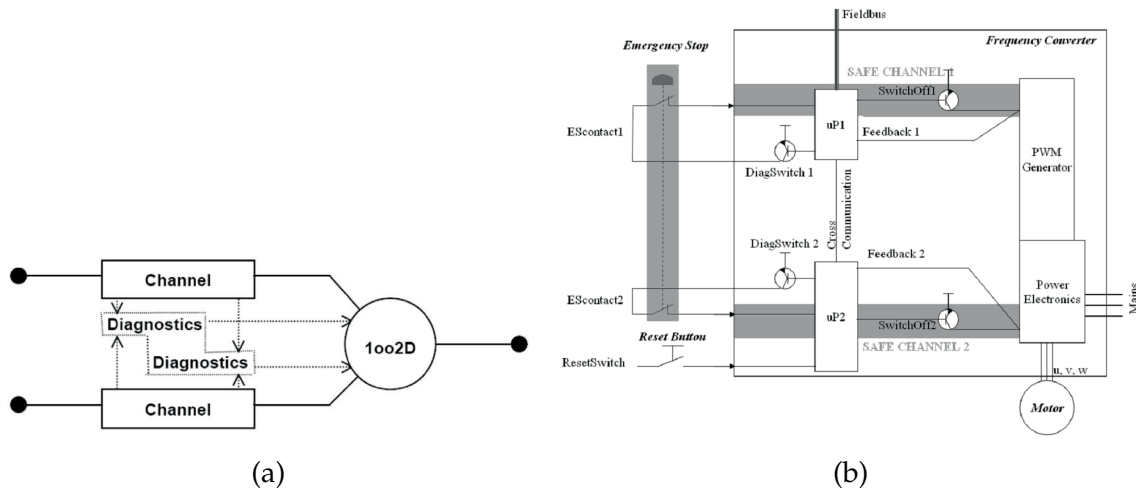


Figure 2.7.: 1002D architectures. (a) High level architecture as described in IEC 61508 [IEC10b]. (b) Block diagram of a safety-related frequency converter, which uses the 1002D architecture (from [BM07]).

### 2.4.3. Example of a Safety Device Realized

This section presents an example from [BM07] of how useful the presented safety patterns can be. The example is taken from. The paper gives detailed information about the IEC 61508 measures and methods which were applied for the presented example. This example from [BM07] is a frequency converter (shown in Fig. 2.7(b)) which uses the 1 out of 2 architecture with diagnostics (1002D) (explained in [IEC10b] part 6). The 1002D architecture is also known as homogenous duplex architecture. As can be seen from Fig. 2.7(a), the 1002D architecture consists of two channels and the diagnostics. The channels perform the system's safety function and the diagnostics can activate a safe state independent from the two channels [BM07].

The last column in table 2.5 shows the methods and measures used in the safety frequency converter. As shown in [PKK13a] approximately 70 % of the suggested methods and measures were really used. This proves that there is a good selection of suitable methods from the pattern. The calculated occurrence value (i.e. number of methods suggested by the pattern divided by the overall number of methods in the IEC 61508) is only 10 %. This presents the benefits of the pattern in order for the architectural designer to make an appropriate selection of a huge number of provided methods by the IEC 61508.

Additionally, the presented safety patterns can be used to argue for the safety of the system. As shown in Fig. 2.6 the pattern provides a generic GSN diagram. By replacing the safety tactics in the GSN diagrams with the used methods and



measures it is possible to obtain a full GSN diagram. This diagram can then be used to prove how specific methods or measures contribute to the overall safety in a system. Fig. 2.8 shows the obtained GSN diagram from [PKK13a] for the presented example.

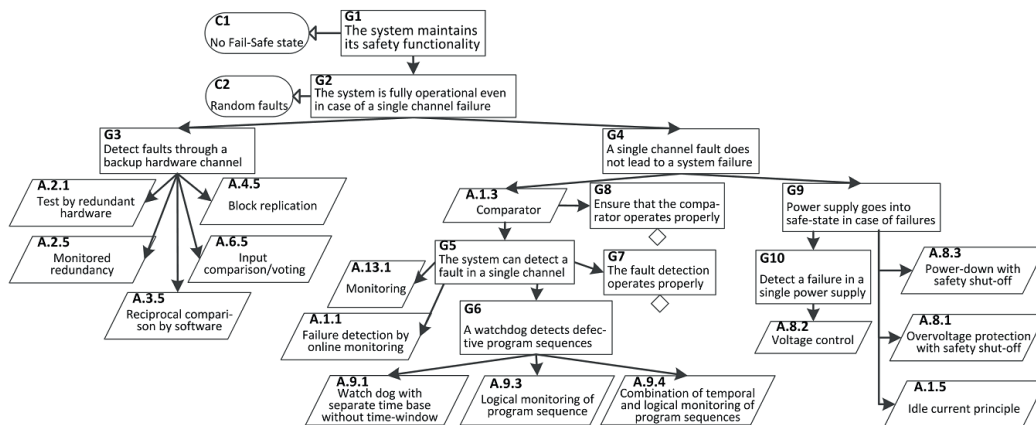


Figure 2.8.: GSN diagram for the safety frequency converter obtained from the homogenous duplex pattern [PKK13a].

## 2.5. Appliance for Pretouch and Collision Detection Systems

The best method to describe and understand the meaning and importance of safety standards by means of pretouch and collision detection systems as presented in this thesis is a simple example. In this section, an imaginary application will be adopted with a pretouch detection system to make it safe by means of the presented safety standards (for example IEC61508 [IEC10b] as a group A standard or IEC62061 [IEC05] as a group B standard). The safety requirements for the pretouch system will be developed as a function of the imaginary application.

Before the design phase of the safety-related control function (SRCF) a risk analysis (or risk assessment) has to be performed. It is described in ISO 14121-1 (see Fig. 2.1) and can involve following steps (according to [Ltd12]):

- Identifying limits of the application
- Identifying the hazards
- Who might be harmed and at which time
- Risk estimation
- Risk reduction (first by safe design, then by safeguarding)



As stated above, if safe design is not possible or not practicable, safeguarding should be used to reduce the risk. [Ltd12] states: “Safeguarding should prevent persons from coming into contact with hazards.” This is similar to the motivation and aims of this thesis (see section 1.1): “Prevent injuries of humans in areas where they just should not be”.

The design of a safeguarding system can be split into 5 steps:

1. Risk assessment (defining the power of the safeguarding system)
2. Breakdown of the safeguarding system into function blocks (specification)
3. Defining the safety requirements for each function block
4. Evaluation of safety requirements
5. Verification and validation

Each of the steps is described below using the example of a home robot that assists with personal domestic applications (one can imagine a more powerful version of a vacuum-cleaning robot). The aim is to reduce risk of a collision between the robot and the human being through a SRCF.

### 2.5.1. Risk Assessment

The necessary SIL is evaluated by breaking down the risk related to the identified hazard into different parameters, namely:

- Severity of the harm (SE)
- Frequency and duration (FR)
- Occurrence probability of the hazardous event (PR)
- Probability of limiting or even avoiding the harm (AV)

The recommended classification for each parameter is provided in tables 2.6 to 2.8 (according to [Ltd12]). The severity of injuries does have a huge influence on the estimated SIL. For a domestic robot, one could imagine that a collision will hardly cause a human to lose a finger or similar injury. The worst will probably be the need for a medical practitioner or even less (e.g. first aid). Thus, we will calculate with a severity of  $SE = 2$  or  $SE = 1$ . As the standard IEC 62061 is used, a SIL target of 4 would not be considered. For SIL 4 see IEC 61508 [IEC10b].

In order to estimate the next three parameters  $FR$ ,  $PR$ , and  $AV$ , the use of a task analysis is recommended to find the correct values. For this example the values are set according to a subjective evaluation. A domestic cleaning robot is usually be active while nobody is at home. Thus, no person would need to access the hazardous zone. However, in the worst case the robot is cleaning while a child or baby is playing on the floor. Thus, the robot will (depending on the cleaning area)

Table 2.6.: Estimation of the severity parameter according to IEC 62061 [IEC05].

Consequences	SE
Death, losing an eye or arm (irreversible)	4
Broken limb(s) or losing a finger(s)	3
Requiring attention from a medical practitioner (reversible)	2
Requiring first aid (reversible)	1

“interact” with the child very often. Since we have to take the worst case,  $FR$  is set to  $FR = 5$ . The probability of occurrence will be set to “possible” ( $PR = 3$ ). It should be probable that adults avoid harm, but this would be more difficult for children and even impossible for babies. Thus,  $AV$  is set to 5.

Table 2.7.: Frequency and probability of occurrence according to IEC 62061 [IEC05].

Frequency of exposure (> 10 min)	FR	Probability of occurrence	PR
< 1 hour	5	Very high	5
between 1 hour and 1 day	5	Likely	4
between 1 day and 2 weeks	4	Possible	3
between 2 weeks and 1 year	3	Rarely	2
> 1 year	2	Negligible	1

Table 2.8.: Probability of avoiding or limiting harm according to IEC 62061 [IEC05].

Probabilities of avoiding or limiting harm	AV
Impossible	5
Rarely	3
Probable	1

After the 4 parameters ( $SE$ ,  $FR$ ,  $PR$ , and  $AV$ ) are estimated, the respective SIL can be determined according to table 2.9. In this table the class  $Cl$  can be calculated by  $Cl = FR + PR + AV = 5 + 3 + 3$ . In the presented example  $Cl$  will add up to 11. Depending on the chosen severity of harm level the required SIL is 1 or even less (bold values in table 2.9). In this table “OMS” is the synonym for “other

Table 2.9.: Estimating the necessary SIL according to IEC 62061 [IEC05] and adopted from [Ltd12].

<i>SE</i>	<i>CI</i>				
	3 – 4	5 – 7	8 – 10	11 – 13	14 – 15
4	SIL 2	SIL 2	SIL 2	SIL 3	SIL 3
3		OMS	SIL 1	SIL 2	SIL 3
2			OMS	<b>SIL 1</b>	SIL 2
1				<b>OMS</b>	SIL 1

OMS ... other measures suggested

measures suggested”. According to IEC61508 everything under SIL 1 is referred as “not safety-related” in terms of compliance [SS11].

As one can see, the severity of harm level has a huge influence on the required SIL. In this example it can be augmented for SIL 1 or “not safety-related”.

### 2.5.2. Specification of Function Blocks

Each function block (FB) must be described. This comprises details about each SRCF, definition of interfaces to other FBs and definition of fault responses. This gives the designer an initial concept of the architecture of the safety-related electronic control system. Fig. 2.9 provides an example for such a function block structure.

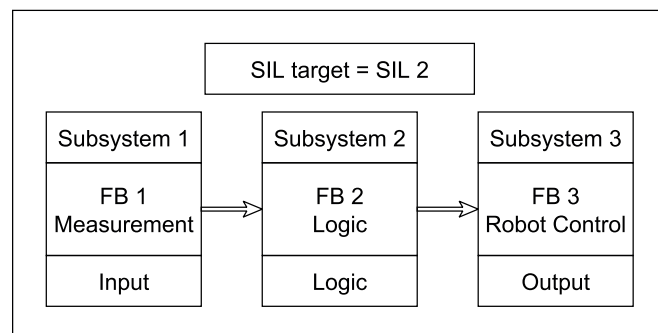


Figure 2.9.: Initial concept for a safety-related electronic control system (SRECS).

### 2.5.3. Safety Requirements for each Subsystem in a Function Block

According to the standard IEC 62061 [IECo5], a subsystem is a system which leads to a failure of the whole SRCF if it fails. Each FB is assigned to a subsystem and more than one FB can be assigned to the same subsystem. Each subsystem can also consist of several elements or diagnostic functions. A safety integrity level claim limit (SILCL) is assigned to each subsystem. This SILCL must not be less than the SIL target. In the presented example all SILCLs must be at least 2. Fig. 2.10 shows the simple subsystem structure used in the example.

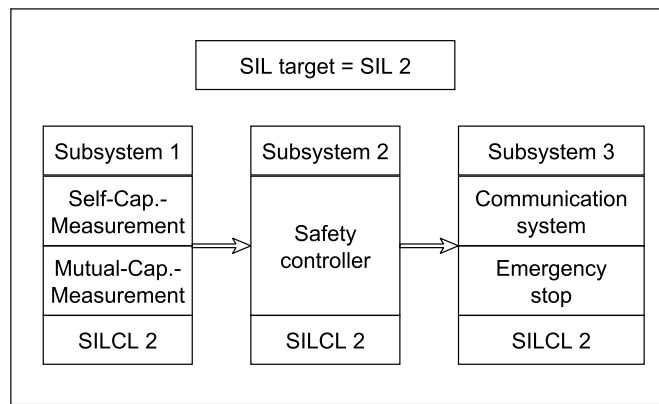


Figure 2.10.: Subsystems of a SRECS for a domestic robot.

### 2.5.4. Evaluation of Safety Requirements

In this step, hardware and software have to be chosen (or designed) for each subsystem. The necessary data has to be obtained from the manufacturer. In this example one is interested in the necessary parameters to achieve. These parameters include:

- $PFH_d$ : Probability of dangerous failure per hour
- $SFF$ : Safe failure fraction
- $HFTN$ : Hardware fault tolerance, where  $N$  means, that  $N + 1$  faults could cause a failure of the SRCF
- $\lambda_D$ : Failure rate of dangerous failures
- $\beta$ : Susceptibility to common cause failure (compare IEC 62061 [IECo5])
- $T1$ : Lifetime or proof test interval (the one which is smaller)
- $T2$ : Diagnostic test interval

- *DC*: Diagnostic coverage
- $B_{10}$ : Number of cycles until 10 % of the population fail

These parameters not only depend on the chosen hardware but also on the architecture in which it is used. The four possible architectures in IEC 62061 are:

- Type *A*: Zero fault tolerance, no diagnostic function
- Type *B*: Single fault tolerance, no diagnostic function
- Type *C*: Zero fault tolerance, with a diagnostic function
- Type *D*: Single fault tolerance, with a diagnostic function

For more information the interested reader is referred to [IEC05; Ltd12] and the literature referenced therein. Tables 2.10 and 2.11 list the necessary parameters which have to be achieved for a given SIL target.

Table 2.10.: Probability of dangerous failure per hour for a given SIL target according to IEC 62061 [IEC05].

SIL	Range of $PFH_d$	
<b>1</b>	$\geq 10^{-6}$	$PFH_d < 10^{-5}$
<b>2</b>	$\geq 10^{-7}$	$PFH_d < 10^{-6}$
<b>3</b>	$\geq 10^{-8}$	$PFH_d < 10^{-7}$

Table 2.11.: Hardware fault tolerance ( $HFT_d$ ) for a given safe failure fraction ( $SFF$ ) according to IEC 62061 [IEC05].

SFF	HFT 0	HFT 1	HFT 2
$< 60\%$	n.a.	<b>SILCL 1</b>	SILCL 2
$\geq 60\%$ to $< 90\%$	<b>SILCL 1</b>	SILCL 2	SILCL 3
$\geq 90\%$ to $< 99\%$	SILCL 2	SILCL 3	SILCL 3
$\geq 99\%$	SILCL 3	SILCL 3	SILCL 3

For the given example, the minimum parameters to be achieved are indicated in bold. If, for example, new hard- or software is used where the presented parameters are not known, these have to be determined before the presented calculations can be made (see IEC 61508 [IEC10b]).

### 2.5.5. Verification and Validation

A verification step each subsystem has to be checked to ensure, that its SILCL is equal or higher to the SIL target of the SRCF. Additionally, the probability of a dangerous fail of the SRCF due to random hardware failures has to be equal or less than the given hardware failure rate ( $\lambda_D$ ).

A validation is necessary before the SRCF can claim a certain SIL target. This validation can be made by analysing (see section 2.4) or testing. The testing is done by simulating certain hardware failures.

### 2.5.6. Result and Consequences

This section has demonstrated what kind of safety requirements are possible for an imaginary robot application and how to determine them according to the standard IEC 61508 [IEC10b].

It was shown that an application such as the presented home cleaning robot is between SIL 1 and “not safety-related”. SIL 1 is the minimum safety integrity level and while implying good design practice it is not very difficult to achieve (compared to the higher SIL levels). Thus, according to [SS11] it would be relatively easy to achieve SIL 1 for such a collision detection system for these kinds of applications. This is especially true if ISO 9001 practices are used to demonstrate Functional Safety Capability.

If the safety system were to be used in a more dangerous environment where a collision for example can cause serious injuries, SIL 2 or even SIL 3 would be necessary.

### 3. Survey of Measurement Systems for Safety Applications

Many measurement principles might be applied to prevent human injuries in areas where they just should not be. This chapter will show that only a few can meet the requirements outlined in section 1.2.

To be able to compare different measurement systems, a kind of reference application is useful. An area of application where nearly all the requirements from section 1.2 have to be met, when it comes to safety applications, is robotics. An emerging research topic in robotics is the safe human-robot interaction [Ryb+12]. As can be seen in Fig. 3.1, especially, in the last five to ten years, a significant increase in research work can be observed in this area of application.

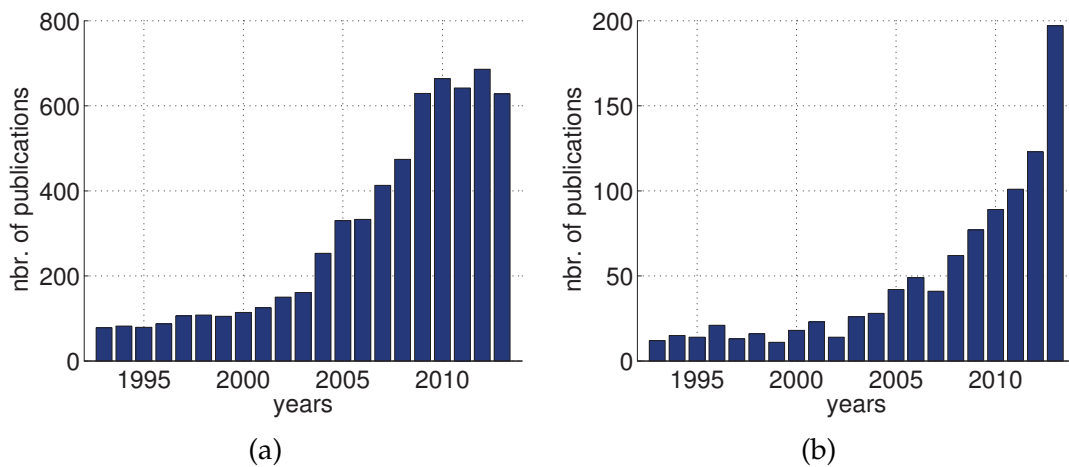


Figure 3.1.: Number of publications matching the terms “\*safe\*” and “\*robot\*” from the years 1993 to 2013. (a) Results obtained from the IEEE Xplore Digital Library search engine. (b) Results obtained from the Science Direct search engine.

The essential goal of this research is to enable robots to safely work and interact with humans [Had+12]. Below, it will be explained why this chapter focuses on robotics as an example for safety applications. A safe human-robot interaction:

- is a timely research topic (e.g. [VB13; LV12; OYF12; NLH12; Hey10]) and thus uses the newest measurement systems.
- covers the requirements, which were proposed in sections 1.1 and 1.2 ([BPCo8]),
- can be easily be used in other fields of applications when considered in terms of sensory and algorithms,

If a sensor system were found or invented that is able to prevent a robot from colliding with e.g. humans, it would be possible to adapt and use this sensor system for other applications (under certain constraints).

The following section presents the state-of-the-art sensor technology for object detection and classification, which can also be used for safety applications. Although the majority of the sensor systems presented are used in robot applications they could easily be used in other applications (for example those presented in section 3.2). According to [CHo8], these sensors belong to the class of exteroceptive sensors, since they take in information from the external environment. This information can include:

- distance from an object
- interaction forces
- tissue density
- other physical properties

At the end of the chapter, a comparison between the sensing technologies presented will be made. Table 3.2 gives an overview of the presented sensors. The attempt was made to provide the reader with an idea of which sensor systems could be used for object detection and/or object classification for safety applications (adapted from [CHo8]). Benefits and drawbacks of these technologies are used to prevent human injuries in areas where humans just should not be.

The second part of this chapter presents existing capacitive sensing technologies for object detection and classification. Different state-of-the-art approaches are presented and compared, as are benefits and drawbacks of the existing systems.

## 3.1. State-of-the-Art Sensor Technology

### 3.1.1. Vision

Vision sensors (e.g. monocular cameras, stereo cameras, panoramic vision, etc.) have been studied in terms of human-robot interactions for a long time [DEo8]. Recently RGB-D cameras, such as the Asus Xtion or the Microsoft Kinect, have become affordable and thus, depth image-based human detection has attracted



attention in robotics research [Fos+12; Cho+13]. Vision sensors can be mounted on the robot or observe predefined areas from the outside. Below, two examples provide promising results. The first example uses cameras mounted on the robot while the second example observes the environment from the outside (i.e. not mounted on the robot). The two examples in this thesis cover the sensor technology and measurement hardware, and attempt to give insight into the possibilities of using vision sensors for human-robot interaction. The examples are also used to show drawbacks and determine potential improvements with other sensors, such as pretouch sensors. The interested reader can refer to [DEo8] and to the literature referenced there for more information on this interesting and extensively studied subject.

### Human Safety in Industrial Workcells [Ryb+12]

There is a high demand in industry to no longer separate humans and active industrial robots, which so far has not been possible because of safety concerns. Sharing workcells, for example, would lead to the more efficient use of time and resources. Thus, in [Ryb+12] a system is presented which uses multiple 3D imaging sensors to separate background, robots and humans (compare Fig. 3.2) and detect possible collisions.

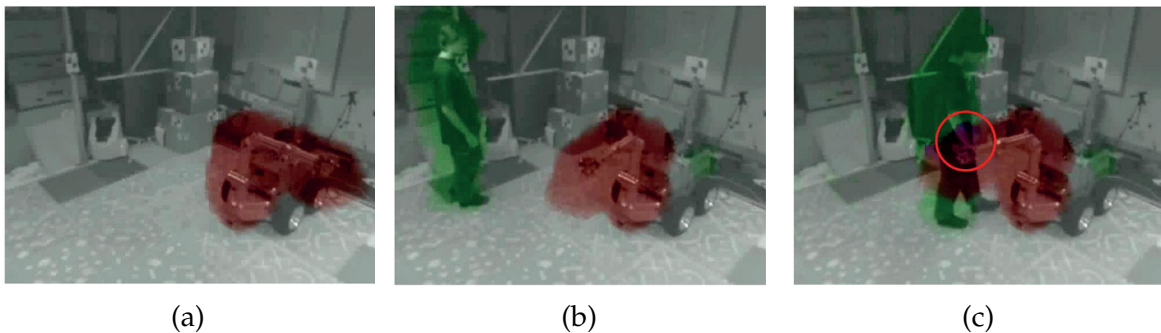


Figure 3.2.: A vision sensor system for human safety in industrial workcells from [Ryb+12]. (a) A picture of one of the four cameras that were used. The red region indicates an adaptive danger zone around the robot, which is based on the robot's position and trajectory. (b) A human is surrounded by an adaptive (green) safety zone. It also follows the human as he moves around in the workcell. (c) The danger and safety zone intersect, because the human comes too close to the robot (indicated by the red circle). In such situations the robot stops or slows down to avoid collisions.

The system presented in [Ryb+12] can be used with a variety of 3D cameras such as stereo cameras, range cameras (i.e. flash lidar), structured light or the Kinect sensor. The experiments in [Ryb+12] were done with four cameras (two range cameras and

two stereo cameras). This sensor fusion approach enables the system to use the benefits of the different sensing devices and avoid/eliminate their drawbacks.

As stated in [Ryb+12] the presented approach has several drawbacks when it comes to safety applications, including:

- The necessary calibrations (intrinsically and extrinsically) for each workcell to obtain distance information and a reference frame from multiple cameras.
- The robots in the workcell (i.e. dangerous objects) have to be known (e.g. joint positions and velocities).
- Occlusions in the workcell can lead to blind zones for safety applications where no collision avoidance is possible.
- All other moving objects (other than the known robots) are interpreted as humans.
- Heavy signal processing (due to e.g. sensor fusion).
- Rather slow detection rate at approximately 10 Hz.

A different approach using the Microsoft Kinect camera and a depth space approach is presented in [Fla+12]. Its performance in terms of object collision avoidance between a robot arm and, for example, a human is promising.

### **Depth cameras on indoor mobile robots for fast human detection [Cho+13]**

In this work a Microsoft Kinect sensor was mounted on a mobile robot to detect humans in different environments. The algorithm runs at 30 Hz on a mobile robot using a single core CPU [Cho+13]. The algorithm consists of four different stages shown in Fig. 3.3:

1. Taking the depth image with a Microsoft Kinect camera.
2. Depth image segmentation.
3. Region filtering and merging.
4. Candidate classification.

Properties of the presented algorithm are

- Relatively high speed for a computer vision detection algorithm (30 Hz).
- Relatively low computational effort.
- Detection of partially occluded humans.

However, the algorithm is only used for the detection of humans. No distance or proximity determination is done. This prohibits its use in a general safety measurement system in the context of the requirements of this work. Additionally, more than one camera has to be used if a 360° observation angle around the robot

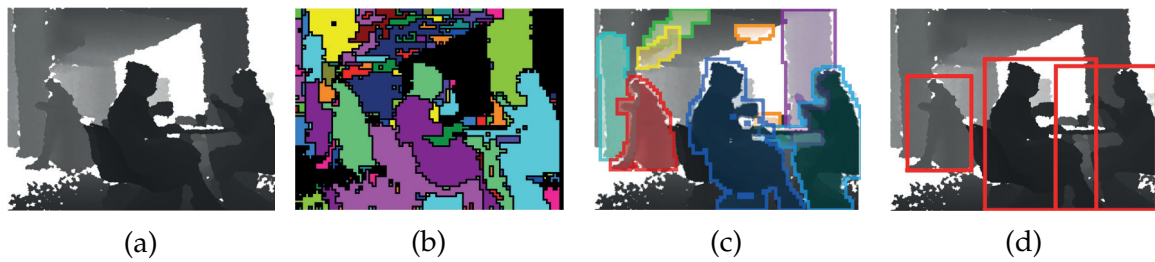


Figure 3.3.: Different stages of the detection process for RGB-D camera-based human detection from [Cho+13]. (a) A picture of the raw depth image from the Microsoft Kinect camera. (b) Different regions after the segmentation process. (c) Possible candidates after the filtering and merging step. (d) Final detected humans indicated by red squares.

is necessary. This would increase the computational effort and reduce the detection rate.

### 3.1.2. Radio frequency identification (RFID)

Radio-frequency identification (RFID) is mostly used in the area of field and service robots (e.g. domestic robots) for positioning purposes (i.e. determination and control) [PKo8; SKo8].

Using such a sensor system for safety applications makes it necessary to attach so-called “tags” to each object of interest. Thus, approaching objects can be identified and their distance can be estimated. Uncertainties in the distance estimation can be improved by sensor fusion with e.g. ultrasonic sensors [Cho+11].

### 3.1.3. Time-of-flight Sensors

Time-of-flight sensors are capable of determining the distance between the sensor surface and an object in front of the sensor surface. For most sensors there has to be a line of sight between these two points [FKo8]. The distance estimation is achieved by measuring the time of e.g. an excited wave with a certain frequency traveling from the sensor to the object of interest and back to the sensor. Thus, the majority of sensors are only capable of determining distances. In [KKo8] sonar systems are described that are also able to do simple target classification. The targeted object surfaces can be classified into planes, cylinders or edges. As far as the author knows there is no time-of-flight measurement system capable of doing object classification in terms of this thesis (e.g. distinguishing between a human and a metallic work tool). Nevertheless, these systems are often used in a fusion approach to improve overall sensor accuracy [DHo8]. Other drawbacks of these

sensors include a limited observation angle resulting in blind spots and the need for a high number of sensors. Additionally, these sensors are usually too big to be mounted on e.g. robot arms or fingers (or other applications limited with respect to spatial dimensions).

Below, the most prominent time-of-flight sensors are listed:

- Ultrasound (US) and sonar.
- Light detection and ranging (Lidar).
- Flash Ladar (laser radar or laser detection and ranging).
- Radar
- Laser

2D and 3D laser range sensors are mainly used for localisation, map building and simultaneous localization and mapping (SLAM) [DEo8]. When not used on the robot but fixed around a region of interest, it has been shown in [Sat+13], that they can also be used to identify people and robots.

#### 3.1.4. Seashell Effect

In [JS12b], a so-called “seashell effect” is introduced for pretouch sensing. It uses the resonant frequency of a cavity, which changes as an object approaches it. This resonant frequency is measured with a microphone, and thus, a distance from an approaching object can be estimated (up to 6 mm). The authors were able to mount the cavity and the microphone into the fingertips of a robotic hand and thus, improve certain grasping tasks.

#### 3.1.5. Magnetic Sensing

Magnetic sensors are useful in pretouch applications to sense conductive objects. In [Sch+13b]’ it was shown that with only two Giant magnetoresistance (GMR) sensors and a static magnetic field, a pretouch sensing system for ferromagnetic objects is feasible. The developed algorithm, comprised of a Gaussian regression and a maximum likelihood estimator, allows an online reconstruction of the position of a ferromagnetic object in the region of interest. Experimental investigations demonstrate the feasibility of this approach. It permits a maximum detection range of 30 mm [Sch+13b]’. Fig. 3.5 shows the measurement setup and the result for one position of an iron bar in the region of interest ( $\Omega_{ROI}$ ).

[Ren+10] presents a measurement system that uses GMR sensors to measure eddy current effects. The system is able to detect hidden conductive objects inside a tube

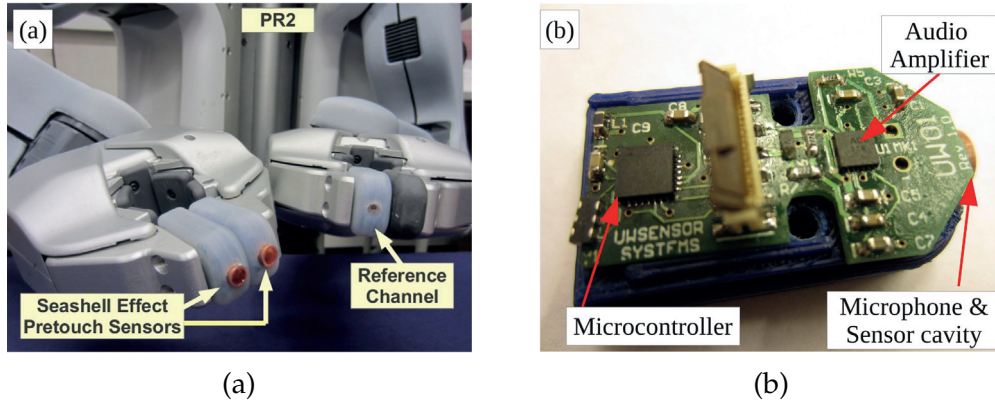


Figure 3.4.: Measurement system using the seashell effect from [JS13]. (a) Fingertips comprising the integrated seashell effect sensor. A microphone is attached to an acoustic cavity to attenuate the ambient sound. The reference channel is used to suppress noise from the ambient sound. The printed circuit board comprises the necessary electronic parts and fits into the fingertip of a Willow Garage PR2 robot.

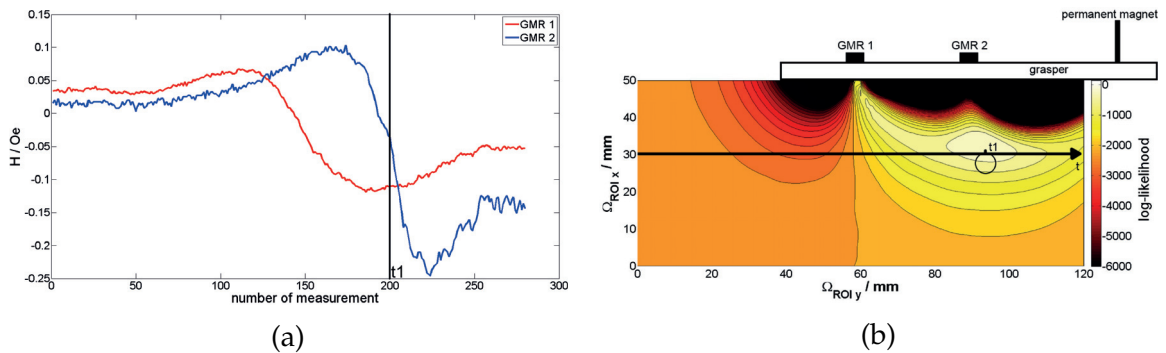


Figure 3.5.: Measurements using a static magnetic field and two GMR sensors to reconstruct the position of an iron bar in  $\Omega_{ROI}$  from [Sch+13b]'. A picture of the measurement setup is shown in Fig. 3.11(a). (a) Measurement readouts from the two GMR sensors. The iron bar was moved in  $\Omega_{ROI}$  from left to right at a distance of 30 mm. (b) Snapshot of the real-time reconstruction of  $\Omega_{ROI}$  while the iron bar was moved along the y-axis at time  $t_1$  (according to (a)). The black circle depicts the true position of the bar and the colorbar depicts the value of the log likelihood.

with a diameter of max. 60 mm. Thus, it appears possible to also use such a system for collision avoidance in open environment sensing applications.

### 3.1.6. Tactile Sensing

Tactile sensors are not able to perform collision avoidance since these sensors only become “active” once a collision has already occurred. However, tactile sensors can be used for impact force reduction and collision detection, whereby the latter can also be used for future force-reduction behaviours [Pha+11]. There exist a huge variety of tactile sensors. The following list is not intended to be exhaustive but to give a brief overview of possible measurement principles that could be used [CHPo8]:

- Optical sensors [Kam+04],
- Piezoresistive sensors [Shi+04],
- Piezoelectric (stress rate) sensors [HC93],
- Skin acceleration sensors [HC89],
- Capacitive sensors [Pha+11],
- Whiskers and antenna sensors [RB+11].

Whiskers or antenna sensors are used by every mammal except for humans. It is possible to rapidly acquire information about objects in the vicinity of the root of the whiskers. Collisions of the body and approaching objects can be avoided as the first contact point is moved from the body surface to the whiskers [Sch+13a]. Thus, whiskers and antenna sensors can also be seen as proximity or pretouch sensors [RB+11].

### 3.1.7. Proprioceptive Sensing

Proprioceptive sensors measure the internal state of a robot. This might include

- position and/or velocity of different joints,
- temperature of different parts,
- voltage,
- motor current,
- forces and torques.

The motor current, force and torque sensors can be used to detect and reduce impact effects in the case of collisions with machinery made up of these sensors. This is especially necessary if no other sensor can be mounted on the machinery or robot and a physical human-robot interaction is unavoidable. For further details



on these proprioceptive sensors the interested reader is referred to [BPCo8; Shi+11; Had+12] and the references therein.

### 3.1.8. Comparison of State-of-the-Art Sensor Technology

table 3.2 gives an overview of the presented measurement systems as they are used for safety applications. The benefits and drawback of the different measurement principles are highlighted (“+” for positive, “-” for negative, and “o” for neutral). As can be seen, only vision sensors have a good sensing range compared with a feasible object classification. These properties are only valid for the externally-mounted vision sensors (i.e. not mounted on the robot). However, vision systems mounted on external positions do suffer for example from possible inclusions due to not having a line of sight. RFID sensors also perform quite well, but as mentioned above, every object has to have an RFID tag in order to be detectable. If no RFID tag is mounted on an approaching object, the object would not be recognized. Sensors based on whiskers also appear to be an interesting approach. As shown in [Sch+13a], these sensors have a lot of similarities to electric field sensors and can be an interesting alternative for pretouch sensing. However, according to [CFm14]: “A whiskered robot would use tactile information in place of cameras to picture out its surroundings but this type of whisker can be a long way off.”

All other sensors have a smaller sensing range and most of them do not provide the opportunity for object classification. Thus, none of the presented measurement systems seems to provide a perfect solution for safety devices under the requirements mentioned in section 1.2. In the second part of this chapter, capacitance measurement systems are investigated for their properties and performance in terms of proximity sensing and object classification.

## 3.2. Safety Through Capacitive Sensing

This section aims to give an overview of existing capacitance measurement systems which are used for open environment (safety) applications according to the definition introduced in section 1.2: “To measure objects where they are not allowed to be”. Several examples show the wide field of application where capacitive sensing can be used. They also describe the benefits and drawbacks of each application and the applied measurement hardware (e.g. in the given applications each piece of measurement hardware is made for its unique application). The differences between the approach presented in this thesis (see section 4.5) and the approaches in the presented applications below will be explained.

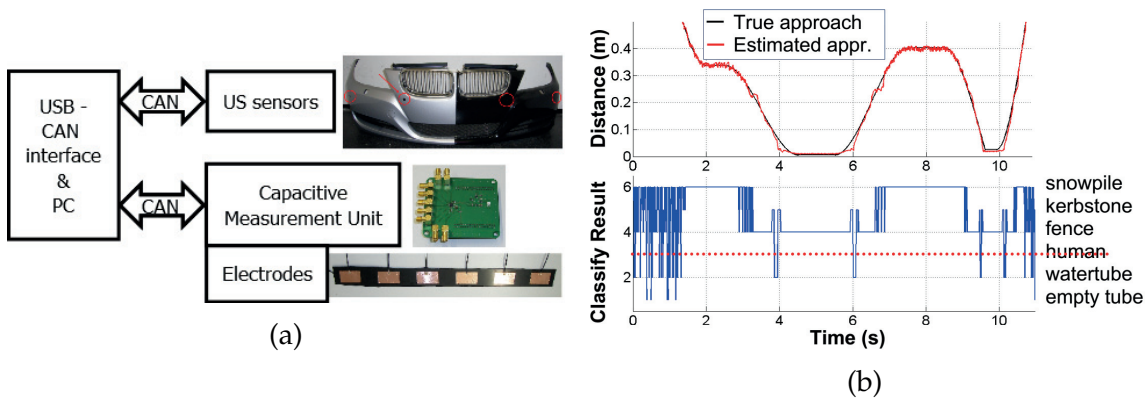


Figure 3.6.: Sensor fusion system comprising capacitance and US measurements on a car bumper. (a) Measurement setup for a sensor fusion system in automotive applications. It comprises US and capacitive sensors for proximity sensing and classification. (b) Distance estimation of an approaching and leaving human and selected object class based on a Kalman filter with an ML criterion [Sch+11]<sup>1</sup>. The object class human was deleted from the stored measurements to simulate real-world situations and demonstrate the robustness of the algorithm that was used.

### 3.2.1. Car Bumper<sup>1</sup>

In [Sch+10; Sch+11]<sup>1</sup>, a sensor fusion concept is presented that incorporates capacitance and ultrasonic (US) measurements for proximity determination in automotive applications (see Fig. 3.6(a)). Although ultrasonic sensors are a well-accepted technology for distance sensing applications, they reveal drawbacks in the closest vicinity of a vehicle (e.g. blind spots due to limited observation angle). Capacitive sensors used in this application are suited to proximity measurements of up to 0.3 m and also provide information about the approaching object itself. Thus, it can be used as a safety feature in terms of object classification. The measurement range of this fusion concept reaches up to 2 m whereby blind spots are avoided. The feasibility of this approach and its robustness against environmental influences is demonstrated by means of experimental investigations in [Sch+10; Sch+11]<sup>1</sup>.

The capacitance measurement system uses a commercially available capacitance-to-digital converter integrated in the Analog Devices IC AD7143 [Ana14]. Measurement results are shown in Fig. 3.6(b). It shows the sensor fusion systems estimated approaching line of a human (capacitance measurement system in combination with an US system). Several other approaching objects were measured and their capacitance measurement traces were stored. To simulate real-world conditions the capacitance measurement trace of the approaching human was deleted from the stored ones for the presented case. As can be seen in Fig. 3.6(b) the estimated

<sup>1</sup>Parts of this section have been published in [Sch+11]<sup>1</sup>



approaching line nearly matches the true approaching line. The algorithm, which is based on a Kalman filter with a maximum likelihood (ML) criterion, estimates the objects that are most similar to a one of the human (in the presented case the object was a fence). Thus, the proximity sensor works as desired and also features a classification scheme that can be used to differentiate between approaching object classes. This classification scheme enables the system for further safety features.

### 3.2.2. Icing

Another kind of application is shown in Fig. 3.7. A capacitive ice sensor working with a capacitive energy harvesting system is used for monitoring overhead power lines ([Mos+09; Mos+10; Mos+11]). Although the sensor is especially used to detect the beginning of icing, it represents a safety device according to our definition because it detects an object (i.e. ice) in a region where it should not be (e.g. overhead power line). Other sensor systems for icing (e.g. presented in [Di +04; BLBo8]) are wired and thus, limited to, e.g., transformer stations [Mos+11]).

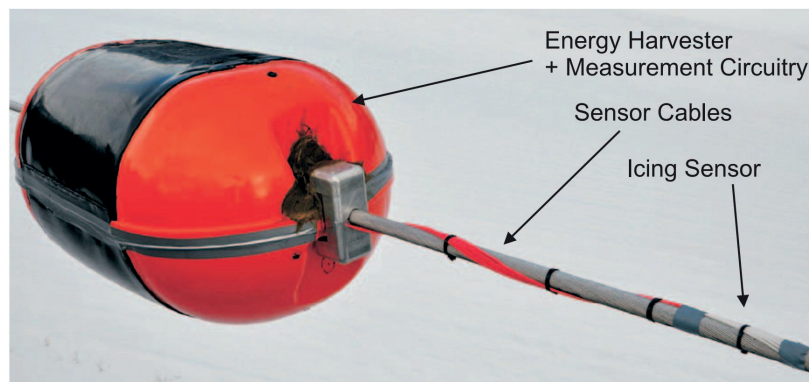


Figure 3.7.: Photo of a capacitive ice sensor mounted on an overhead power line [Mos+10]. The energy harvester shell also comprises the measurement circuitry. The sensing electrodes are directly mounted on the power line.

The ice detection system presented in [Mos+10] uses an integrated capacitance-to-digital converter operating at a nominal frequency of 240 kHz. The measurement system works in the mutual capacitance mode with one transmitter and two receiver electrodes. It was shown that the occurrence of icing on an overhead power line can be detected in laboratory measurements (e.g. a climate room) as well as in a field test. There, the sensor system was mounted on a power line at a hilltop location in Austria. In both cases early icing could be detected and distinguished from melting. This is especially important for the de-icing process. The safety system comprises a

capacitance measurement system for object detection (i.e., ice detection) and object classification (i.e., distinguishing between ice and water).

### 3.2.3. Protection of Power Line Contacts

[ZPN<sub>10</sub>] presents a protection system for construction workers to prevent electrocution. The worker has to wear the proposed capacitance sensor and the system sounds an alarm if a live power-circuit is approached. Since contact with overhead power lines was the most frequently occurring event in the construction industry in the United States from 2003 to 2006 ([Jano8]), such types of safety sensor systems are of particular interest.

The protection system for construction workers uses capacitance measurement hardware comprising a variable high-gain preamplifier, a narrow 60 Hz bandpass filter, a fixed gain post amplifier, an ADC and a communication unit for the connection with a host computer [ZPN<sub>10</sub>] (see Fig. 3.8). The measurement results presented in [ZPN<sub>10</sub>] show that approaching a power line at both 120 V and 9000 V can be detected starting at a distance of approximately 1 m. Thus, for the safety of construction workers, a proximity sensor for an energized power circuit was realized. Every human or object which needs to be protected must wear the proposed sensor system.

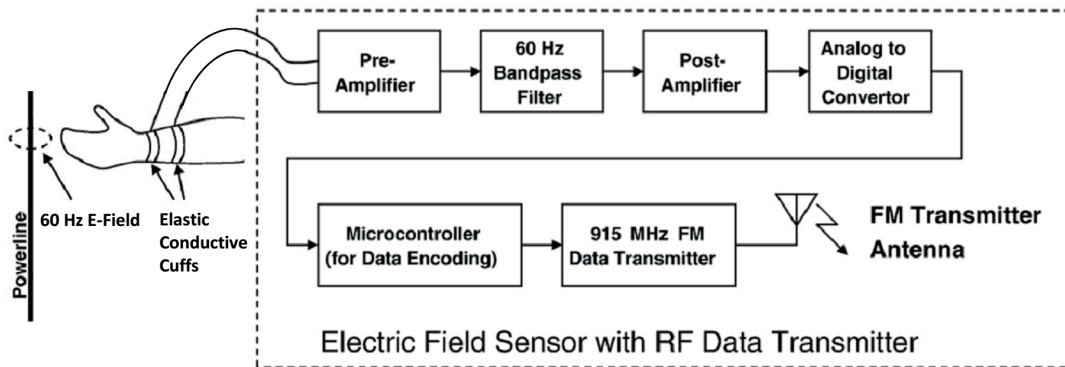


Figure 3.8.: Block diagram of the power line contact protections system [ZPN<sub>10</sub>]. A FM transmitter is used to send the measurement data to a receiver for the purposes of indication signalling and further decoding and analysing.

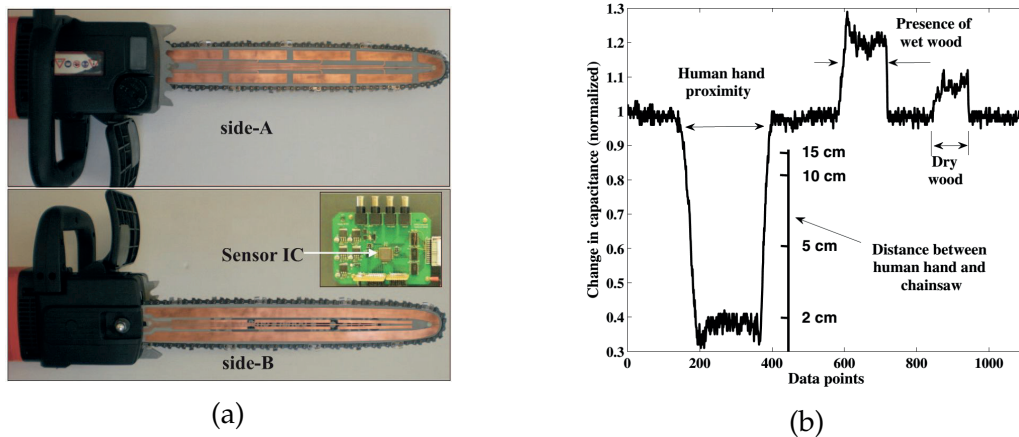


Figure 3.9.: Capacitive safety system on a chainsaw [GZBo8]. (a) Picture of both sides of the chainsaw sword and the measurement circuitry. (b) Measurement results for different approaching objects.

### 3.2.4. Chainsaw

In [NSo7] a capacitive sensor system is presented that switches off a machine (e.g. a chainsaw) if an object (e.g. human hand) comes too close. A conductive material has to be integrated into the object of interest (e.g. a garment with a built-in wire cloth). This conductive material is connected to a radio frequency generator. The generator is a 80 kHz Wien bridge oscillator and the receiver detection unit, mounted on the chainsaw, has to measure this signal level. The 80 kHz signal level directly depends on the distance between the object and the chainsaw. It was shown in [NSo7] that a rectified mean value detector is able to measure the signal value through the capacitive connection between the transmitter and the receiver. Thus, a proximity switch is realized. It switches off the chainsaw at a distance of about 100 mm (equals a threshold of 300 mV which is early enough considering a maximum blade speed of 2 m/s and a whole-system response time of 10 ms).

[GZBo8] showed that it is possible to detect humans and animals with a capacitance measurement system mounted on the chainsaw without the counterpart on the object of interest (i.e. no generator is necessary, see Fig. 3.9). Thus, the safety feature is not only limited to one object. As can be seen in Fig. 3.9(b) different approaching objects (human hand and wood) can be distinguished by the proposed measurement system in [GZBo8].

### 3.2.5. Object Ranging and Material Type Identification

In addition to proximity sensing, [Kir+08] also performed material type identification. It is proposed that a material type identification can be made by obtaining measurements for one object at several different frequencies and obtaining information about the conductivity of the unknown objects by analysing the variations of the sensor signals. This kind of classification is necessary for safety applications since certain objects are allowed to be in areas where others are not.

The proximity and classification sensor presented in [Kir+08] uses two electrodes in a mutual capacitance system. The measurement hardware used was presented in [NW91; NF92; FN94]. It uses a sinusoidal signal as transmitter (first electrode) and a charge amplifier as receiver (second electrode). The measurements are done at three frequencies to obtain a material classification. Four types of material were tested: human, concrete, wood and metal. The promising results are shown in table 3.1. The material classification result is used in the proximity determination

Table 3.1.: Material classification results in [%] [Kir+08].

Material tested	Concrete	Metal	Wood	Human
Concrete	<b>100</b>	0	0	0
Painted mild steel	0	<b>99.7</b>	0	0.3
Aluminum	0	<b>99.3</b>	0	0.7
Thick mild steel	0	<b>100</b>	0	0
Wood	0	0	<b>88.3</b>	11.7
Thick wood	0	0	<b>97.3</b>	2.7
Human	0	0	0	<b>100</b>

Bold values highlight the correct classification.

algorithm resulting in a better distance estimation compared to the distance sensing without a classification.

### 3.2.6. Pretouch for Robot Grasping<sup>2</sup>

So-called “pretouch sensors” are especially useful in robotic applications to close the gap between vision and tactile sensors. Pretouch sensors are not only able to benefit manipulation but also add a safety feature if an object classification is

<sup>2</sup>Parts of this section have been published in [Sch+13b]

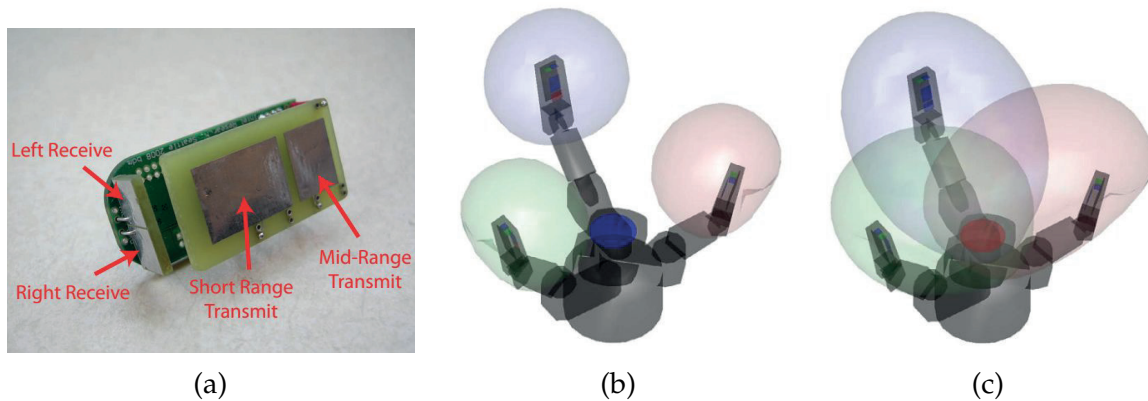


Figure 3.10.: Robotic pretouch sensor mounted on the fingertips of a robot hand from [MLS10]. (a) Sensor hardware presented in [MLS10] which is mounted in the fingertips. (b) Signal surfaces for short-range sensing. (c) Signal surfaces for mid-range sensing.

possible (e.g. a robot grasper is not allowed to grasp if a human hand is in the way). Below, two different approaches are presented:

### Pretouch sensing for object alignment

In [MLS10; JS12a] a capacitive (also called electric field) pretouch sensor is presented, which is designed to be mounted into the fingers of a robot hand (a Barret hand in this case). The sensor shown in Fig. 3.10(a) is used to align the three fingers of the robot hand around the object to be grasped. Thus, when grasping the object all three fingers make contact with it without displacing it.

As shown in Fig. 3.10(a) each fingertip consists of four electrodes (two transmitter and two receiver electrodes) which are used for short range ( $< 2$  cm, Fig. 3.10(b)) and mid range ( $< 5$  cm, Fig. 3.10(c)) sensing, respectively. Another electrode is positioned in the palm and is used as transmitter electrode. Using this palm transmitter and the fingertip receiver, long-range sensing (10 cm to 15 cm) is possible. The robot hand was able to pick up an object it was tuned for. Additionally it was able to grasp for an object which was brought into the vicinity by a human. As soon as the human disengaged the object, the robot hand moved to a certain position with the object. Little information about the measurement circuitry and speed is given in [JS12a]. Although the sensor system showed a promising performances with objects for which it was tuned, it failed with objects that differed in size. However, the experiment with the human interaction showed the possibilities of such a capacitive sensing system for safety applications in robot applications.

Another promising approach is presented in [LCY09]. A capacitance sensor system is shown, which was able to switch between proximity measurement and tactile

measurement. In the paper metallic objects as well as a human hand could be detected.

### **Pretouch sensing using an ECT approach<sup>3</sup>**

Another pretouch application is presented in [Sch+12; Sch+13b]'. It uses a robot grasper attached with capacitive and GMR sensors (shown in Fig. 3.11(a)). Using the capacitance measurement data in an ECT manner (refer to section 4.4) the region of interest (ROI) is reconstructed by means of 2D images of the spatial permittivity distribution (see Fig. 3.11). The measurement results of the GMR sensors are compared to simulation results of a 3D finite element method (FEM). The FEM results were precomputed for several positions of the object of interest. A maximum likelihood estimator (MLE) was used to estimate the position of the ferromagnetic object. The results for one position (i.e., likelihood of the position of the iron bar in the ROI) is shown in Fig. 3.11.

The sensor fusion approach in this application is specific to two types of materials. These are dielectric and ferromagnetic materials, which are commonly found in many industrial environments. Electric and magnetic fields are applied in the ROI and the distortion of these fields caused by objects is measured. Thus, a safety feature can be added: The grasper shown in Fig. 3.11 only grasps at certain objects (e.g. ferromagnetic objects) and does not grasp at e.g. a human hand or dielectric object in the ROI.

Although the reconstruction algorithms for the capacitance measurement part are taken from an ECT application without adaptation to the open environment, the reconstruction shows promising results (shown in Fig. 3.11). Dielectric objects (e.g. PVC bar) and ferromagnetic objects (e.g. iron bar) can be detected by this measurement system. However, because of the parasitic effects of the open environment (explained in section 4.3.2) the iron bar cannot be reconstructed using the capacitance measurement system at certain positions. This system uses the mutual capacitance mode in a Low-Z scheme. With an additional self-capacitance measurement system (i.e., measuring the displacement current originating from the sensing electrodes) it should be possible to overcome the parasitic effects, which originally resulted in blind spots for certain objects.

---

<sup>3</sup>Parts of this section have been published in [Sch+13b]'



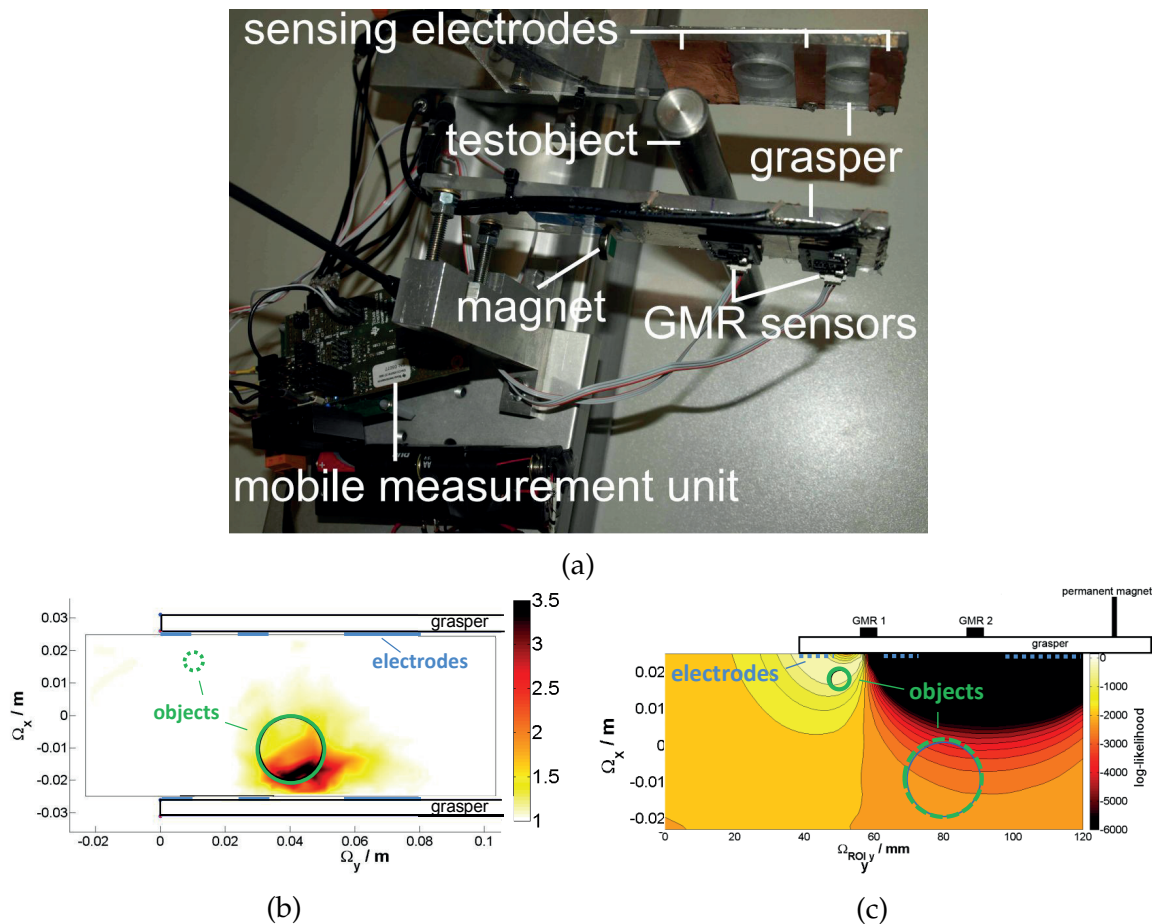


Figure 3.11.: Robot grasper with GMR and capacitive sensing capability. (a) Picture of the test objects. The metallic bar can be detected by the GMR sensors. Dielectric objects can be detected with the capacitance measurements. Reconstruction results of the ECT robot grasper for the two objects (ferromagnetic and dielectric) are shown in (b) and (c). (b) Likelihood for the position of an iron bar. The small green circle indicates the true position of the iron bar and the dashed green circle the true position of a polyvinylchlorid (PVC) bar which is not recognized by the GMR sensors. (c) Reconstruction of the region of interest in an ECT manner. The spatial permittivity distribution is reconstructed. The true position of the PVC bar (indicated by the green circle) matches the reconstruction result. However, the shape cannot be reconstructed.

### 3.3. Comparison of (Safety) Sensor Systems

The last section in this chapter comprises the sensing techniques presented in table 3.2. Although the evaluation of the sensor systems is a subjective value, the table can infer the performance of each system with respect to safety applications. The capacitance measurement systems tend to outperform the measurement systems presented in section 3.1 (except for the outside-in vision sensor). Although most capacitance measurement systems do suffer from a short sensing range, the sensors have benefits when it comes to the size of the sensor's front end, measurement hardware complexity, power consumption, and the sensitivity to different objects.

As explained above, each presented capacitance measurement system was designed and intended to be use with special applications. This prohibits a more general usage and adoption for different applications. Another drawback is the measurement rate. Although the maximum possible measurement rate is high compared to other sensor systems (for example vision sensor), it is still too slow for highly reactive machinery, for example (an example was given in the introduction in section 1.2).



Table 3.2.: Overview and comparison of presented exteroceptive sensors including different capacitance sensor systems. The evaluation is based on the presented applications and the values are subjectively chosen by the author.

Sensor type	References	Sensing range	Classify objects	Sensitivity diff. obj.	Parasitic influence	Size	Hard. compl.	Power cons.	Meas. rate	Costs
Vision oi <sup>a</sup>	[Ryb+12]	+	+	+	○	-	+	-	○	-
Vision io <sup>b</sup>	[Cho+13]	○	○	+	○	-	○	-	-	-
RFID	[PKo8]	-	○	-	+	+	-	+	+	+
Tof	[FKo8]	+	○	○	○	-	+	-	+	○
Seashell	[JS12b]	-	○	○	-	+	-	○	○	+
Magnetic	[Sch+13b]'	-	-	-	○	+	-	+	+	+
Tactile	[Pha+11]	-	-	-	+	○	-	○	+	○
Whiskers	[RB+11]	○	○	○	+	○	○	○	+	○
Propriocep.	[Had+12]	-	-	-	○	+	-	+	+	+
Capacitance measurement systems:										
Car bump.	[Sch+11]'	○	+	+	-	+	+	+	○	+
Icing	[Mos+11]	-	○	-	○	+	+	+	○	-
Powerline	[ZPN10]	+	-	-	+	○	+	○	+	○
Chainsaw	[NSo7; GZBo8]	○	+	+	○	+	-	-	+	-
Obj. Ident.	[Kir+08]	○	+	+	○	○	○	○	○	○
Pretouch 1	[MLS10; JS12a]	○	○	○	○	+	+	+	+	○
Pretouch 2	[Sch+13b]'	○	+	+	○	+	+	+	○	+

<sup>a</sup> oi... outside in

<sup>b</sup> io... inside out

## 4. Capacitive Sensing and the Open Environment

This chapter aims to give the reader an understanding of capacitance measurements and how they are used initially in this work. With this in mind, the chapter starts with an introduction and short history of capacitance measurement, and describes the physics behind this old sensing principle. It will be shown that state-of-the-art capacitive sensing can be split into two parts with different problems and different ambitions. The term “open environment” is explained and arising problems with this measurement environment are presented. An approach taken in attempting to solve the problems that arose is introduced and the methods taken from ECT are presented in addition to ECT itself. As required, a novel measurement system was developed in this thesis and is presented in the last section of this chapter. Illustrative measurement results and comparisons with commercial available systems conclude this chapter.

### 4.1. Capacitive Sensing in a Nutshell

This sections aims to give a short overview of the history of capacitive sensing and introduce the physics behind so-called “electric field sensing”.

#### 4.1.1. The First Capacitive Sensor

Electric field sensing (or capacitive sensing) has been known for a long time. In nature, different kinds of fish are able to generate electric voltages from millivolts (for example, the Mormyridae family) up to approximately 800 V and about 50 A (for example, the Torpedinidae family) [SST08]. The ability to generate electric fields (see Fig. 4.1) facilitates hunting and defense but also localization and communication. Fish that are able to localize and communicate through electric fields also have sensory receptors called Mormyromasts (which can be seen as an electric field or capacitive sensor) [Sm99].

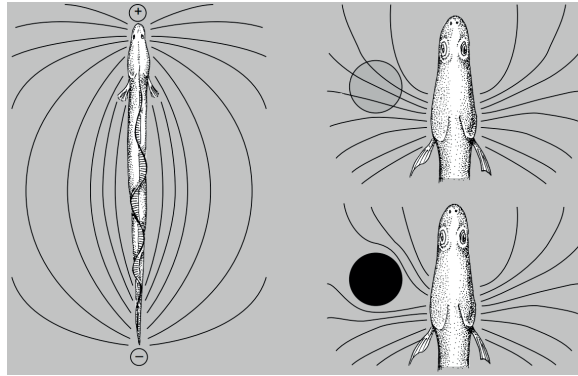


Figure 4.1.: Electric field produced by a Mormyridae to detect objects which are differentiated by their relative permittivity (for example, the black circle) adopted from [Bra97].

At the same time, the Theremin can be seen as the first human implementation of an electric field (or capacitance) proximity sensor. It is an electronic musical instrument controlled without contact between the player and the instrument [Sal10]. It was first presented in the early 1920s.

Although capacitive sensing has been known for such a long time, it was not used in a wide field of applications until the last two decades. Since then, necessary hardware has been made available in integrated circuits (ICs) and capacitive sensing is now used in commercial applications such as touch screens ([SS91; Gou+90]), in mobile phones and many other applications ([Pue93; KLY11; TRL12]).

#### 4.1.2. Physics Behind Capacitive Sensing and Simulation

Capacitive sensing consists of at least two conductors (called electrodes) that are separated by a non-conducting material. The distant ground potential can also be seen as one of these two electrodes. An electric field occurs whenever the two electrodes are on different electrical potentials. Capacitive sensing is well described by the Maxwell equations. Simplification such as ignoring magnetic fields is often possible without relevant loss of accuracy [Bax97]. These systems are also often used as electroquasistatic, which is defined as follows: “The electroquasistatic approximations are justified if time rates of change are slow enough (frequencies are low enough) so that time delays due to the propagation of electromagnetic waves are unimportant.” ([HM13])

This is always the case for the measurement systems presented in this thesis (highest measurement frequency is 1 MHz which equals a wavelength of  $\approx 300$  m

and electrode lengths are always smaller than 0.2 m). Thus, a simplified version of Maxwell's equations can be used [Bax97]:

$$\nabla \times \mathbf{E} = -\frac{\partial}{\partial t}\mu_0\mathbf{H} \approx 0 \quad (4.1a)$$

$$\nabla \times \mathbf{H} = \frac{\partial}{\partial t}\epsilon_0\mathbf{E} + \mathbf{J} \approx 0 \quad (4.1b)$$

$$\nabla \cdot \epsilon_0\mathbf{E} = \rho \quad (4.1c)$$

$$\nabla \cdot \mu_0\mathbf{H} = 0 \quad (4.1d)$$

This means that a given charge density  $\rho$  results in an electric field intensity  $\mathbf{E}$  and the magnetic field intensity  $\mathbf{H}$  is supposed to be 0. The constant  $\mu_0$  denotes the magnetic vacuum permeability and is defined to a value of  $4\pi \times 10^{-7} \text{ N/A}^2$ . With the speed of light  $c$  the electric vacuum permittivity  $\epsilon_0$  is defined as  $\epsilon_0 = 1/\mu_0 c^2 = 8.854\,187\,8 \times 10^{-12} \text{ F/m}$ .

The electric field is the gradient of the voltage:

$$\mathbf{E} = -\nabla V \quad (4.2)$$

If homogenous isotropic medium is used (constant and scalar relative permittivity  $\epsilon_r$ ) and no free charges reside in the ROI ( $\rho = 0$ ), equation (4.2) can be rewritten as Laplace's equation to the well-known form:

$$\nabla \cdot (\epsilon_0\epsilon_r\nabla V) = 0 \quad (4.3)$$

This equation possesses a unique solution when boundary conditions (for example, Dirichlet boundary conditions, which are potentials on electrodes) are known. More details can be found in [HM13; Bax97; Dyeo4] and the literature referenced therein.

Unfortunately, only for simple electrode configurations is an analytic solution of equation (4.3) possible [Bax97]. For the reconstruction of the ROI, the so-called "forward problem" (i.e. equation (4.3)) has to be solved several times as explained later in this section. In this work the FEM is used to solve the equation (4.3) for different electrode geometries and approaching objects. Although the FEM is often used to solve electromagnetic problems, it can generally be used for all boundary-value problems characterized by a partial differential equation and a set of boundary conditions. [Polo6] provides a very good introduction into the FEM for electromagnetics. Below, only the most relevant steps necessary to understand the new concepts for the reconstruction process presented in section 4.3.4 are taken from [Polo6] and explained below. The problem at hand is a real-world 3D problem. However, as will be shown later in this chapter, the aim in this thesis is to reduce this problem to two 2D problems. Thus, the following equations are valid for 2D.

The expansion to 3D is straightforward but solving the integrals will not be as simple as in the 2D space with linear shape functions.

In 2-D space, equation (4.3) can also be written as

$$\frac{\partial}{\partial x}(\varepsilon \frac{\partial V}{\partial x}) + \frac{\partial}{\partial y}(\varepsilon \frac{\partial V}{\partial y}) = 0 \quad (4.4)$$

This is a special case of a generic second-order partial differential equation of the form

$$\frac{\partial}{\partial x}(\alpha_x \frac{\partial u}{\partial x}) + \frac{\partial}{\partial y}(\alpha_y \frac{\partial u}{\partial y}) + \beta u = g \quad (4.5)$$

where  $u = V$ ,  $\alpha_x = \alpha_y = \varepsilon$ ,  $\beta = 0$ , and  $g = 0$ . Two types of boundary conditions can apply. The Dirichlet boundary condition with

$$u = u_0 \text{ on } \Gamma_1 \quad (4.6)$$

and the mixed type with

$$(\alpha_x \frac{\partial u}{\partial x} \hat{a}_x + \alpha_y \frac{\partial u}{\partial y} \hat{a}_y) \cdot \hat{a}_n + \gamma u = q \text{ on } \Gamma_2 \quad (4.7)$$

where  $\hat{a}_n$  denotes the unit vector normal to the boundary  $\Gamma_2$  and  $\gamma$  and  $q$  are constants. The method of weighted residual and the Galerkin approach are used [Sch91] where the left hand side (lhs) of equation (4.5) is subtracted by its right hand side (rhs) for one element with the domain  $\Omega_e$ . Since the numerical solution obtained by the FEM is not exact, this difference is not zero. Thus, this approach aims to minimize the residual in a weighted sense whereby the residual is multiplied by a weight function  $w$ , integrated over the area  $\Omega_e$  and set to zero:

$$\iint_{\Omega_e} w \left[ \frac{\partial}{\partial x}(\alpha_x \frac{\partial u}{\partial x}) + \frac{\partial}{\partial y}(\alpha_y \frac{\partial u}{\partial y}) + \beta u - g \right] dx dy = 0 \quad (4.8)$$

Due to the substitution and rearranging equation (4.8) can be rewritten as:

$$\iint_{\Omega_e} \left( \frac{\partial}{\partial x} \left( w \alpha_x \frac{\partial u}{\partial x} \right) + \frac{\partial}{\partial y} \left( w \alpha_y \frac{\partial u}{\partial y} \right) \right) dx dy - \iint_{\Omega_e} \left[ \alpha_x \frac{\partial w}{\partial x} \frac{\partial u}{\partial x} + \alpha_y \frac{\partial w}{\partial y} \frac{\partial u}{\partial y} \right] dx dy + \iint_{\Omega_e} \beta w u dx dy = \iint_{\Omega_e} w g dx dy \quad (4.9)$$

By using Green's theorem for the first integral of the equation above and substituting it back the differential equation reduces to

$$- \iint_{\Omega_e} \left[ \alpha_x \frac{\partial w}{\partial x} \frac{\partial u}{\partial x} + \alpha_y \frac{\partial w}{\partial y} \frac{\partial u}{\partial y} \right] dx dy + \iint_{\Omega_e} \beta w u dx dy = \iint_{\Omega_e} w g dx dy - \oint_{\Gamma_e} w \left( \alpha_x \frac{\partial u}{\partial x} n_x + \alpha_y \frac{\partial u}{\partial y} n_y \right) dl \quad (4.10)$$

Following the Galerkin approach, the weight functions  $w$  are the same as the shape functions  $N_j$ . The shape functions  $N_j$  are used for interpolation of the unknown quantity  $u$ , which is  $V$  in our case, in the discretized area. With  $u = \sum_{j=1}^n u_j^e N_j$ , where  $n$  is the number of nodes per element, and with rearranging, equation (4.10) becomes:

$$\begin{aligned}
& - \iint_{\Omega_e} \left[ \alpha_x \left( \frac{\partial N_i}{\partial x} \right) \left( \sum_{j=1}^n u_j^e \frac{\partial N_j}{\partial x} \right) + \alpha_y \left( \frac{\partial N_i}{\partial y} \right) \left( \sum_{j=1}^n u_j^e \frac{\partial N_j}{\partial y} \right) \right] dx dy + \\
& \iint_{\Omega_e} \beta N_i \left( \sum_{j=1}^n u_j^e N_j \right) dx dy = \iint_{\Omega_e} N_i g dx dy - \oint_{\Gamma_e} N_i \left( \alpha_x \frac{\partial u}{\partial x} n_x + \alpha_y \frac{\partial u}{\partial y} n_y \right) dl, \\
& \hspace{25em} \text{for } i = 1, 2, \dots, n \quad (4.11)
\end{aligned}$$

This equation can be written in matrix form by:

$$\mathbf{M}u + \mathbf{T}u = f + p \quad (4.12)$$

where

$$M_{ij} = - \iint_{\Omega_e} \left[ \alpha_x \left( \frac{\partial N_i}{\partial x} \right) \left( \frac{\partial N_j}{\partial x} \right) + \alpha_y \left( \frac{\partial N_i}{\partial y} \right) \left( \frac{\partial N_j}{\partial y} \right) \right] dx dy \quad (4.13)$$

$$T_{ij} = \iint_{\Omega_e} \beta N_i N_j dx dy \quad (4.14)$$

$$f_i = \iint_{\Omega_e} N_i g dx dy \quad (4.15)$$

$$p_i = - \oint_{\Gamma_e} N_i \left( \alpha_x \frac{\partial u}{\partial x} n_x + \alpha_y \frac{\partial u}{\partial y} n_y \right) dl \quad (4.16)$$

With the substitution of  $\mathbf{K} = \mathbf{M} + \mathbf{T}$  and  $b = f + p$ , equation (4.12) can be written in the convenient form:

$$\mathbf{K}u = b \quad (4.17)$$

As stated earlier, for a typically electrostatic problem,  $\beta = 0$  and  $g = 0$ . Thus, the matrix  $\mathbf{T}$  and the vector  $f$  vanish. If only Dirichlet boundaries (equation (4.6)) apply, the contour integral in equation (4.16) is also discarded. As will be shown in section 4.3.4,  $\mathbf{T}$  will be used to implement the leakage current into the FEM forward problem.

The evaluation of the entities of  $\mathbf{M}$  depends on the type and order of the shape functions used (i.e. interpolation functions). For linear triangular elements these entities can be derived analytically. Below, only the results are given. The derivation

can be found in [Pol06]. With the notation  $\bar{x}_{ij} = x_i - x_j$  and  $A_e$  denoting the area of a finite element (i.e. triangle) the entities of the symmetric matrix  $M$  result in:

$$M_{11} = - \left[ \alpha_x \frac{\bar{y}_{23}^2}{4A_e} + \alpha_y \frac{\bar{x}_{32}^2}{4A_e} \right] \quad (4.18a)$$

$$M_{22} = - \left[ \alpha_x \frac{\bar{y}_{31}^2}{4A_e} + \alpha_y \frac{\bar{x}_{13}^2}{4A_e} \right] \quad (4.18b)$$

$$M_{33} = - \left[ \alpha_x \frac{\bar{y}_{12}^2}{4A_e} + \alpha_y \frac{\bar{x}_{21}^2}{4A_e} \right] \quad (4.18c)$$

$$M_{12,21} = - \left[ \alpha_x \frac{\bar{y}_{23}\bar{y}_{31}}{4A_e} + \alpha_y \frac{\bar{x}_{32}\bar{x}_{13}}{4A_e} \right] \quad (4.18d)$$

$$M_{13,31} = - \left[ \alpha_x \frac{\bar{y}_{23}\bar{y}_{12}}{4A_e} + \alpha_y \frac{\bar{x}_{32}\bar{x}_{21}}{4A_e} \right] \quad (4.18e)$$

$$M_{23,32} = - \left[ \alpha_x \frac{\bar{y}_{31}\bar{y}_{12}}{4A_e} + \alpha_y \frac{\bar{x}_{13}\bar{x}_{21}}{4A_e} \right] \quad (4.18f)$$

With the entities of  $M$  the equation (4.17) can be solved for an electrostatic problem using triangular elements and linear shape functions (i.e. solving for the unknown vector  $u$  which is the electric potential  $V$  for electrostatic problems). Thus, the forward problem (for example potentials in the region of interest and thus capacitance values) can be solved and used for reconstruction purposes described later in this chapter.

## 4.2. State-of-the-Art Capacitive Sensing

A benefit of capacitive sensing is its functionality with a wide variety of materials. However, it is therefore also sensitive to disturbers like objects of no interest, dirt, moisture, etc. Thus, state-of-the-art capacitance sensors are trained (or calibrated) for only a few specific objects of interest in the environment in which they are used and which is uncertain. However, if the environment is known, defined within certain limits, or its influence can be neglected, it is possible to reconstruct the objects by means of their spatial permittivity distribution (for example in ECT [Zan+07]). Thus, a huge variety of different objects can be measured. Below is an example for each of the two above-mentioned cases (also see section 3.2 for an overview of state-of-the-art safety capacitive sensing systems).

### 4.2.1. Well-known Objects<sup>1</sup>

If the variety of arising object types is known, experimental investigations showed the ability to estimate the distance of an approaching object to the sensor surface. Due to the prior knowledge of approaching object types, the environment in which the sensor is used may vary in certain limits (see section 3.2).

Fig. 4.2(b) shows capacitance measurement results (in mutual capacitance mode) for different object types and two receiving electrodes  $R1$  and  $R2$  (i.e. two measurements per approaching object type). The complete measurement setup is described in section 3.2.1. It is apparent that no distance estimation is possible with only one electrode due to ambiguity. The reason for this ambiguity is known as coupling and shielding and is described in section 4.3.3. With two receiving electrodes and a limited number of different objects a distance value can be matched with a pair of capacitance measurements. Fig. 4.2(a) shows different object types approaching and leaving the same sensor surface plotted over time. If the approaching object type is known, the distance can be estimated with the prior information of the initial measurements in Fig. 4.2(b).

If different object types are approaching (as shown in Fig. 4.2(a)) an object type classification has to be made before a distance from the sensor surface can be estimated. In [Sch+11] a Bayes risk decision in combination with a maximum-likelihood detector was used for object classification and distance estimation.

It was shown that distance estimation and even object classification are possible with capacitive sensing under certain circumstances. The presented approach can only be successful if:

- A limited number of different object types are approaching.
- Object types do not change properties. This would lead to different capacitance measurements for one and the same object type (for example small and big objects from the same type would lead to different measurements and wrong classification).
- External environmental influences are limited (for example moisture on the sensor surface would lead to a virtually increased sensor surface as shown in [Sch10]).

---

<sup>1</sup>Parts of this section have been published in [Sch+11]



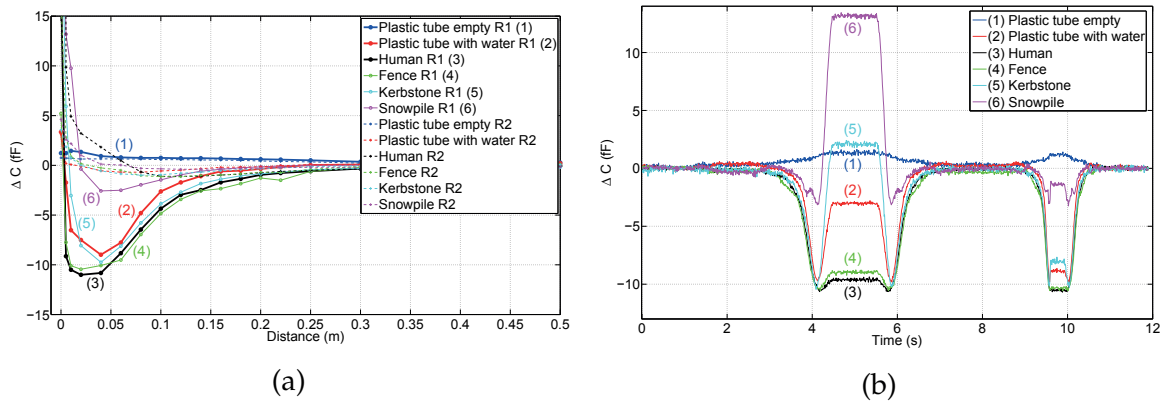


Figure 4.2.: Capacitance measurement results for different objects with two scenarios in mutual capacitance mode (from [Sch+11]). See section 3.2.1 for the whole measurement setup. (a) Change of capacitance for different objects approaching the sensor surface and two receiving electrodes (R1 and R2, plotted over the distance). It can be seen that coupling only occurs for with receiving electrode R1. (b) Change of capacitance for the receiving electrode R1 plotted over time and two approaches to the sensor surface (final distance to sensor surface 10 mm and 30 mm).

#### 4.2.2. Well-Known Environment

A related technology is ECT. One of its uses is in industrial processes to obtain 2D cross-sectional images of the material (i.e. permittivity) distribution within pipes [NSW12]. ECT is essentially an array of capacitive sensors with heavy signal processing to calculate an image of the region of interest ([Neu+11; WF09; YP03]). The calculation has to deal with a nonlinear and ill-posed inverse problem [SL05] with a higher number of unknowns (i.e. number of pixels) than independent measurements (i.e. number of capacitance measurements). Thus, the reconstruction method typically needs some kind of regularization or prior knowledge (e.g. Tikhonov regularization, total variation). The calculation or reconstruction methods for online reconstruction can typically be divided into two types [Isa96]: Non-iterative algorithms (for example Offline Iteration/Online Reconstruction [Liu+04], Optimal Approximation [Zan+07] and Singular Value Decomposition) as well as iterative algorithms (for example Gauss-Newton methods [BHW03] also in combination with statistical methods like Particle Filter [WSB07] or Kalman Filter [TGA04; M V+07]). Other approaches presented in [NBB95] and [Zan+06] use neural networks for solving this inverse problem. An example of an ECT system is given in the following section.

Fig. 4.3(a) shows a schematic of an ECT system. Different measurement modes exist that differ in the measurement circuitry used. Detailed information about the different measurement modes and their benefits can be found in [Weg+05]. In

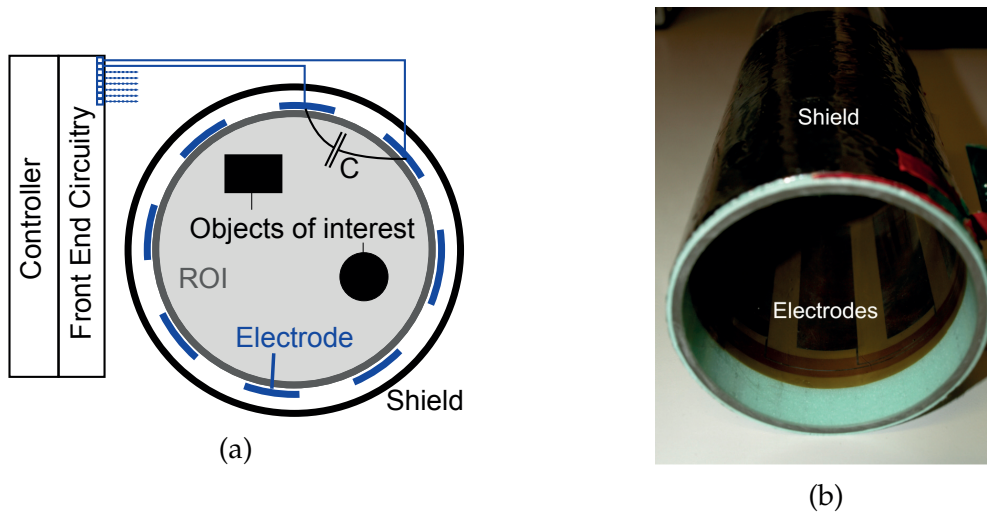


Figure 4.3.: Schematic of a state-of-the-art ECT system to reconstruct the inside of a pipe (ROI). (a) Sketch of an ECT system comprising the measurement hardware (controller and front end circuitry) and the sensor (electrodes) mounted on a pipe. Capacitance  $C$  exemplarily indicates exemplarily the measurand between two electrodes. (b) Picture of a prototype ECT sensor mounted on a pipe made of acrylic glass.

Fig. 4.3(a),  $C$  exemplarily depicts the measured capacitance between two electrodes. A picture of a pipe with a prototype ECT sensor is shown in Fig. 4.3(b). The electrodes mounted on a nonconductive pipe (acrylic glass in Fig. 4.3(b)) are covered by a conductive shield. This permits the sensor to be sensitive only inside the pipe which is the region of interest (ROI). The final goal of ECT is to generate an image of the spatial permittivity distribution. This goal is achieved by measuring the capacitances between the electrodes and signal processing as explained above.

Because of the enclosed structure of an ECT system, the environment does not change and the sensor is barely influenced by external disturbers (for example by moisture or electrostatic discharge). Additionally some other simplifications can be applied:

- No interaction between electric and magnetic field.
- No charges inside the pipe.
- Length of sensing electrodes compared to objects of interest lengths can be neglected.

These properties (and of course the heavy signal processing) permit a reconstruction of the spatial permittivity of the inside of the pipe (i.e. generating a 2D cross-sectional image of the inside).

Fig. 4.4 shows the picture of a prototype ECT system used at the Institute of Electrical Measurement and Measurement Signal Processing at the Graz University

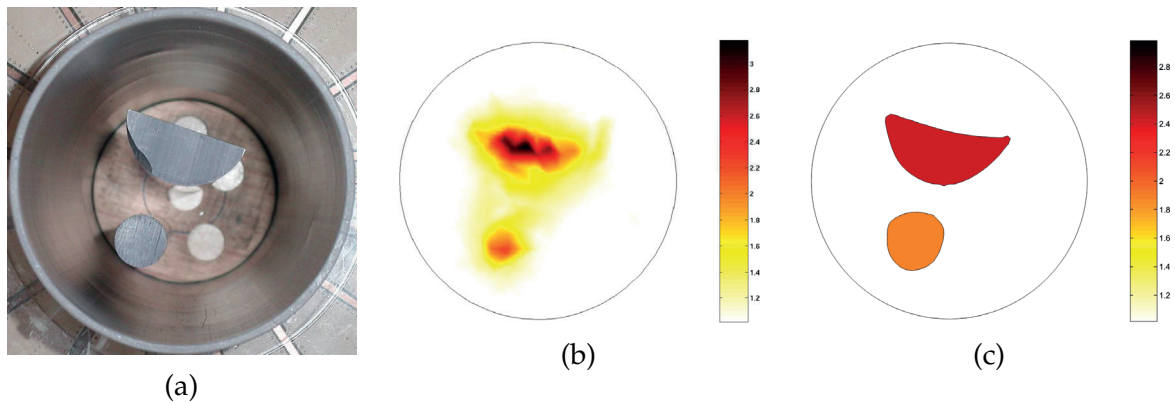


Figure 4.4.: ECT example and reconstruction results from [Koro6]. (a) ECT measurement setup with two PVC objects in ROI. (b) Reconstruction results with a FEM based algorithm. (c) Reconstruction results with a BEM based algorithm.

of Technology and two images obtained from the same measurement signals but different signal processing afterwards from [Koro6]. The intention in this case is not to compare the two algorithms based on a FEM and a boundary element method (BEM) as shown in Fig. 4.4(b) and Fig. 4.4(c), respectively. Rather, to show the capability of such an ECT system and the huge influence on the chosen reconstruction algorithm.

Compared to state-of-the-art “reconstruction results” in open environment sensing in section 4.2.1, ECT results contain much more information while needing less prior information about the objects of interest. Thus, the best possible outcomes for an improved capacitive open-environment sensing system are reconstruction results similar to ECT.

### 4.3. Capacitive Sensing in the Open Environment

When using a capacitance measurement system for a broad field of applications in the open environment, neither can the environment be defined nor can potential approaching objects be preassigned. Thus, certain issues have to be taken into account before using capacitive sensing in an uncertain environment. Below, a short introduction into an approach to open environment sensing is given, followed by a description of the effects that occur when using it. These effects described below do not occur solely in open environment sensing, but most of the time occur all at once. Additionally, the influences can change from one sensing situation to another.

### 4.3.1. Not Well-known Environment and Objects

Another formulation for “not well-known” can be “undefined”. If an entire environment is undefined, the presented measurement systems described in section 3.2 will not work as reliably as presented. One could envision a measurement task as described in section 3.2.1 (car bumper) but without any prior information about the approaching objects. The object classification algorithm will eventually fail because it is difficult if not nearly impossible to train the system for every object in every situation. Furthermore, a reliable distance estimation will not work due to the different capacitance measurement results for each object (see Fig. 3.6).

To overcome the drawbacks of capacitive sensing in the open environment, a different approach is presented in this thesis. In order to obtain a combination of the two approaches presented in sections 4.2.1 and 4.2.2, additional information from the capacitance measurement has to be used. This could include the “leakage information” for example (presented later in this section). The overall goal is to classify objects according to some of their electrical properties. The connection of the objects to the ground can be one of these classification properties, as is, obviously, the relative permittivity (similar to ECT). The aim is to use the additional information to reconstruct a 2D picture of the environment above the sensor surface similar to an ECT image (see Fig. 4.26). Consequently, unknown objects will be classified according to the defined electrical properties. Additionally, a distance estimation that is neither constrained by the approaching objects nor by the environment itself is not possible.

### 4.3.2. Parasitic Effects<sup>2</sup>

In order to assess the advantages and disadvantages of possible circuitry for capacitive sensing a model of the sensor front-end is necessary. Fig. 4.5 shows a model of an extension to the equivalent circuit used in [Zano05; Bra+05]. It additionally considers an approaching object (if measuring in the open environment) and electromagnetic compatibility (EMC). The three main parasitic effects shown in Fig. 4.5 are:

- Parasitic connection to ground through the equivalent parallel circuits ( $R_{GND}$ ,  $L_{GND}$ ,  $C_{GND}$ ,  $R_{1,GND}$ ,  $L_{1,GND}$ ,  $C_{1,GND}$  and  $R_{2,GND}$ ,  $L_{2,GND}$ ,  $C_{2,GND}$ ) connected to the sensing electrodes 1 and 2 and the approaching object. Thus, only a part of the displacement current (indicated by red arrows) originating from electrode 1 is entering electrode 2 and is measured in the mutual capacitance mode (see section 4.5.1).

<sup>2</sup>Parts of this section have been published in [SZ14]

- Capacitive crosstalk from disturbers and electrostatic discharge (ESD) to the sensing electrodes indicated by  $U_{D1}$  and  $U_{D2}$ . This is especially a problem in open environment measurements and its influence can be reduced by e.g. methods shown in [Bra03].
- Resistive path  $R_{1,2}$  parallel to the capacitance of interest  $C_{TR}$ .

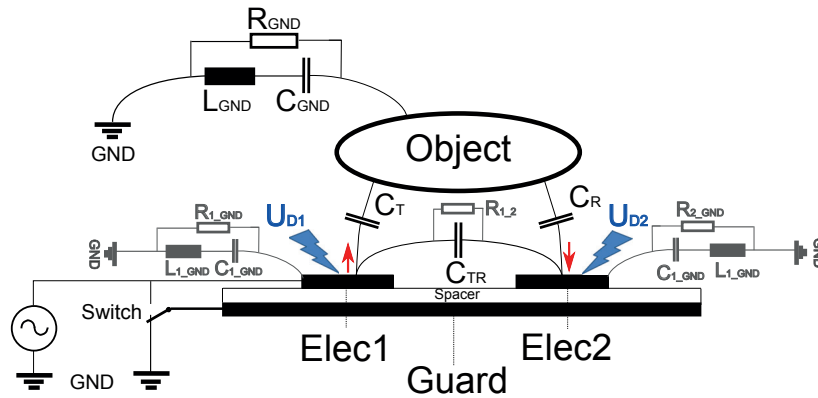


Figure 4.5.: Sketch of a two-electrode capacitive sensor front end including several parasitic effects. Red arrows indicate the displacement current originating from electrode 1 (Elec1) and entering electrode 2 (Elec2).  $U_{D1}$  and  $U_{D2}$  denote capacitive crosstalk from disturbers in the vicinity and ESD to Elec1 and Elec2. The main parasitic effects to ground are shown by the equivalent parallel circuits connected to the electrodes and the object. Depending on the measurement mode (refer to section 4.5.1) the guard electrode can be set ground or the excitation signal (i.e., active guarding).

The measurement circuitry has to deal with these parasitic effects [ZN10]. Table 4.3 gives an overview of how these parasitic effects influence the different measurement circuitries.

### 4.3.3. Shielding and Coupling<sup>3</sup>

There are two other effects that can be observed with capacitive sensing (in mutual capacitance mode), which are the so-called “coupling” and “shielding” effects [Zano5]. These effects occur only in the mutual capacitance mode, which is described later in section 4.5.1. Thus, when writing about shielding and coupling effects, one implicitly acts on the assumption that the mutual capacitance mode is used. Shielding and coupling occur for certain objects and depend on the properties of these approaching objects. Among others, the capacitive connection of the objects to the distance ground is an important property.

<sup>3</sup>Parts of this section have been published in [Sch+11]

As shown in Fig. 4.5 and simplified in Fig 4.6(a) it mostly depends on the capacitances  $C_{GND}$ ,  $C_T$ ,  $C_{TR}$  and  $C_R$ . If a capacitive sensor system is measuring in mutual capacitance mode (see section 4.5.1) and an object approaches, the displacement current (indicated by red arrows in Fig. 4.5) originating from electrode 1 flows to electrode 2 and to the distance ground  $GND$ . The relation of current flowing to electrode 2 and to  $GND$  depends on the relation between  $C_{GND}$  (which stays nearly constant for an approaching object) and the capacitance of the parallel circuit of  $C_T$ ,  $C_{TR}$  and  $C_R$  (which increases for an approaching object). A bigger portion of the displacement current flows from electrode 1 through  $C_T$  and  $C_{GND}$  to the distance ground for an object further away (since the capacitance of the parallel circuit  $C_{GND}$ ,  $C_T$ ,  $C_{TR}$  is rather small). Thus, the measured capacitance decreases with an approaching object for further distances. This is called shielding mode.

At a certain distance to the sensor surface, the capacitance of the parallel circuit  $C_{GND}$ ,  $C_T$ ,  $C_{TR}$  has a higher influence than  $C_T$  and  $C_{GND}$  and more displacement current flows from electrode 1 to electrode 2 than to the distance ground. The measured capacitance increases for an approaching object for very close distances. This is called coupling mode.

Fig. 4.6(b) and Fig. 4.6(c) show a sketch of the shielding and coupling effect, respectively. For purposes of representation, they are highly simplified and only serve to visualize an initial understanding of both effects and their impacts on the measurement results. Because both effects strongly depend on the approaching object, they can also be used for classification of the approaching object as shown in [SZ11]'. Both effects can be observed in the measurements presented in section 4.5.2.



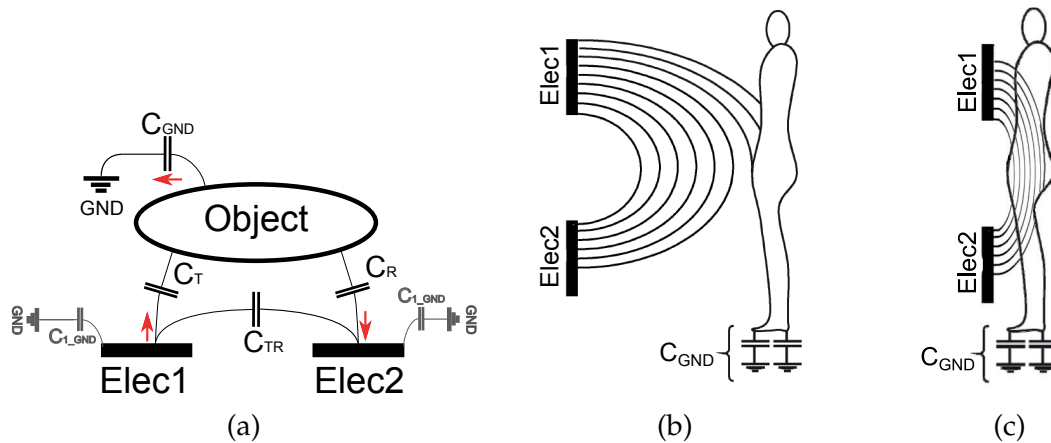


Figure 4.6.: Sketch of the shielding and coupling effect (simplified). (a) Sketch of the capacitive connections for a sensor with two electrodes (Elec1 and Elec2 act as the transmitter and receiver electrodes, respectively) and an approaching object (simplified from Fig. 4.5). (b) Pictorial representation of the shielding effect showing electric field lines between the transmitter and receiver electrodes (adopted from [Geo+09]). Parts of the electric field are shielded by an object at a certain distance from the sensing electrodes and also connected to ground (indicated with the lumped capacitance  $C_{GND}$ ). (c) Pictorial representation of the coupling effect for an object very close to the sensor surface. Electric field lines between the transmitter and ground are not shown for clarity.

#### 4.3.4. Leakage

When measuring in mutual capacitance mode, the leakage displacement current  $i_L$  can be defined as the current originating from the transmitter electrode but not entering the receiver electrode. Instead, it returns through other grounded surfaces or the distance ground. The sketch in Fig. 4.7 illustrates this effect, whereby the leakage current is a 3D effect which does not appear in a 2D simulation.

The presented shielding effect described in section 4.3.3 can be seen as a part of this leakage in 2D. However, leakage (as defined in this thesis) includes displacement currents originating from the transmitter electrodes and entering the distance ground (and not the receiving electrode) without any object in the vicinity of the sensor surface.

#### Proposed Method

A method is proposed which enables the 3D leakage effect to be simulated in a 2D simulation. This is necessary for later reconstruction techniques taken from ECT and presented in section 4.4.2. The difference between a 3D simulation (i.e. real world setup) and the simplified 2D simulation is shown in Fig. 4.8. It shows

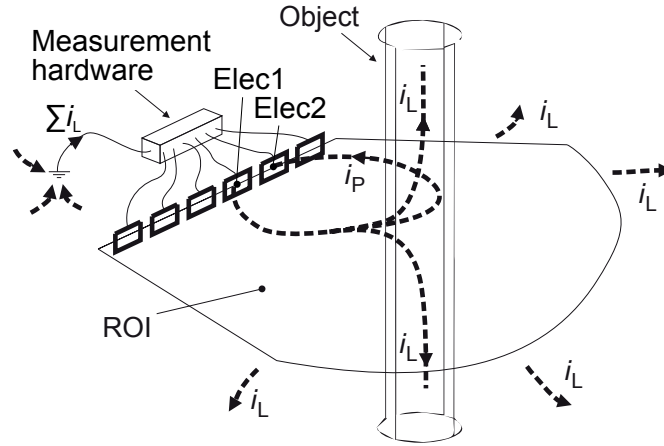


Figure 4.7.: A pictorial description of the leakage effect adopted from [Zan09]. In contrast to the coupling displacement current  $i_P$ , the leakage displacement current does not return to the receiving electrode (Elec2) but through other grounded surfaces. The leakage current has a higher influence than the coupling current on certain objects and situations. Thus, it is reasonable to attempt to measure the leakage current for object localization and classification.

the profile of both simulations (i.e. 3D and 2D). A 2D simulation reduces the 3D problem to 2D space by assuming that the 3D geometry does not change in one axis (e.g., no change in  $z$  axis: geometry indefinitely long). A setup as shown in Fig. 4.7 has different lengths in  $z$  direction for objects and electrodes. Thus, the displacement current shown in Fig. 4.7 cannot be simulated in an ordinary 2D simulation because it does not exist.

To simulate the effects of this leakage displacement current, a space charge is placed into  $\Omega_{ROI}$  of the electro static 2D simulation. A cutout of Fig. 4.8(b) (indicated by the dashed green line) is shown in Fig. 4.8(c).

Gauss' law states that the total flow of charge due to the displacement current through a surface is found by integrating  $D$  over that surface:

$$\Psi_{\Omega} = \int_{\Omega} D d\Omega \quad \text{in } C \quad (4.19)$$

with  $\Omega$  an elementary area,  $D$  the electric flux density normal to  $d\Omega$  and  $\Psi_{\Omega}$  the displacement charge [Bax97]. In other words, the total electric flux through any closed surface is equal to the number of charges enclosed by this surface. For a slice as shown in Fig. 4.8(c) (cutout of Fig. 4.8(b)), one can imagine the total displacement charge as

$$\frac{\int D d\Omega_A + \int D d\Omega_B}{V} = \rho \quad \text{in } C/m^3 \quad (4.20)$$



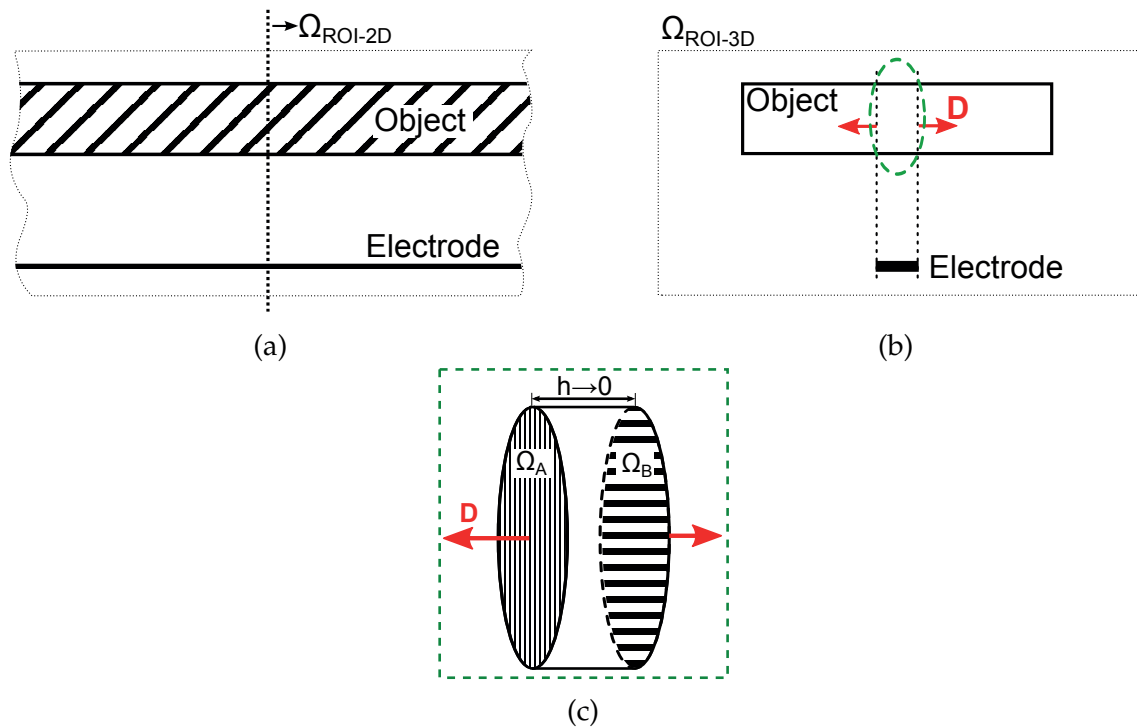


Figure 4.8.: Profiles of a 2D and 3D simulation setup and cutout to explain leakage displacement. (a) Profile of a 2D simulation where an unchanging  $z$  axis is assumed (i.e. indefinitely long electrode and object). (b) Profile of a similar 3D simulation with different length of electrode and object. Due to its different length an electric flux density  $D$  exists in 3D which cannot be simulated in the 2D simulation. (c) Cutout of the profile shown in (b).

as the height  $h$  is reduced to zero for the 2D case. Thus, it is proposed that putting a negative space charge into  $\Omega_{ROI}$  in the 2D simulation can be used to compensate for the 3D leakage effect (i.e. displacement  $D$  in 3D simulation shown in Fig. 4.8(b)).

### Validation of the Proposed Method

To validate this method, a measurement setup is simulated in 3D and compared with the same setup in 2D with and without the “leakage method”. The validation is structured into five simulations, where each simulation compares the 3D and 2D results:

1. Empty measurement setup with no objects in  $\Omega_{ROI}$
2. Measurement setup with an object ( $\epsilon_r = 80$ ) in  $\Omega_{ROI}$  (object has the same length as the electrodes)
3. Same object in  $\Omega_{ROI}$  as in step 2, but 200 mm longer than electrodes
4. Same object in  $\Omega_{ROI}$  as in step 2, but 400 mm longer than electrodes
5. Measurement setup with an approaching object

The test setup is the same for all five simulations and comprises two electrodes separated from a ground plane by a spacer with a relative permittivity  $\epsilon_r = 2$  and is shown in Fig. 4.9.

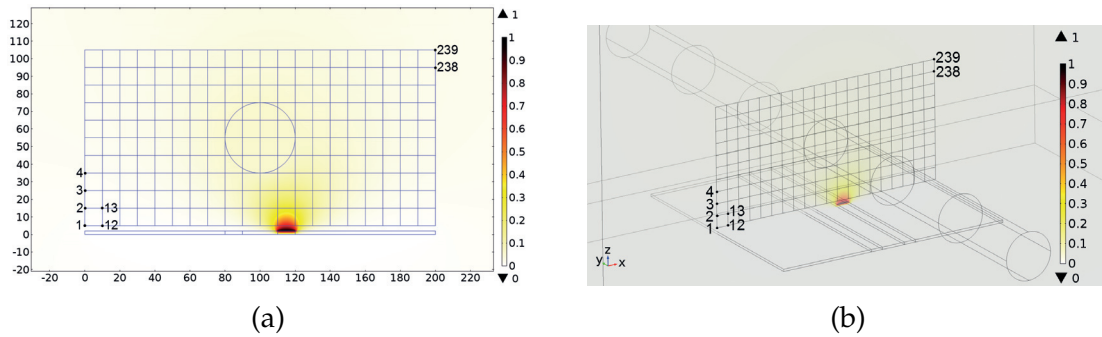


Figure 4.9.: Simulation setup in 2D and 3D to validate the leakage effect and the approach to compensate for it. (a) 2D simulation of the simulated capacitive sensor. The relative permittivity of the object (circle in the center) is set to  $\epsilon = 1$  for the first simulation and  $\epsilon = 80$  for the other simulations. To also simulate the leakage effect in 2D, a negative space charge proportional to the potential  $V$  is placed in  $\Omega_{ROI}$ . The intersection points on the grid are used to measure the potential at this point and compare it with the 3D simulation for validation purposes. (b) The 3D simulation is used as a reference. The “true” leakage effect is caused by the far boundary of the simulation setup (similar to real world experiments). While the object’s relative permittivity stays the same, the length is increased in order to change the leakage effect.

The proposed method uses negative space charges in the 2D simulation to compensate for the 3D leakage effect. The amount of charge is proportional to the electric potential  $V$  in  $\Omega_{ROI}$ . In the first four validations the capacitance between the electrodes is calculated in 3D. Then the attempt is made to get the same capacitance by changing the proportional factor of the space charge in 2D. After solving this optimization problem, the potential values at the intersection points on the grid (shown in Fig. 4.9) are plotted for all three cases (i.e. 3D simulation, 2D simulation and 2D simulation with proposed “leakage method”). This plot aims to provide better understanding of the improvements of this approach compared to a usual 2D simulation. Another indicator for the improvements (the 2-norm  $\|3D - 2D_x\|_2$ ) is shown in table 4.1.

Fig. 4.10(a) shows the simulated potentials of the 3D simulation compared with a “normal” 2D simulation and a 2D simulation including the proposed method (i.e. using negative space charges to compensate for the 3D leakage effect). In this simulation setup no object is present in  $\Omega_{ROI}$ . However, the leakage effect occurs in 3D. With the proposed method the 2D simulation can be improved to better represent the 3D problem. The voltages at the intersection points have similar values in the 3D simulation and the 2D simulation using the negative space charge whereas the potentials for a usual 2D simulation are too high.

Table 4.1.: Simulation results of the leakage effects and the compensation of the leakage effect by placing negative charges into  $\Omega_{ROI}$  in 2D (with and without an object in the vicinity of the sensor surface).

object length and fig. nr.	$C_{3D}$ [fF]	$C_{2D}$ [fF]	$C_{2D,leak}$ [fF]	$2 - norm$ $\ 3D, 2D\ _2$	$2 - norm_{leak}$ $\ 3D, 2D_{leak}\ _2$
no object, 4.10(a)	107.85	113.73	107.86	0.1327	0.0377
equal elec., 4.10(b)	102.71	111.00	102.71	0.1992	0.0273
400 mm, 4.10(c)	96.25	111.00	96.26	0.3009	0.0315
600 mm, 4.10(d)	93.61	111.00	93.62	0.3397	0.0289

The difference between the simulation setups 2 to 4 is the size of the object in  $\Omega_{ROI}$ . The length of the object is increased in each simulation to increase the leakage effect in the 3D simulation. As can be seen in Figs. 4.10(b) to 4.10(d) and table 4.1, the leakage effect can be compensated for by the proposed method by increasing the proportional factor of the space charge. Table 4.2 shows the results of the optimization problem for this factor (the resulting charge is the electric potential times the proportional factor). Higher negative charges are necessary for bigger objects. Thus, the necessary space charge used to compensate for the 3D leakage

effect can be used as a piece of additional information about the object in  $\Omega_{ROI}$  (i.e. the objects connection to ground).

Table 4.2.: Change of the proportional factor of the space charge according to the length of the object (a bigger object results in stronger leakage effect).

object length and fig. nr.	$\Omega_{ROI}$ space charge [nC/m <sup>3</sup> ]	objects' space charge [nC/m <sup>3</sup> ]	objects' $\epsilon_r$ [1]
no object, 4.10(a)	-0.42	-0.42	1
200 mm), 4.10(b)	-0.42	-1.29	80
400 mm, 4.10(c)	-0.42	-9.20	80
600 mm, 4.10(d)	-0.42	-13.75	80

In the fifth simulation, an approaching object ( $\epsilon_r = 80$ ) is simulated at different positions above the same sensor surface. This simulation is done in 2D and 3D (see Fig. 4.11). To avoid errors in the simulation results stemming from changing meshes, the approaching object is placed at each simulated position and only the relative permittivity value is changed from one simulation to another. Thus, in Fig. 4.11, 13 objects are shown but only one object has a relative permittivity of  $\epsilon_r = 80$ .

The capacitance between the two electrodes is evaluated for different distances between the object and the sensor surface. This is done in a 2D and 3D simulation. As can be seen from Fig. 4.12, although the same setup is used, there is a significant difference in the evaluated capacitances, which increase as the objects gets closer to the sensor surface. The simulated capacitance is always higher in 2D compared to the result in 3D.

This error in 2D is caused by the objects' "different" connection to ground. If, for example, a negative charge is placed at the approaching object in the 2D simulation, this charge has the same effect as a capacitive ground connection into the third dimension (compare the first four simulations above). The negative charge has to increase as the object approaches the sensor surface and the electric potential increases. In the first four simulations this was achieved by using a charge proportional to the electric potential.

The effect of such a negative charge placed on the approaching object is shown in Fig. 4.12. As shown in this section, this approach not only enables the 3D effect to be balanced, but also allows additional information about the objects' connection to ground to be obtained. Furthermore, no 3D simulation with its high computational effort is necessary.

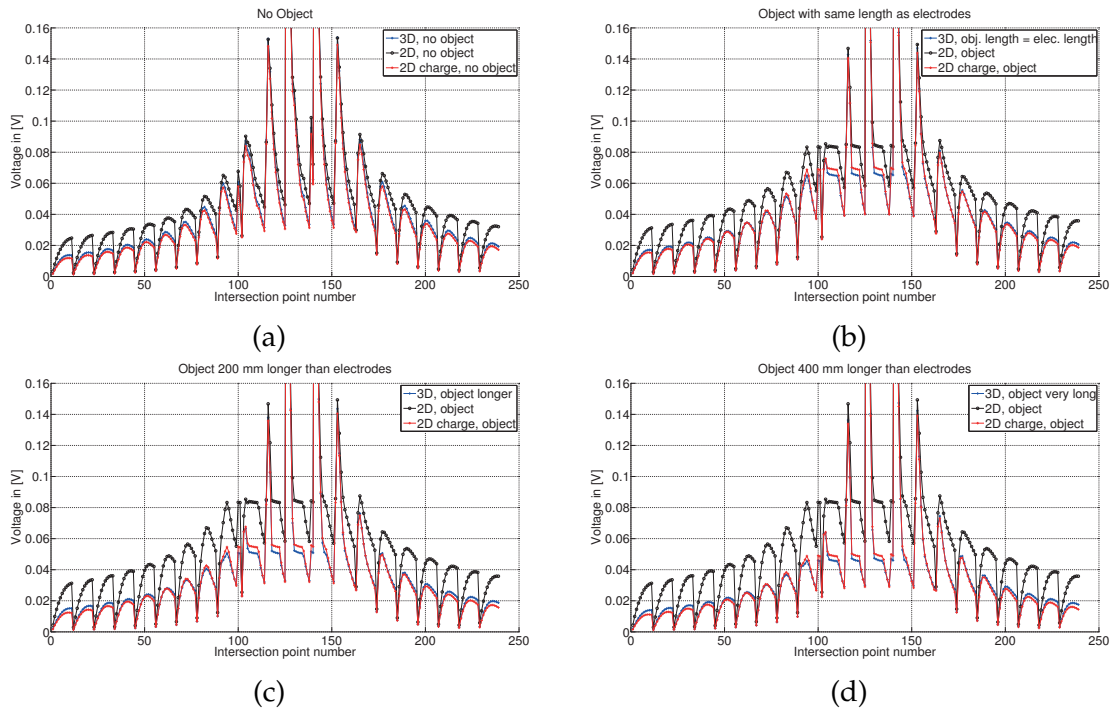


Figure 4.10.: Simulation results for the leakage effect. (a) Simulation results showing the potential values at the intersection points of the grid in (a). The leakage effect can almost be compensated for by placing charges at the intersections. (b) A higher leakage current can be observed with an object with a high relative permittivity. However, when placing higher negative charges in the area of the object, the leakage effect can again nearly be compensated for in the 2D simulation. (c) . (d) .

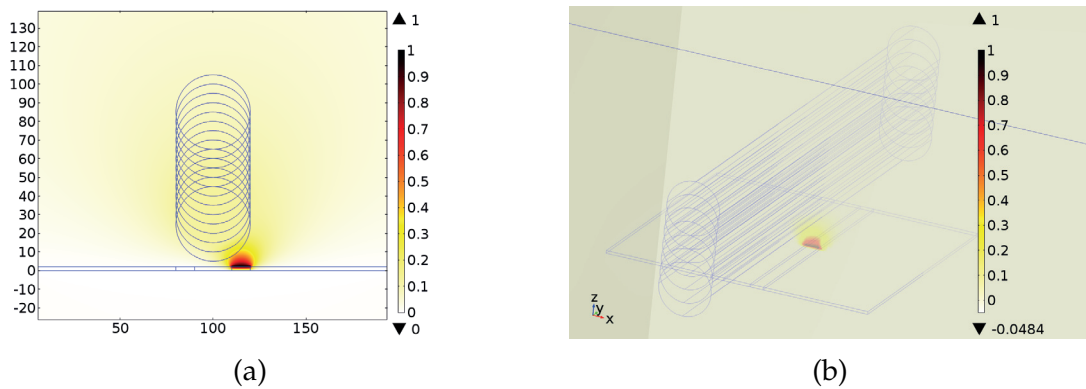


Figure 4.11.: Simulation setups to validate the leakage effect with an approaching object. Both simulations (2D and 3D) use the same scenario and dimensions of the test setup. (a) The 2D simulation is easier to set up and faster to solve. Although, as shown in Fig. 4.12, the results differ from the 3D simulation. (b) A 3D simulation delivers a more accurate result (Fig. 4.12), but is also more difficult to set up and requires more time for solving the forward problem.

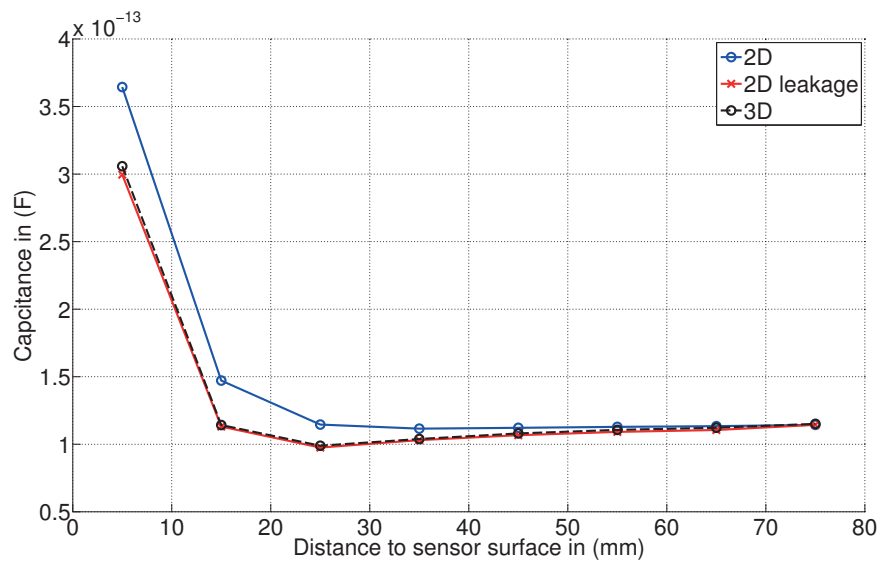


Figure 4.12.: Simulation results presenting the difference between a 2D and a 3D (setups are shown in Fig. 4.11). As can be seen here, the capacitance between the two electrodes for an approaching object differs between the 2D and 3D simulation (traces “2D” and “3D”). Using a changing negative charge (placed at the approaching object) in the 2D simulation, this difference can be eliminated (simulation trace “2D leakage”).

With the five simulations above, the high impact of the leakage effect has been shown. When measuring in mutual capacitance mode (see section 4.5.1), this leakage effect also has a high impact on the measurement results and thus on the reconstruction results. An illustrative reconstruction example is shown in Fig. 3.11. Because of the leakage current, a conductive object could not be reconstructed at certain positions in the ROI. Due to the high impact of the leakage effect in open environment sensing, additional information can be gained compared to only measuring coupling displacement currents. As described in section 4.5.1, capacitive sensors using the self capacitance mode measure the displacement current between the transmitter electrode and the distance ground. That is the presented leakage current. Proximity sensors using the self capacitance mode usually have a good signal-to-noise ratio (SNR) but at the same time lack a clearly defined observation region [Zan09; Sch+13a].

### Reconstruction of the Leakage Effect

This thesis employed two approaches to using the leakage current as an additional source of information for proximity detection and classification of objects. Both approaches followed the idea of reconstructing the 2D ROI twice:

1. Reconstruction of the ROI based on coupling displacement currents.
2. Reconstruction of the ROI based on leakage displacement currents.

Since the leakage current is a 3D effect, it contains information about the 3D environment. With the combined reconstruction of the coupling and leakage current (for example as shown in Fig. 4.13), 3D information could be obtained from only 2D 2D reconstructions. This is called a 2.5D ECT system in [Zan09]. It has the advantage of the computational effort of a 2D reconstruction while providing the information of a 3D environment. A 3D simulation would have higher computational effort with which the necessary real time capability could not be achieved.

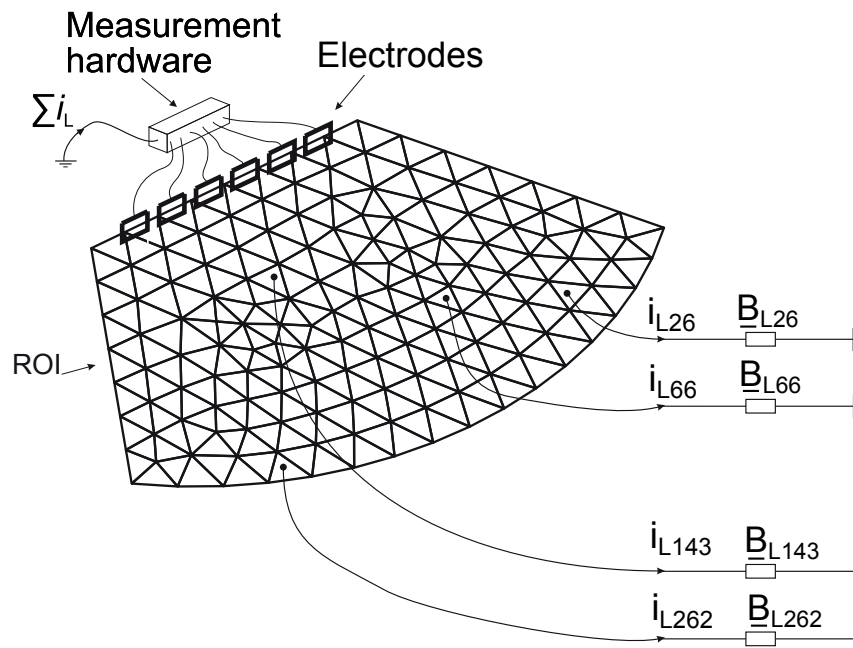


Figure 4.13.: A pictorial representation of a leakage map adopted from [Zan09]. If it were possible to separate the coupling displacement current and the leakage displacement current, two tomographic pictures could have been achieved. The first picture would be similar to an ECT picture (i.e. spatial permittivity distribution). The second picture would reconstruct the susceptances  $B_{Lx}$  between the distance ground and each reconstruction element.



### Simulation of the Leakage Current

As explained in section 4.1.2 and for example in [Polo6], capacitive sensing can be simulated (i.e. solving the forward problem) by solving Laplace's equation shown in equation (4.3) or rewritten for 2-D in equation (4.4). How this problem is solved numerically using the FEM is also shown in section 4.1.2. To be able to reconstruct the leakage current presented above, the additional term  $\beta$  is added to Laplace's equation. The generic second-order partial differential equation in (4.5) reduces to

$$\frac{\partial}{\partial x}(\alpha_x \frac{\partial u}{\partial x}) + \frac{\partial}{\partial y}(\alpha_y \frac{\partial u}{\partial y}) + \beta u = 0, \quad (4.21)$$

where  $u = V$ ,  $\alpha_x = \alpha_y = \varepsilon$  and  $\beta = B$  (a constant proportional the susceptance connected to ground as shown in Fig. 4.13). Consequently following the same approach as in section 4.1.2, the matrix  $T$  is no longer zero and has to be evaluated.  $T$  was defined in equation (4.14) and is re-stated here for convenience of the reader:

$$T_{ij} = \iint_{\Omega_e} \beta N_i N_j dx dy.$$

For linear shape functions and with the generic formula from [ZTZoo]:

$$\iint_{\Omega_e} (N_1)^l (N_2)^m (N_3)^n dx dy = \frac{l! m! n!}{(l + m + n + 2)!} 2A_e, \quad (4.22)$$

the entities of the symmetric matrix  $T$  can be evaluated to:

$$\begin{aligned} T_{11} = T_{22} = T_{33} &= \frac{\beta A_e}{6} \\ T_{12} = T_{21} = T_{13} = T_{31} = T_{23} = T_{32} &= \frac{\beta A_e}{12}. \end{aligned} \quad (4.23)$$

With this extension of the Laplace's equation, each finite element in the ROI will not only be assigned to a relative permittivity value  $\varepsilon_r$  but also to a susceptance value  $B$ . This permits a 3-D effect to be simulated (i.e. the leakage current) in a 2-D FEM simulation as indicated in Fig. 4.13.

The two approaches leading to the necessary measurements for a reconstruction of the leakage current are described below. With the first approach (i.e. leakage current suppression), the leakage current could not be completely suppressed. The second approach (i.e. simultaneous measurement in self capacitance mode and mutual capacitance mode) was successfully used in this work. It is described hereafter in more detail.



### Suppression of leakage currents

The suppression and admission of leakage displacement currents is supposed to be one way to get a leakage tomographic picture. Several arrangements were used, three of which are shown in Fig. 4.14:

- Switches.
- Current compensated coils (wide frequency range).
- Band-stop filter (frequency selective).

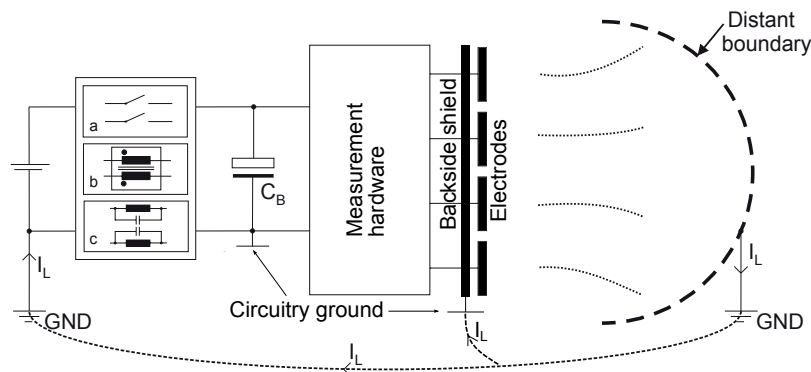


Figure 4.14.: Sketch of possible leakage suppressing methods adopted from [Zan09]. The main goal is to be able to measure with and without leakage currents. This can be achieved in several ways: (a) Switches can be used to separate the circuitry ground from the distance ground. Additional energy buffering ( $C_B$ ) has to be considered. (b) Current compensated coils can be used to suppress the leakage current for a wide frequency range. Additional switches must be measured with the leakage currents included. (c) A band-stop filter can be used for frequency selective leakage suppression.

The main disadvantage of this method is the circuitry ground. Even if one of the possible suppression techniques worked perfectly, there has to be a circuitry ground. Even worse, most of the time the sensor front end has to be sensitive in only one direction (or has to be shielded from disturbers at the back). Therefore, most sensor front ends are built up similarly to the one shown in Fig. 4.20(a) and Fig. 4.20(b). In general they consist of:

- Measurement electrodes (at the top).
- Some kind of spacer to separate top and bottom (in the middle).
- Backside shield, which is connected to circuitry ground in mutual capacitance mode (at the bottom).

Usually the grounded backside shield is as big as the sensor surface. Thus, it provides a return path for the leakage current which should be suppressed (as shown in Fig. 4.14).

Fig. 4.16 shows the measurement results for the setup shown in Fig. 4.15. The setup uses the approach (a) in Fig. 4.14 (switches are used to separate the circuitry ground from the distance ground). If the device is in “leakage suppression mode”, data transfer is done over an RF - link and batteries supply the circuitry with power. If the switch is closed and measurement is done including leakage currents, the data and power are transferred over the implemented USB connection.

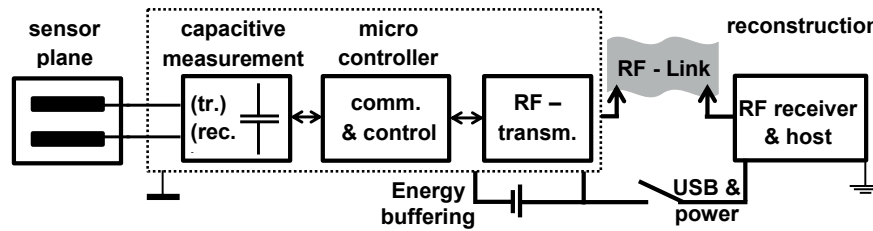


Figure 4.15.: Block diagram of measurement hardware for leakage suppression. A switch can be used to separate the distance ground from the circuitry ground to suppress leakage currents. If the switch is opened, data transfer is done over a RF link and power is supplied by batteries.

Different objects are used to validate this leakage suppression approach:

- Human hand
- Iron rod (connected and not connected to world ground)
- PVC bar

As can be seen in the measurement results in Fig. 4.16, a much higher capacitive change in the coupling mode can be measured for the approaching human hand if leakage suppression is used. However, the shielding effect is still present for distances further away from the sensor surface. Leakage current flows from the transmitting electrode to the backside shield and back to the circuitry ground as explained above and shown in Fig. 4.14. A reduced difference in the measurement results is observed if the approaching object is smaller and thus, the capacitance-to-world ground is smaller (i.e. less leakage current) compared, for example, to a human hand. Fig. 4.16(e) and 4.16(f) show the results of using an approaching iron rod (not connected and connected to the distance ground, respectively). In both cases, leakage current is still present (decreasing capacitance in the beginning of the approach). With the third approaching object (a PVC bar) no leakage current can be measured with the setup used. The capacitance to the distance ground is very small, as are the size and relative permittivity ( $\epsilon_r \approx 3$ ). Thus, similar measurements are obtained with and without leakage suppression.

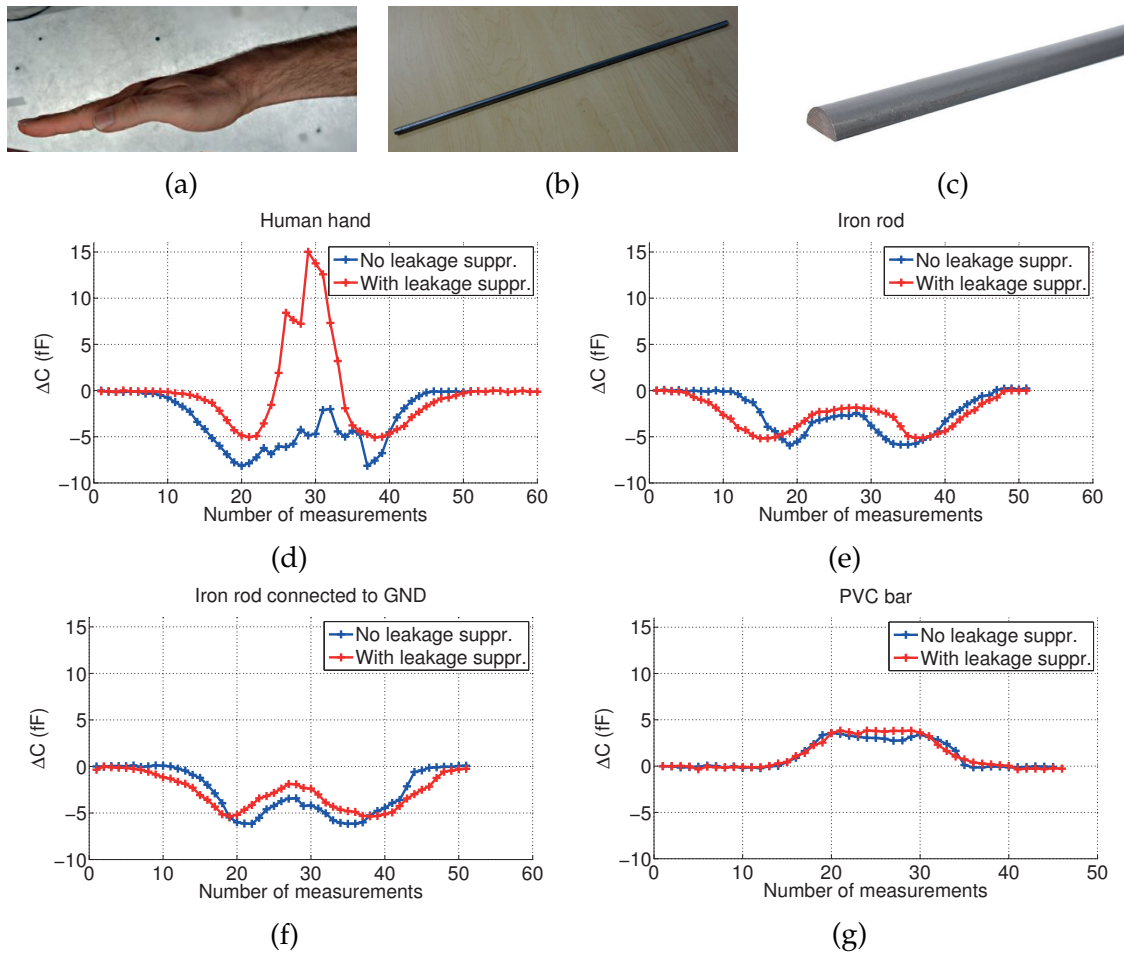


Figure 4.16.: Experimental measurement results for leakage suppression. Three objects (human hand, iron rod and PVC bar) are used to evaluate the leakage suppression of the measurement setup shown in Fig. 4.15. (d) A human hand produces the highest capacitance change since it is the biggest object with the highest permittivity. Part of the leakage current can be suppressed resulting in a lower decrease and higher increase of the measured capacitance. (e) and (f) An approaching iron rod not connected and connected to the distance ground, respectively, is shown. Leakage current still flows and small effects of the leakage suppression can be observed. (g) The PVC bar does have a minor connection to the distance ground (minor leakage current flows) and thus, the measurements obtained are similar.

### Measuring simultaneously in mutual- and self capacitance mode

The second approach aims to reconstruct the leakage current by measuring in both capacitance measurement modes (i.e. self and mutual capacitance mode). These modes are described in more detail in section 4.5.1. If a capacitance measurement system is able to work in both modes simultaneously, all displacement currents ( $i_p$  and  $i_L$  in Fig. 4.7) are measured. In contrast to the first approach, the leakage current  $i_L$  is not suppressed when measuring in the mutual capacitance mode. The coupling current  $i_p$  cannot be measured on its own. Thus, the leakage current still affects the measurements and the reconstruction results.

Fig. 4.17 shows a sketch of a system using mutual- and self capacitance modes. The shield on the backside of the electrodes has to be able to work in two modes. If the mutual capacitance mode is used (compare Fig. 4.17(b)), the shield has to be set to ground. When measuring in the self capacitance mode, the shield has to act as an active guard (set to the excitation signal as shown in Fig. 4.17(a)). The reason for switching the potential on the backside shield, is the resulting offset capacitance  $C_{Off}$  between the transmitter electrode and the backside shield (in the self capacitance mode) or the receiving electrode and the backside shield (in the mutual capacitance mode).  $C_{Off}$  is indicated with dashed lines in Fig. 4.17. If the backside shield is not used as active guard in the self capacitance mode (for example, it is set to ground potential) or used as active guard in the mutual capacitance mode,  $C_{Off}$  would be very high (several magnitudes higher than the capacitances of interest). Thus, a reliable measurement would be very difficult.

As the switching of the backside shield is essential, simultaneous measurement in both modes is not possible. Thus, in this work attempts to switch between both measurement modes fast enough so that only minor changes to the measurands and the environment would occur (see section 4.5.2).

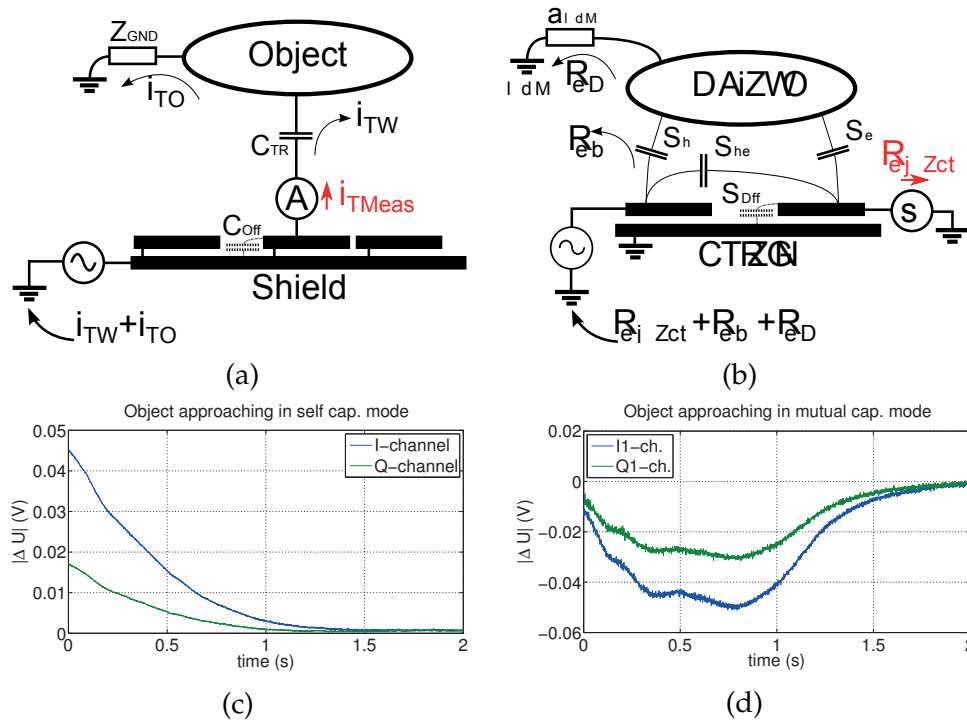


Figure 4.17.: Sketch and measurements of the self- and mutual capacitance measurement mode. (a) In the self capacitance mode, the current originating on one electrode is measured. The backside shield has to work as an active guard. Otherwise the main part of  $i_{TMeas}$  would flow from the electrode to the shield. (b) In the mutual capacitance mode the received displacement current on one electrode is measured. In this mode, the backside shield has to be set to circuitry ground. Otherwise the main part of  $i_{RMeas}$  would come from the shield. (c) Measurements for the self capacitance mode. For an approaching object with a relative permittivity higher than 1,  $i_{TMeas}$  is increasing. (d) Due to parasitic effects (compare section 4.3.2) an approaching object first decreases the received displacement current in the mutual capacitance mode. At a certain distance the received current increases very quickly.

### 4.3.5. Geometric Effects for Elongated Open Environment Capacitive Sensing<sup>4</sup>

One benefit of capacitance sensors is the possibility of installing them on planar and non-planar surfaces. The sensor elements (i.e. the electrodes) are incomparably simple while providing high versatility with respect to geometrical constraints. Hence, this technology also allows complex structures or machines to be monitored, where traditional systems e.g. those based on a line of sight principle, fail. However, the individual shapes of the sensor electrodes dictate the coupling mechanisms between the electrodes to objects in the environment. Below, analysis of the 3D sensitivity distribution of an example sensor setup by means of numerical analysis and comparative studies with equivalent circuit models are provided. Furthermore, impacts are analysed and demonstrated by means of experimental investigations and numerical simulations.

#### Experimental Setup

The developed test setup is shown in Fig. 4.18 . It uses three electrodes (one transmitter electrode and two receiver electrodes) to determine the distance to an approaching object. A sketch in Fig. 4.18(a) shows the different layers of the test setup. The electrodes are positioned under a sheet of black synthetic fibre and two layers higher density polyethylene . They are materialized by 1 m long and 0.51 mm thick simple electric wires, which permit the realization of a very flexible electrode structure. To make the sensor sensitive in only one direction (above the electrodes) a ground plane made of an aluminium foil beneath the electrodes is used. The frame itself is built up with polystyrene (Styrofoam). To determine the capacitance between a pair of electrodes, a commercially available capacitance-to-digital converter was used [Ana14]. A wireless transmitter connects to a host controller for evaluating the measurement results and permitting a portable and flexible experimental setup. Measurement results for an approaching human hand are shown in Fig. 4.18(d).

#### Sensitivity Analysis of the Electrode Structure

The capacitance between a pair of electrodes separated by  $c$ , with a length  $L$ , a radius  $a$ , and a distance  $b$  between the electrodes and the ground plane (all in

---

<sup>4</sup>Parts of this section have been published in [SBZ11]

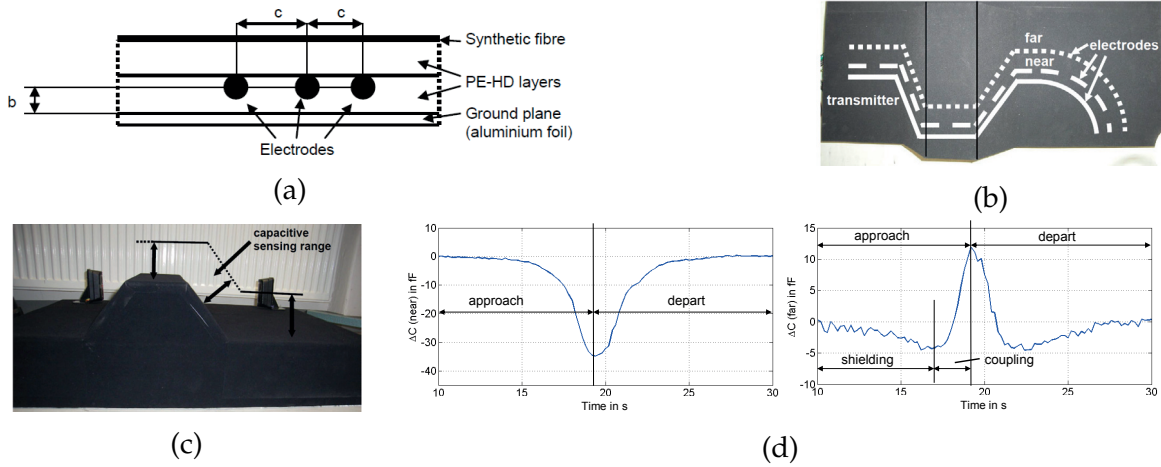


Figure 4.18.: Experimental test setup used for sensitivity analysis of bending electrode structures. (a) Cross section of the experimental setup with the different layers (not in scale). (b) and (c) Pictures of the experimental test setup comprising three electrodes with a length of 1 m. (d) Measurement results for an approaching human hand above a parallel electrode area of the experimental test structure. The results of the near and far electrodes are shown in the left and right pictures of (d), respectively.

metres) can be approximated by [Bax97]:

$$C \approx \frac{\pi \epsilon_0 \epsilon_r L \ln\left(1 + \frac{2b}{c}\right)}{\left(\ln \frac{2b}{a}\right)^2} \quad (4.24)$$

For the presented parallel electrode structure with the length of 1 m and a relative permittivity  $\epsilon_r$  of 1, capacitances of 1276 fF and 361 fF for the near and the far electrode, respectively, can be calculated. However, the capacitance change for an approaching object is only about 35 fF and 15 fF for the near and far electrodes, respectively. As already mentioned in section 1, the capacitance measurement system has to be able to work with such high offset capacitances.

The investigation of sensitivity impacts due to bending electrode structures is based on finite element simulations. Two scenarios for an approaching object are chosen and compared to the ideal situation (i.e. parallel electrode structure, see Fig. 4.18(b)). The simulation setup is shown Fig. 4.19(a), corresponding results are shown in Fig. 4.19(b). The approaching object was simulated as a whole block, with slices of different relative permittivity  $\epsilon_r$  to simulate an approach while keeping the same mesh. As can be seen from Fig. 4.18(d) and Fig. 4.19(b), the simulation results match the measurement results. Small differences originate from differences between the experimental setup and the simulated geometry (e.g. laying of electrodes).



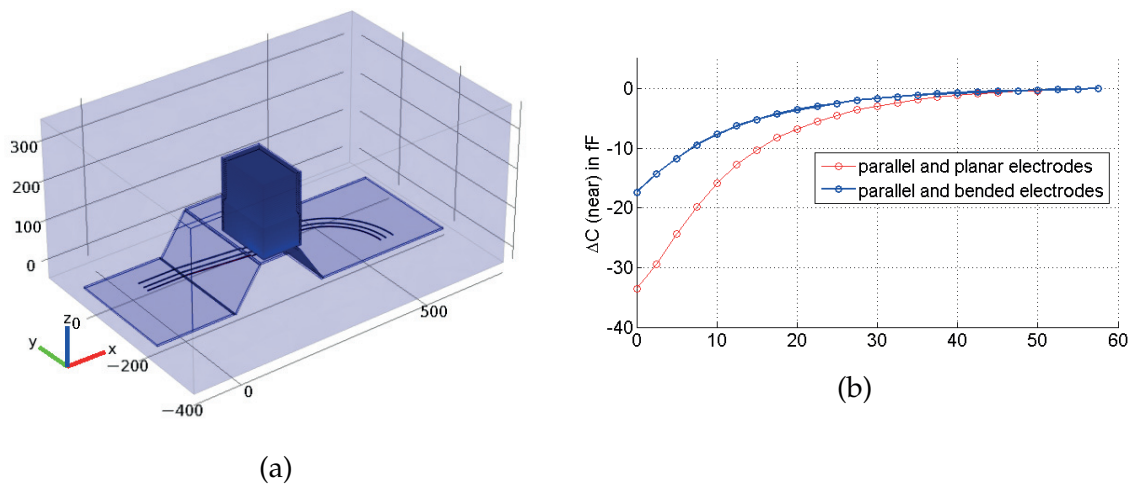


Figure 4.19.: Simulation setup and results for an object approaching different positions. (a) Picture of the FEM simulation setup to recreate the experimental setup. (b) Simulation results for two electrode structures (near and far) and one object approaching different positions of the setup surface.

In curved areas the sensitivity of the sensor deviates from the sensitivity obtained by a planar sensor arrangement. As can be seen in Fig. 4.19(b), the sensitivity increases for objects approaching above the curved electrode structures. Due to the increased covered electrode area, a higher capacitance is measured. Thus, the approaching object appears closer than it really is. Especially for short distances, this effect would lead to an incorrect distance measurement for the whole sensor arrangement if no countermeasures were made. If only the curved electrode structure is exposed to an approaching object, distance measurement is still possible because of the unambiguousness of the near and the far electrodes. If an object approaches in a non parallel configuration (e.g. rising area of the experimental test setup in Fig. 4.18(c)), a smaller capacitance is measured as shown in Fig. 4.19(b). If an object enters the vicinity of such a structure, the measured capacitance is smaller compared to the ideal case. Thus, a measurement system would provide a distance that is farther away than the object.

To overcome these difficulties of elongated and non-planar capacitive sensors, the sensitivity of the sensor has to be increased or decreased in the particular areas. Possibilities would be a decrease or increase of

- the distance between the sensor electrodes,
- the relative permittivity  $\epsilon_r$  (e.g. another spacer material), or
- the electrode surface

in the desired areas.



## 4.4. The ECT Approach

After a short introduction to ECT, an approach is presented which aims to combine results from the work leading to this thesis and from research results in the field of ECT. In the first part, a mobile and wireless ECT system is presented and measurement results are shown. The second part presents the leakage effect in the ECT system. Although this effect is usually not considered, it can have a significant influence on the ECT measurement results. The third and last part will show how to use and adopt the presented ECT system for capacitive sensing in the open environment.

### 4.4.1. A Mobile and Wireless ECT System<sup>5</sup>

Below, a multi channel capacitive measurement system used for an ECT sensor (see subsection 4.2.2) will be presented. The system is capable of determining the capacitances of all pairs of electrodes of an arrangement consisting of  $N_{elec}$  electrodes. For simplified instrumentation, the system features wireless data transmission to a host. This indicates that cabling can be avoided making the system versatile and in particular useful in applications with difficult measurand access like in the case of operation on high voltage parts or on moving parts. The system is not limited to specific electrode designs and thus permits the use of optimized electrode designs for specific tasks. With its small geometric outline, low weight and low power consumption, the measurement system is well suited for the fast prototyping of ECT systems.

Fig. 4.20(a) depicts a sketch and Fig. 4.20(b) a photography of the flexible electrodes. Eight electrodes were placed on a flexible printed circuit board (PCB) material such that the sensor could be fitted to the circumference of a specific pipe. In order to be insensitive with respect to the backside region of the electrodes, the sensor is shielded using a screen, which was created with aluminium foil. This can be seen in Fig. 4.20(c). The screen is connected to the measurement ground. To minimize the offset capacitance caused by the screen, the relative permittivity of the spacer material has to be low. Following the recommendations on the design of ECT sensors presented in [Yan10], two axial screens in the upside and downside direction of the sensor were applied.

Fig. 4.20(c) depicts the complete system consisting of the ECT sensor and the multichannel capacitive measurement system. The pipe is made out of acrylic glass. As can be seen, the design and the setup of the ECT sensor are kept on an overall simple level. With the setup it is possible to determine the capacitance matrix  $C$

<sup>5</sup>Parts of this section have been published in [SNZ12]

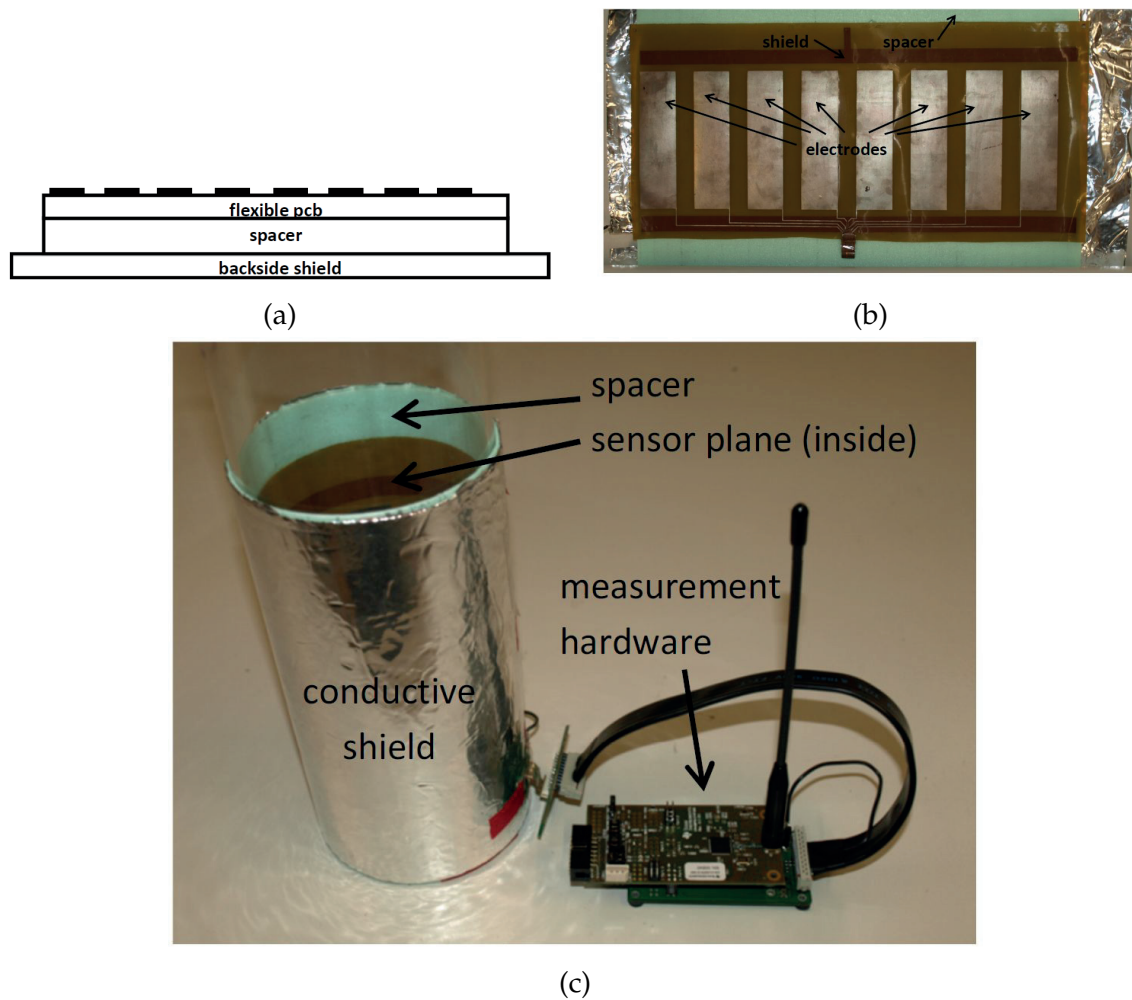


Figure 4.20.: A mobile and wireless ECT measurement system [SNZ12]. (a) Sketch of the different layers of the sensor plane. A spacer between backside shield and PCB is used to keep the offset capacitance low. (b) Eight electrodes and two axial end screens on the top and bottom side of the PCB, respectively, are used for the ECT system. (c) Picture of the measurement setup comprising the sensor plane attached on a pipe made of acrylic glass and the measurement hardware including the RF transmitter.

which contains the capacitances between all possible pairs of electrodes ( $8 \times 8$  matrix because of eight electrodes).

### Solving the Inverse Problem

This section summarizes the algorithmic approach to determining the spatial permittivity distribution inside the pipe from measurements  $\tilde{\mathbf{d}}$ . For a brief overview and a general introduction to the inverse problem of ECT the reader is referred to [Neu+11].

Let  $\partial\Omega$  denote the screen bounding of the problem domain  $\Omega$  and  $\Omega_{\text{ROI}}$  denote the domain inside the pipe. The boundaries of the electrodes are referred to as  $\Gamma_i$ ,  $i = 1 \dots N_{\text{elec}}$ . Using an electrostatic formulation of Maxwell's equations, electric fields in  $\Omega$  are governed by the potential equation  $\nabla \cdot (\varepsilon_0 \varepsilon_r \nabla V) = 0$ , where  $V$  is the electric scalar potential.  $\varepsilon_0$  and  $\varepsilon_r$  are the absolute and the relative permittivity. The boundary conditions are of Dirichlet type and given by  $V_{\partial\Omega} = 0$  on the screen,  $V_{\Gamma_j} = V_0$  on the transmitter electrode and  $V_{\Gamma_i} = 0$ ,  $i \neq j$ , on the remaining  $(N_{\text{elec}} - 1)$  receiver electrodes. The inter electrode capacitances are computed by Gauss's law

$$c_{i,j} = \frac{1}{V_0} \int_{\Gamma_i} \vec{n} \cdot \varepsilon_0 \varepsilon_r \nabla V_j ds, \quad (4.25)$$

and stored in the matrix  $\mathbf{C} = [c_{i,j}]$ , where each column corresponds to one transmitter electrode and each line to one receiver electrode.

The computation of  $\mathbf{C}$  given the permittivity distribution is referred to as forward map  $F : \mathbf{x} \mapsto \mathbf{C}$ . Hereby the state vector  $\mathbf{x}$  denotes a parametric description of the material distribution in  $\Omega_{\text{ROI}}$ . The numerical evaluation of  $F$  is done by means of the FEM.  $\mathbf{x}$  contains the relative permittivity inside of the corresponding finite elements. For the determination of  $\mathbf{x}$ , given the measurements  $\tilde{\mathbf{d}}$  we use a nonlinear approach. Let  $\mathbf{y}$  denote the components of  $\mathbf{C}$  corresponding to the measurements collected in  $\tilde{\mathbf{d}}$ . Then  $\mathbf{x}$  can be found by solving an optimization problem of form

$$\mathbf{x}^* = \arg \min_{\mathbf{x}} \|\mathbf{y}(\mathbf{x}) - \tilde{\mathbf{d}}\|_2^2 + \alpha \|\mathbf{L}\mathbf{x}\|_2^2. \quad (4.26)$$

The first term minimizes the misfit between the model and the data. The second term is a so-called "regularization term", which is necessary to achieve a numerical stable solution. This is required due to the ill-posed nature of the inverse problem.  $\mathbf{L}$  is referred to as regularization matrix and  $\alpha$  is the regularization parameter. For the solution of (4.26) a Gauss-Newton (GN) method is applied to find  $\mathbf{x}^*$  in an iterative way by

$$\mathbf{x}_{k+1} = \mathbf{x}_k + s \left( \mathbf{J}\mathbf{J}^T + \alpha \mathbf{L}^T \mathbf{L} \right)^{-1} \left( \mathbf{J}\mathbf{r} + \alpha \mathbf{L}^T \mathbf{L}\mathbf{x}_k \right), \quad (4.27)$$

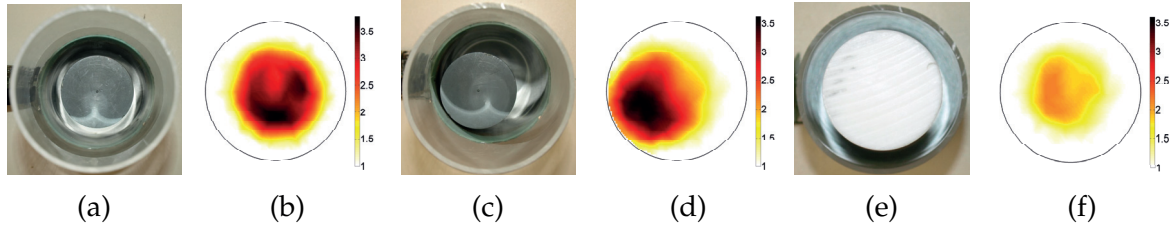


Figure 4.21.: Experimental results from the presented ECT system. (a) and (b) PVC bar at the centre of the pipe ( $\epsilon_r \approx 3.5$ ). (c) and (d) Same PVC bar positioned on the left side. (e) and (f) Teflon bar ( $\epsilon_r \approx 2.2$ ) positioned at the centre (different scale).

where  $J$  denotes the Jacobian and  $s$  is a step width parameter and  $r = \mathbf{y} - \tilde{\mathbf{d}}$  is the residual vector.

It has to be mentioned that a reconstruction of measured data requires a calibration strategy in order to minimize the difference between the physical process  $P : x \mapsto \tilde{\mathbf{d}}$  (the sensor) and the forward map  $F$  [Neu11]. For model-based inversion techniques, calibration has to be applied if the model error  $e = P - F$  outweighs the measurement noise. For the presented ECT system, a two-point calibration is used with an air-filled pipe and a solid PVC block filling the entire pipe. Then, an affine transformation  $\hat{c}_{i,j} = \rho_{i,j}c_{i,j} + c_{0,i,j}$  is applied to the output of  $F$  and  $\hat{C} = [\hat{c}_{i,j}]$  is used to assemble  $\mathbf{y}$ . Hereby, the gain  $\rho_{i,j}$  and the offset  $c_{0,i,j}$  are determined from the calibration measurements. This approach can also be applied to calibrate the measurements  $\tilde{\mathbf{d}}$ . Then  $\mathbf{y}$  is obtained from  $C$ .

## Experimental Results

Below, experimental results are shown to give the reader an idea of the capabilities of the proposed approach. Fig. 4.21 depicts the measurement setups and the corresponding simulation results.

In the first experiment shown in Fig. 4.21(a) a 65 mm-diameter PVC block was placed in the centre of the pipe. The reconstruction result of the non-invasive measurement is shown in Fig. 4.21(b). As can be seen, the relative permittivity distribution in the inside of the pipe can be reconstructed. According to the so-called “soft field nature” [Bax97] of the capacitive measurement system, a certain smoothness occurs to the reconstructed relative permittivity distribution in the inside of the pipe. Fig. 4.21(c) and (d) show the true position and reconstruction result of the same PVC block at a different position inside the pipe. Again it is possible to reconstruct the position of the PVC bar in the inside. The third measurement in Fig. 4.21(e) and (f) a 50 mm-diameter bar made of polytetrafluoroethylene (polytetrafluorethylen (PTFE) or Teflon) is positioned in the centre of the pipe. It is possible to reconstruct the

true relative permittivity  $\varepsilon_r \approx 2.2$  of the bar. The position inside the pipe can also be estimated.

#### 4.4.2. ECT and Leakage

ECT systems usually work in one of two measurement modes [Neu+11]

- Low-Z measurement
- High-Z measurement

In both measurement modes, ECT specific simplifications are made. For example, it is assumed that the length of objects in the ROI extends the length of the electrodes. Thus, a reduction of the 3D problem to a 2D problem is allowed for simulation purposes [Neu+11] and for solving the forward problem (refer to section 4.4.1). Both measurement modes belong to the mutual capacitance mode (refer to section 4.5.1). Although not considered in ECT applications, it will be shown in this section the leakage effect (described in section 4.3.4) can also occur in ECT applications. The effects in the forward problem and the reconstruction results, if leakage is present, are shown. Additionally, measures are presented to detect and reconstruct leakage.

For the following investigations, the ECT system presented in section 4.4 and shown in Fig. 4.20(c) is used. Fig. 4.22 shows the reconstruction result for a simulated setup of this ECT system. To avoid a so-called “inverse crime” [Neu+11] (since the same forward map  $F : \boldsymbol{x} \mapsto \boldsymbol{C}$  is used for simulation and reconstruction) a different mesh structure is used. As can be seen in Fig. 4.22, a coarser mesh is used for solving the forward problem (Fig. 4.22(a)) than for the reconstruction shown in Fig. 4.22(c). The simulation results of the forward problem are shown in Fig. 4.22(b)). In this figure each inter electrode capacitance of the matrix  $\boldsymbol{C}$  is plotted for two situations. The upper part of Fig. 4.22(b) shows the plots for an empty pipe (filled with air,  $\varepsilon_r = 1$ ) and for an object (PVC bar,  $\varepsilon_r \approx 3$ ) in  $\Omega_{ROI}$ . The bottom part shows the difference of each inter electrode capacitance between these two situations ( $C_{PVC} - C_{Air}$ ). Since  $\boldsymbol{C}$  is an  $8 \times 8$  matrix, 64 measurements are plotted.

As can be seen in Fig. 4.22(b), a dielectric object in  $\Omega_{ROI}$  increases most of the inter electrode capacitances. Capacitance which decrease are effected from the shielding effect presented in section 4.3.3. Since shielding also occurs in 2D, it can be simulated in 2D and thus, does not have an effect on the reconstruction results shown in Fig. 4.22(c).

For validation of the forward problem, a real measurement is taken with a PVC bar at the same position (shown in Fig. 4.23(a)). Although the measurement results shown in Fig. 4.23(b) differ slightly from the simulation results in Fig. 4.22(b),



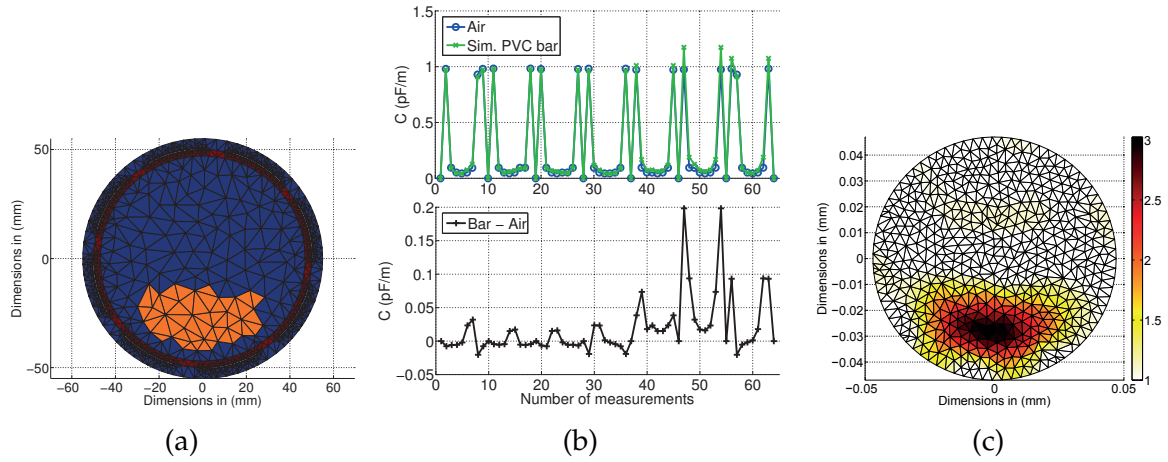


Figure 4.22.: ECT simulation and reconstruction results for a PVC bar. (a) Simulation setup with a coarser mesh to avoid an “inverse crime”. (b) Simulation results of the setup with a PVC bar with  $\varepsilon_r \approx 3$  and for an empty pipe (filled with air,  $\varepsilon_r = 1$ ). The bottom picture shows the difference between the two situations. (c) Reconstruction of the spatial permittivity distributions in  $\Omega_{ROI}$ .

the reconstruction results are similar. The misfit between measurement data and simulation results is considered due to the use of a calibration scheme as explained in section 4.4.1. This minimizes the difference between  $P$  (physical process) and  $F$  (the forward map).

The leakage effect is not considered in ECT systems. Fig. 4.23 and Fig. 4.22 above showed an “usual” ECT scenario. With the formulations presented in section 4.3.4, it is possible to define a forward problem addressing the leakage effect. Thus, the reconstruction of the “leakage of objects” in  $\Omega_{ROI}$  is possible. Below, the novel formulation from section 4.3.4 is used to solve a “leakage forward problem” and reconstruct it in an ECT manner. A real-world experiment is used to show the effect of leakage in an ECT application and a reconstruction proves the presumptions made in the sections above.

Fig. 4.24 shows the 2D reconstruction of the “3D leakage effect” in ECT. A small area in  $\Omega_{ROI}$  (three FEM elements) is set to a negative charge (shown in Fig. 4.24(a) and mathematically described in section 4.3.4). The simulation results (solution of the forward problem) resulting in the inter electrode capacitances are shown in Fig. 4.24(b). As can be seen, the inter electrode capacitances decrease compared to the capacitances of an empty pipe. This is because the leakage effect is simulated by the negative charge. The reconstruction algorithm used was the same one as for the reconstruction of the spatial permittivity distribution. The reconstruction of the leakage effect was based on the extended Laplace equation (4.21) as described in section 4.3.4.

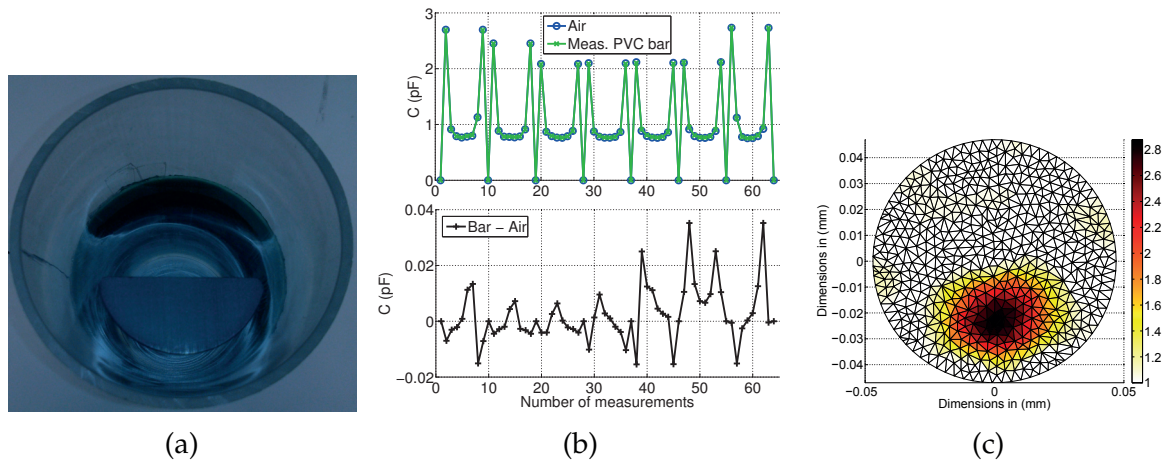


Figure 4.23.: ECT measurement and reconstruction for a PVC bar. (a) Picture of the setup comprising the PVC bar and the ECT pipe with the sensing electrodes. (b) Measurement results showing the inter electrode capacitances for a pipe filled with only air, a pipe with the inside as shown in (a) and the difference between the two (bottom figure). No transmitter measurements were taken. Thus, the main diagonal of  $C$  consists only of zeroes. (c) Reconstruction result of the spatial permittivity distribution in  $\Omega_{ROI}$ .

Fig. 4.24(c) and 4.24(f) show the results. The position of the negative charge (i.e. object with a parasitic connection to the 3D ground) can be estimated. The amount of charge that is doubled in Fig. 4.24(a) compared to Fig. 4.24(d) can also be reconstructed.

To prove the simulation from above, real-world experiments were conducted. Fig. 4.25 shows the setup results. To simulate a “leakage object” inside  $\Omega_{ROI}$  an electric wire was used. As shown in Fig. 4.25(a) the wire was spanned through the ECT pipe. In the first experiment the wire was connected to world ground (Fig. 4.25(b) and 4.25(c)). In the second experiment it was disconnected and left floating (Fig. 4.25(d) and 4.25(e)). As can be seen, the inter electrode capacitances decrease compared to an empty pipe (similar to the simulation results). In both reconstruction results (based on simulation and measurements) the position of the leakage object can be estimated. Additionally, the connection to ground can be reconstructed.

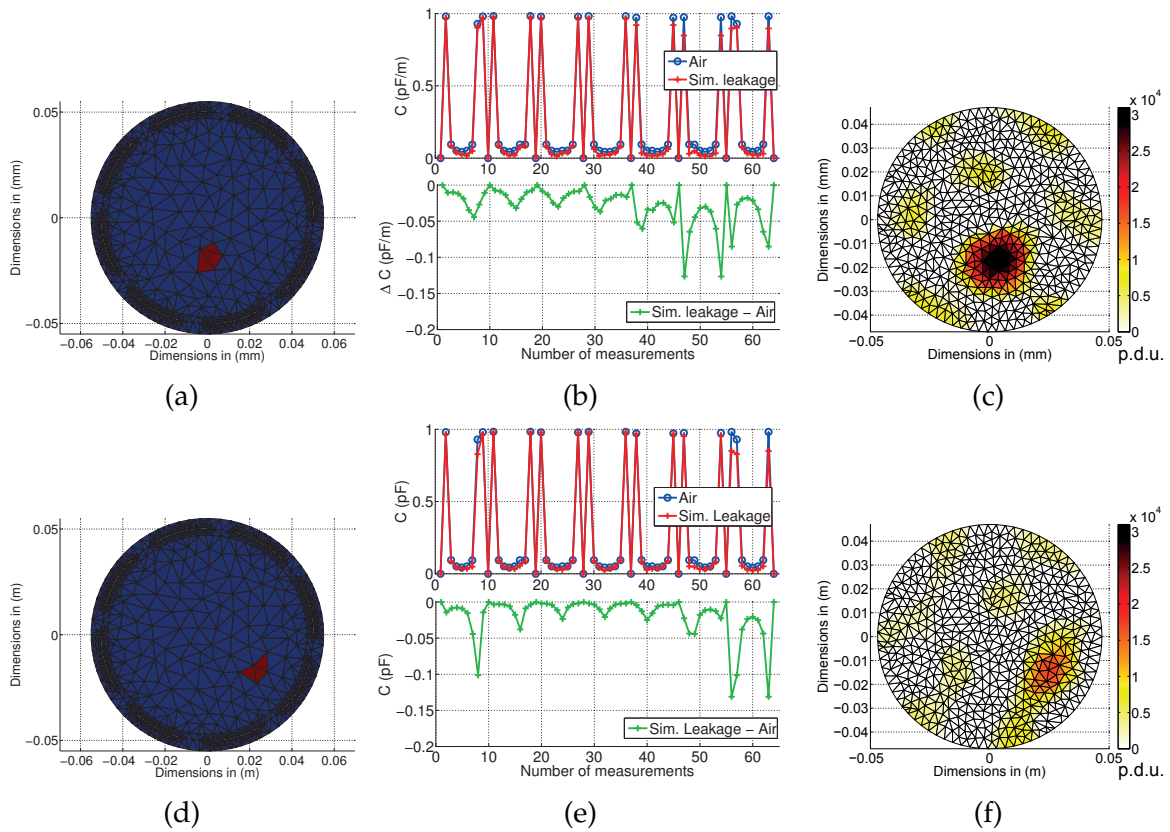


Figure 4.24.: ECT simulation of the leakage effect. (a) and (d) Simulation setups of an ECT pipe including a small area, which is set to a negative charge to simulate the leakage effect. In (a) the amount of negative charge is doubled compared to (d). (b) and (e) Simulation results showing the inter electrode capacitances of an empty pipe, the setup in (a), and the difference of the two (bottom figure). As can be seen, all inter electrode capacitances decrease with a negative charge inside  $\Omega_{ROI}$ . (c) and (f) The reconstruction of the charge in  $\Omega_{ROI}$  matches the true position and the amount of charge can also be reconstructed ((c) nearly doubled compared to (f)).



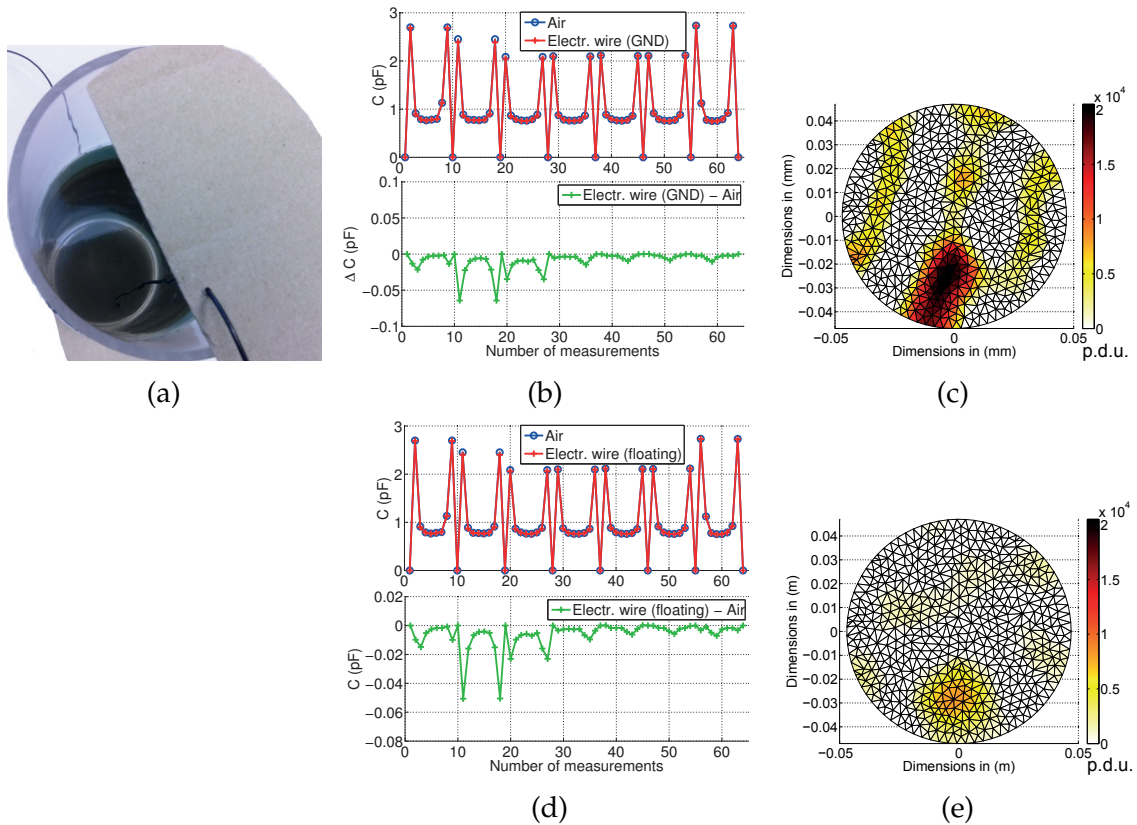


Figure 4.25.: ECT measurements and reconstruction results for a leakage object. (a) Picture of the measurement setup comprising the ECT pipe with the sensing electrodes and an electric wire spanned through  $\Omega_{ROI}$ . The electric wire is connected to world ground (results in (b) and (c)) and left floating (results in (d) and (e)). (b) and (d) Measurement results showing the inter electrode capacitances of an empty ECT pipe, the pipe including the electric wire (connected and not connected to ground, respectively). (c) and (e) Reconstruction results of the electric wire inside  $\Omega_{ROI}$ . The position of the wire can be reconstructed and also the type of connection to ground can be estimated.

### 4.4.3. From ECT to Open Environment Sensing<sup>6</sup>

Fig. 4.26 presents the idea of using an ECT approach for open environment capacitive sensing applications. The enclosed structure of the capacitive array is opened and attached to the surface of interest. The measurements obtained by the measurement circuitry are processed in an ECT manner. Compared to ECT, the open environment is very uncertain in most cases. Additional parasitic effects (shown in Fig. 4.5) can have a huge influence on the measurement results and the measurement circuitry also has to have the ability to deal with these effects (see table 4.3).

In [Sch+13b]<sup>6</sup> it was shown that such an ECT approach can be transferred to the open environment for things such as safety applications. Although it showed promising results, limitations due to the measurement hardware (presented in section 4.4.1) and open environment effects (described in section 4.3.2) were identified. A brief overview is given in section 3.2.6 and a more detailed explanation about the measurement results can be found in [Sch+13b]<sup>6</sup>.

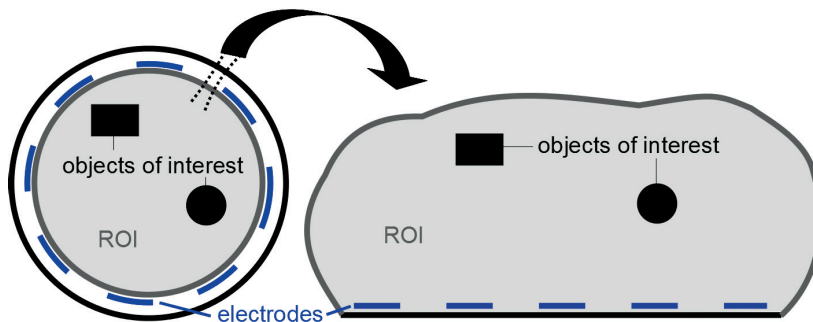


Figure 4.26.: Sketch of the proposed idea of transferring the ECT approach to capacitive sensing for the open environment. The enclosed structure of an ECT system is opened and attached to the surface of interest.  $\Omega_{ROI}$  changes from the well-known inside of e.g. a pipe to the uncertain open environment.

Fig.4.27 shows the measurement electrode setup and the discretized  $\Omega_{ROI}$  for the simulation. The electrodes are made of 100  $\mu\text{m}$  thick copper foil and have a size of 12 mm times 200 mm. Thus, the number of electrodes and their size is in the same range as the electrodes which were used in the ECT configuration. However,  $\Omega_{ROI}$  is approximately 5.6 times bigger in the open environment configuration.

The electrode setup presented here is used for the measurements and reconstruction results in section 5.1.

<sup>6</sup>Parts of this section have been published in [SZ14]<sup>6</sup>

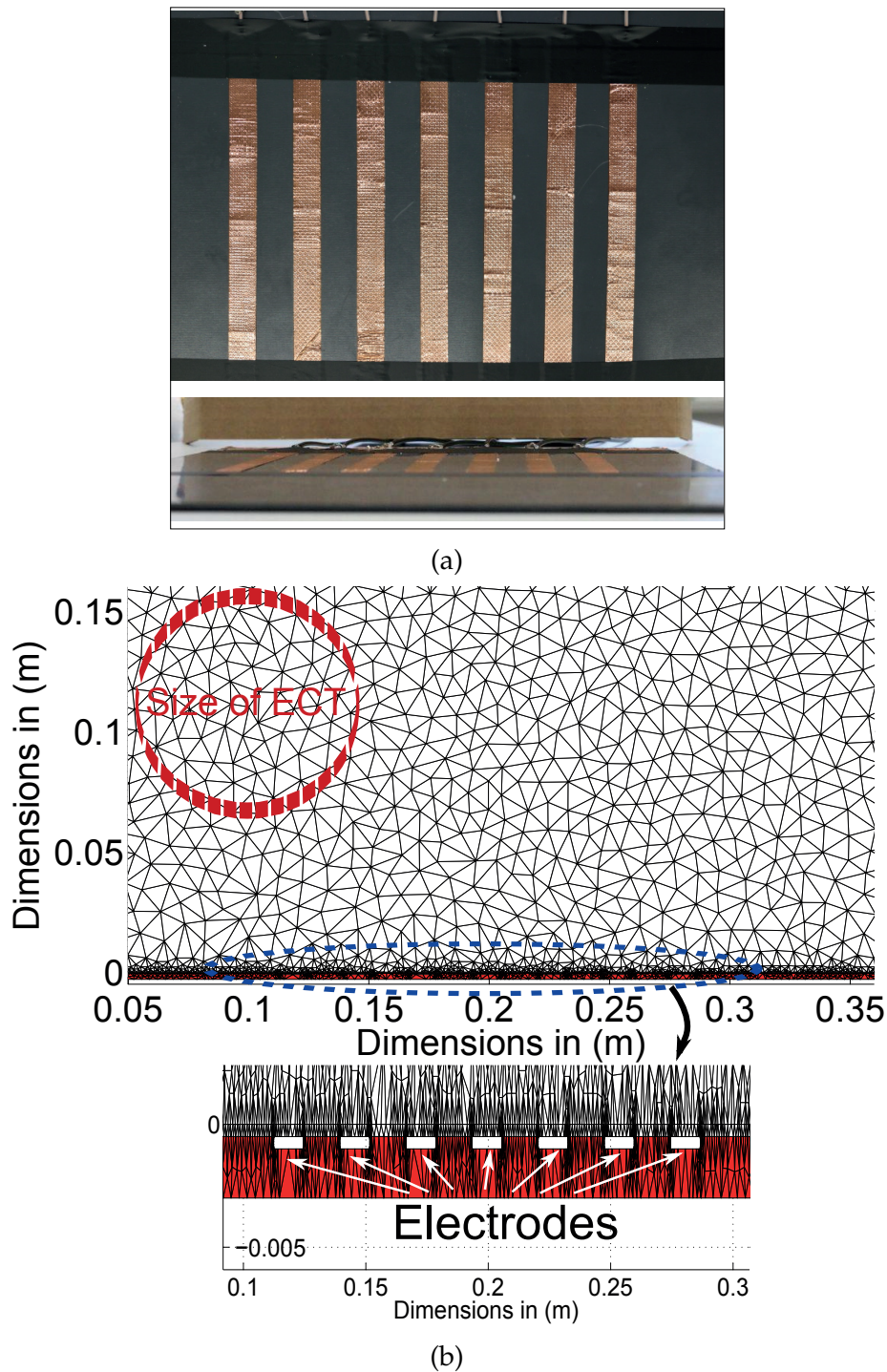


Figure 4.27.: Electrode structure and  $\Omega_{ROI}$  for simulation and reconstruction. (a) Top and front view of the electrode structure used. The seven electrodes and the backside shield (not shown) are made of flexible,  $100\ \mu\text{m}$  thick, copper foil. The 2 mm-thick black spacer is made of polyethylene high-density (PEHD). (b)  $\Omega_{ROI}$  with a detailed close-up of the electrodes. The size is approximately 6 times bigger than  $\Omega_{ROI}$  in the ECT case.

## 4.5. Measurement System for Open Environment Applications

The last section of this chapter deals with the measurement hardware used to obtain the capacitance values of interest. First, possible circuitries and measurement modes are introduced and compared to each other and the requirements acquired in this chapter. Since no commercially available hardware was able to fulfill the stated requirements, a new capacitance measurement device was developed, designed and built. It is presented in the second part of this section. Illustrative measurement results prove the feasibility of the design and close this section and chapter.

### 4.5.1. Measurement Circuitries and Modes<sup>7</sup>

There exist a huge variety of measurement circuitries for measuring electrical capacitances. A coarse classification presented in [Bax97] can be listed as follows

- Direct DC
- Oscillators
- Single-ended
- High-Z
- Low-Z
- Bridge

Table 4.3 gives an overview of the circuitries most commonly used for proximity sensing (i.e., direct DC and single-ended measurement systems are not taken into account). This work focuses on the effects that arise when capacitive sensing gets into the open environment (which is most often the case in safety applications) rather than on the different properties of the circuitries. The interested reader can refer to [Bax97; Cui+11; Weg+05] and to the literature referenced therein for more information on capacitance measurement circuitries.

It is also possible to distinguish the sensing system by the measurement mode used. The two different modes are often denoted as

- Mutual capacitance mode.
- Self capacitance mode.

The first mode utilizes measurements of the capacitance between two electrodes by applying voltage on one electrode and measuring e.g. the displacement current on the other electrode (i.e., Low-Z circuitry). The second mode utilizes measurements of the displacement current originating from one electrode to the distance ground.

---

<sup>7</sup>Parts of this section have been published in [SZ14]

Table 4.3.: Comparison of different capacitive sensor front-end circuitry (adopted from [Zano5]). The lower part of the table indicates whether a circuit is sensitive (-) or insensitive (+) to one of the parasitic effects shown in Fig. 4.5.

Class Circuit	Oscillators		High Z		Low Z		Bridge CF
	RC	SC	CF	DC	CA	CF	
Guarding	active	passive	active	active	passive	passive	passive
ADC required?	no	no	yes	yes	yes	yes	yes
BP filtering	no	no	difficult	diff.	possible	possible	possible
Complexity	low	low	high w. guarding	low	medium	high	high
Sens. to res. shunt	yes	minor	yes	yes	medium	minor	minor
Extended wire length?	minor	minor	no	no	minor	yes	yes
Long time stability	moderate	moderate	low to medium	low to medium	moderate	low to medium	medium/low
Short time stability	good	good	good	good	good	good	good
EMC emission	low	SR limit.	very low	very low	SR limit.	SR limit.	SR limit.
EMC sensitivity	high	medium	low	high	medium	low	low
Spark discharge sens.	low	low	(freq. shifting)	high	low	(freq. shifting)	(freq. shifting)
Measurement rate	low	low	high	high	low	low	low
Matching	medium	good	medium	high	high	medium	medium
Power consumption	low	low	medium	medium	good	good	good
			moderate	low	low	moderate	medium
Suppression of:							
$R_{1\_GND}$	+	+	+	+	+	+	+
$C_{1\_GND}$	+	+	+	+	+	+	+
$R_{1,2}$	-	+	-	-	+	+	+
$R_{2\_GND}$	+	+	-	-	+	+	+
$C_{2\_GND}$	+	+	-	-	+	+	+
$U_{D1}$	-	+	+	+	+	+	+
$U_{D2}$	+	-	-	-	-	-	+
ESD 1	-	+	+	+	+	+	+
ESD 2	+	+	-	-	+	+	+

RC: Resistor/Capacitor; SC: Switched Capacitor; CF Carrier Frequency; CA Charge Amplifier; DC Direct Current; SR limit.: Slew rate limitation required.

A difficulty associated with the self capacitance mode is the fact that the sensitivity is quite high at the edges of the electrodes in particular when conductive objects reside in the vicinity, e.g. as the carrier of the electrode. In this case, moisture and contamination may significantly affect the measurement and a reliable proximity determination might not be possible. A commonly used method to cope with this problem is active guarding where a guard is placed between the actual electrode and a metallic carrier. Thus, the sensitivity moves away from the edges of the electrodes. However, this also leads to reduced sensitivity with respect to small objects in the vicinity of the electrodes. On the other hand, the self capacitance mode usually offers a higher SNR than the mutual capacitance mode and, in conjunction with active guarding, a high robustness. The mutual capacitance mode usually has a worse SNR but has the capability to detect objects in situations where the self capacitance mode is blind. Thus, a measurement circuitry that combines both measurement modes is preferable for applications where objects of different sizes and permittivities in different distances from the sensor surface have to be measured (e.g. in safety applications).

In the following section, the different types of measurement hardware used in the example applications in section 3.2 are presented. Measurement results are shown where applicable and the different approaches for safety applications are compared.

#### 4.5.2. Capacitance Measurement System<sup>8</sup>

Taking into account the parasitic effects that occur in open environment measurements (presented in section 4.3.2) and following the proposed ECT approach in section 4.4, a new capacitance measurement hardware is presented in [Sch+13a]'. The beneficial nature of this measurement system is described as it compares to the example applications in section 3.2. A comparison against two commercially available capacitance measurement systems highlights the performance of the presented system. Furthermore, the measurement system is tested in a robot application and its feasibility is demonstrated by means of experimental investigations.

##### Design of the Evaluation Circuitry

An overview of the measurement system presented is shown in Fig. 4.28(a). A sinusoidal signal, generated by a direct digital synthesizer (DDS), is applied to one or more electrodes through switch circuitry. The displacement current originating from the electrodes used as transmitters is measured by transmitter circuitry [Sch+13a]'.  

---

<sup>8</sup>Parts of this section have been published in [SZ13; SZ14]'



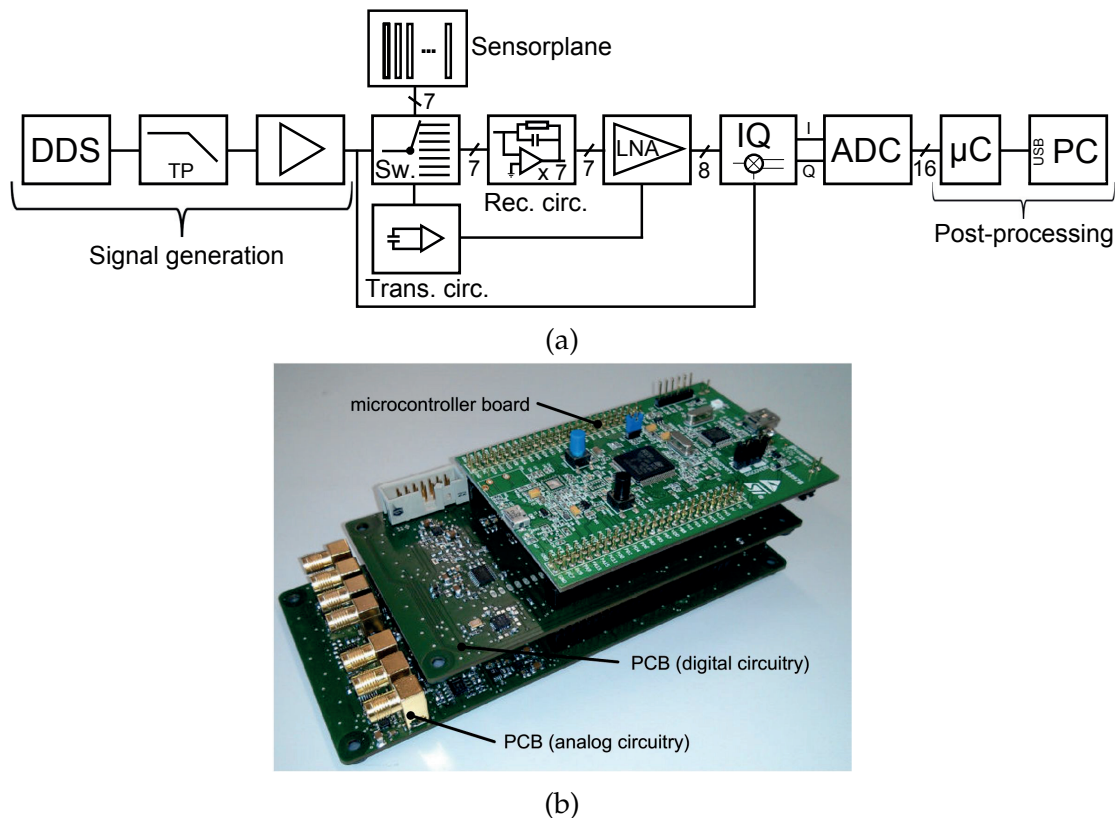


Figure 4.28.: Proposed capacitance evaluation circuitry. (a) Overview of the different parts of the measurement system. (b) Picture of the three stacked PCBs of the evaluation circuitry.

Each electrode is also connected to receiver circuitry. If an electrode is not used as a transmitter, the receiver circuitry measures the displacement current entering this electrode. Since each electrode can be used as a transmitter or a receiver, a total of  $\frac{N_{elec}(N_{elec}-1)}{2}$  independent measurements, where  $N_{elec}$  is the number of electrodes, can be obtained with the mutual capacitance mode. With the additional self capacitance mode, a total of  $\frac{N_{elec}(N_{elec}-1)}{2} + N_{elec}$  independent measurements can be obtained. Additionally, the backside of the sensor can be connected to ground (mutual capacitance mode) or to the excitation signal (i.e., active guarding in self capacitance mode). This function is also possible with each electrode if the electrode is not used as transmitter or receiver. After amplification, an IQ-Demodulator is used to get phase and amplitude information from the measured signals with respect to the excitation signal. The post processing consists of an ADC and a microcontroller ( $\mu C$ ). The  $\mu C$  is used to control the measurement hardware (e.g. analog digital converter (ADC), IQ-Demodulator, DDS, etc.), store the measurement signals and communicate with a host computer to do further post processing (e.g. reconstruction algorithms).



Table 4.4.: Properties of the proposed measurement system compared to state-of-the-art sensors

	Proposed sensor	AD7746	AD7148
Excitation signal	Sinusoidal signal	Square wave	Square wave
Frequency	Tunable from 10 kHz to 1000 kHz	32 kHz	250 kHz
Measurement rate	1.25 kHz (max. 6.25 kHz @ 1 MHz)	10 Hz to 90 Hz	40 Hz
Measurement method	Self cap. and Mutual cap. mode	Mutual cap. mode	Self cap. mode
Shielding	Active guarding and Grounded shielding	Grounded shielding	Active guarding
Number of electrodes	$N_{elec} = 7$	$N_{elec} = 3$	$N_{elec} = 8$
Number of independent measurements	$28 \left( = \frac{N_{elec}(N_{elec} - 1)}{2} + N_{elec} \right)$ for each frequency	2	8

The proposed measurement system (shown in Fig. 4.28(b)) is able to work in mutual capacitance mode and self capacitance mode. It provides a high measurement rate ( $> 1$  kHz). The measurement frequency can be changed between 10 kHz and 1 MHz to any frequency value of interest. Thus, it is possible to obtain additional information about parasitic effects due to their frequency dependency as shown in Fig. 4.5. This also provides additional information for material classification [Kir+08]. Furthermore, a change in measurement frequency can be used to deal with EMC problems as shown in [Bra03].

As shown in Fig. 4.28(b), the measurement hardware consists of three stacked PCB. The top PCB is a commercially available microcontroller evaluation board. The PCB positioned centrally comprises all digital parts (e.g. clock generator, DDS, ADC, etc.). The bottom PCB comprises the analog circuitries such as transmitter and receiver circuitries and IQ-Demodulator.

Since each electrode can be used as a transmitter and receiver, the proposed measurement system can also be used for ECT applications. Thus, it is appropriate for the stated approach to capacitive safety applications in section 4.4.

### Comparison with State-of-the-Art Capacitive Sensors

Table 4.4 gives an overview of the proposed measurement system [Sch+13a] and two commercially available systems [Ana14]. One of the commercially available measurement systems works in self capacitance mode (AD7148) and the other one works in mutual capacitance mode (AD7746). Although there exists a huge variety of capacitance measurement systems (see section 3.2), these systems are appropriate as state-of-the-art systems by means of resolution and speed (i.e., measurement update rate).

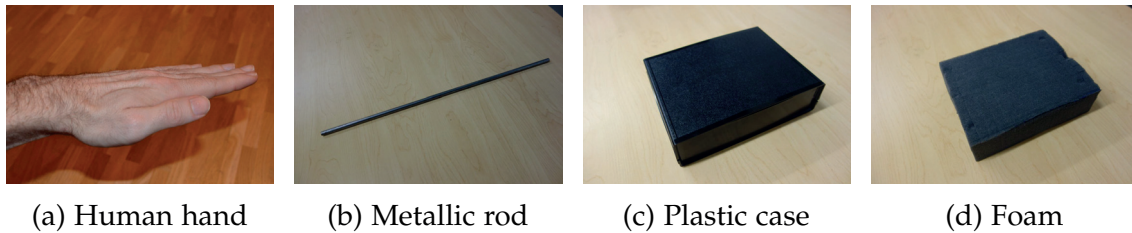


Figure 4.29.: Sample objects to test the capacitive measurement system. (b) An iron rod is used to show the properties for conductive objects (connected and not connected to ground). (c) Dielectric objects such as this PVC case can be detected even if they are small in volume and have a low permittivity ( $\epsilon \approx 2$ ). (d) The foam material consisting of polyurethane (PUR), which has a very small electric permittivity ( $\epsilon \approx 1$ ) shows the limitations of the sensor as it cannot be used for collision avoidance.

Several experiments (Fig. 4.30(a) to 4.30(c)) were carried out in [Sch+13a]’ with the proposed measurement system and different test objects shown in Fig. 4.29. The system is compared to the two commercially available ones (Analog Devices AD7148 and AD7746 [Ana14]). In the first experiments shown in Fig. 4.30(a), a human hand (shown in Fig. 4.29(a)) approaches the sensor surface and then retreats. The human hand can be detected in self capacitance mode as well as in mutual capacitance mode with all three measurement systems (proposed sensor and commercially available ones). However, due to shielding and coupling effects (described in section 4.3.3) at a certain distance from the sensor surface, the measured capacitance increases (marked with arrows in Fig. 4.30(a)). This effect can yield ambiguities in proximity determination. An approaching metal bar (see Fig. 4.29(b)) shows SNRs similar to those of a human hand. It can be detected by all three measurement systems. Objects with low permittivity  $\epsilon_r$  (i.e., close to 1) are difficult to detect with a self capacitance mode measurement system. As can be seen in Fig. 4.30(c), the plastic box shown in Fig. 4.29(c) can be detected by the proposed measurement system in the mutual capacitance mode and for close distances in the self capacitance mode. With the two commercially available measurement systems it is very difficult to detect this kind of object (i.e., low permittivity and low volume). Similarly, it is difficult to detect the foam material shown in Fig. 4.29(d) with the commercially available sensors. The proposed measurement hardware is still able to detect the foam in self capacitance mode.

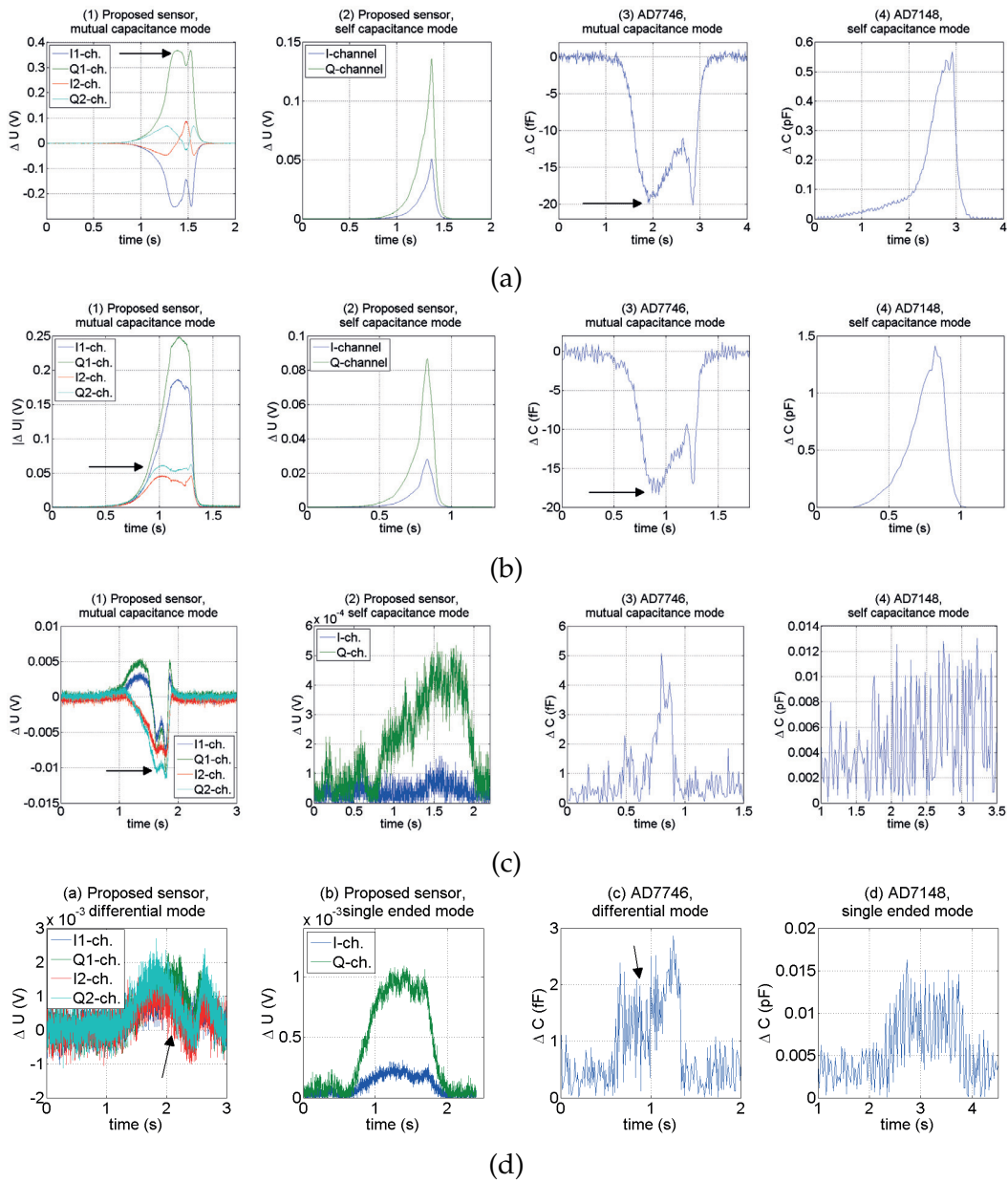


Figure 4.30.: Measurement results for four different objects obtained with the proposed capacitance measurement system and two commercially available systems [Sch+13a]'. (a) A human hand approaching and leaving the sensor surface. Black arrows indicate the transition from shielding to coupling mode (refer to section 4.3.3). (b) A metal bar approaching and leaving the sensor surface. (c) An empty plastic box approaches and leaves the sensor surface. With the self capacitance mode it is difficult to detect the approaching box. However, the proposed measurement system working in mutual capacitance mode is able to detect even objects which have such a low permittivity and small volume. (d) Only the self capacitance mode of the proposed measurement system is able to detect a foam material approaching the sensor surface.

# 5. Object Detection and Classification

This chapter introduces two application examples. Raw measurement results have already shown in section 4.5. The first application aims to show the performance of the developed measurement circuitry (see section 4.5) using the presented leakage reconstruction method (presented section 4.3.4). The second application shows the usage of the capacitance measurement circuitry in a highly reactive robotic application. Together, both applications should give the reader an idea of the wide range of use of the measurement circuitry developed here.

## 5.1. Reconstruction in the Open Environment

Many algorithms could be used to reconstruct the spatial permittivity distribution in an ECT manner (compare [Neu+11]). The approach presented here to reconstruct the spatial permittivity and leakage distribution is based on the algorithm presented in section 4.4 and adopted according to section 4.3.4. Thus, a calibration scheme is necessary and is presented below.

### 5.1.1. Calibration for Open Environment Sensing

A similar reconstruction method as was used in the ECT case above is used in the following open environment setup. Thus, an offset- and gain-calibration (i.e. two point calibration) is used similar to the ECT case. This calibration is also necessary when using simulated data instead of measurement data. It has to be done for the reconstruction of the relative permittivity and the leakage current. In the case of relative permittivity reconstruction, the calibration is the same as within ECT (empty pipe and pipe completely filled with a PVC rod).

The calibration scheme for the leakage reconstruction is different. The first calibration point is similar to the ECT case.  $\Omega_{ROI}$  is measured without any objects (i.e. only with air). Since all electrodes should be influenced by the same leakage current, a conductive plate connected to circuitry ground and at a certain distance from the sensor surface is used for the second calibration point. For the simulation

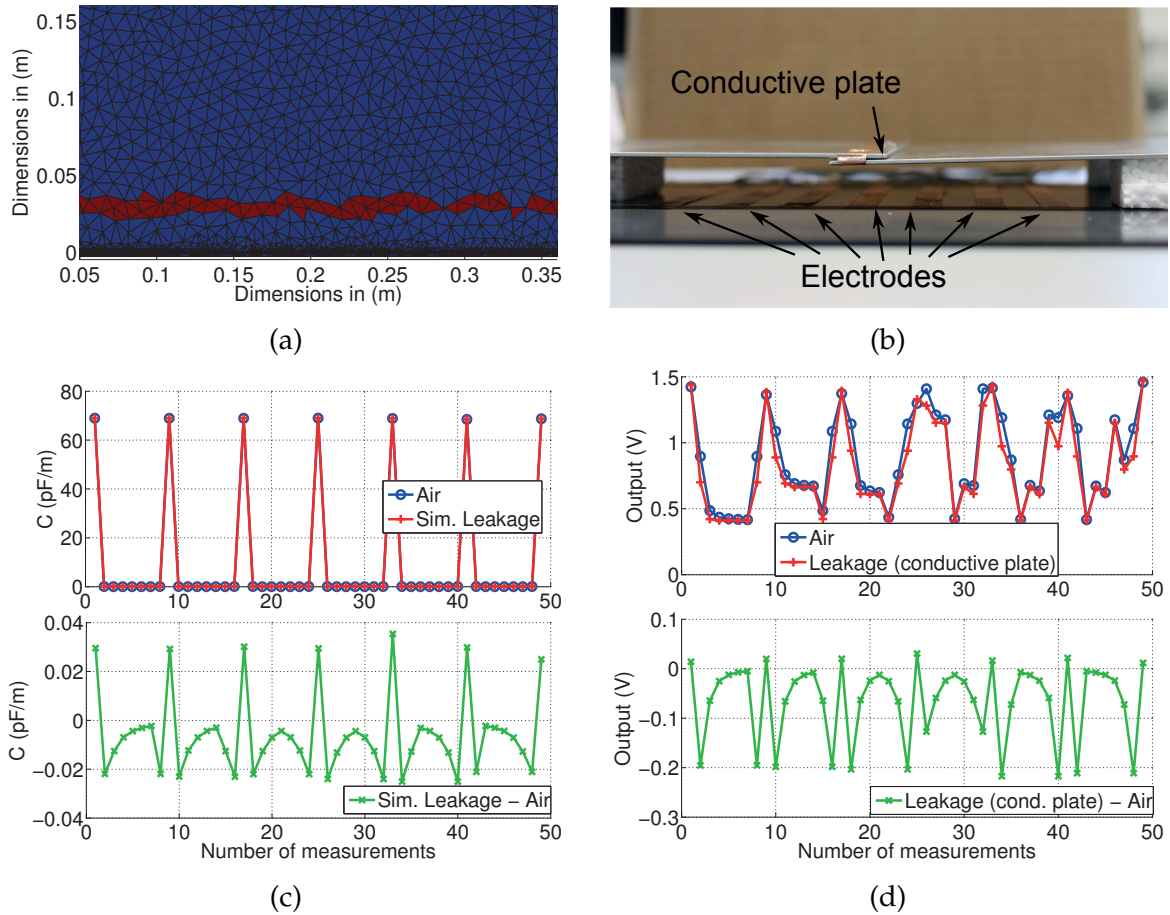


Figure 5.1.: Calibration schemes and measurement results for the leakage effect. (a) . (b) . (c) . (d) .

of the forward problem a rectangular bar with a certain value of  $B$  was simulated above the electrodes. Both cases (simulation and measurement calibration setup) and corresponding results are shown in Fig. 5.1.

Although the transmitting current is much higher in the simulation, the difference between an empty  $\Omega_{ROI}$  and the leakage calibration object is similar in both cases. As can be seen in Fig. 5.1(c) and (d), transmitting currents (i.e. leakage currents) increase while receiving currents (i.e. coupling currents) decrease. Thus, the simulation maps the measurements and the leakage simulation approach from section 4.3.4 can be used for the reconstruction of the leakage map.

## 5.1.2. Reconstruction Results for Dielectric and Leakage Objects

### Dielectric Objects

This sections presents results from reconstructions based on simulated data as well as real-world measurements. The reconstruction algorithms that were used are described in section 4.4 (common ECT reconstruction) and section 4.3.4 (novel leakage reconstruction). The following configurations are reconstructed and presented in this section:

- Simulated dielectric object at different positions
- Measurements of similar dielectric object at different positions
- Simulated grounded object at different positions
- Measurements for two different grounded objects at different positions

Fig. 5.2 shows a simulated dielectric object ( $\epsilon_r = 3$ ) at certain positions in  $\Omega_{ROI}$ . Since the transmitting current has no effect (minor leakage current occurs for small dielectric objects), it is neither simulated nor measured in this measurement setup. The first position farthest away from the sensor surface the simulated results (Fig. 5.2(b)) are nearly equally affected (compared to the simulation results with an air-filled  $\Omega_{ROI}$ ). Thus, the reconstruction result cannot determine the spatial relative permittivity distribution of the object of interest. The result can however, be used as an indication for any object in  $\Omega_{ROI}$ .

In Fig.5.2(d) to 5.2(f) the same dielectric object ( $\epsilon_r = 3$ ) is used but positioned closer to the sensor surface. As can be seen, the simulated results are unequally distributed. Pairs of electrodes closer to the object (for example, electrode pairs in the middle: 3 – 4, 4 – 5) receive a higher capacitance change than, for example, pairs on the left or right side (for example, electrode pair: 1 – 2, 6 – 7). Due to the soft field property of capacitive sensing [Maro6], the size and orientation is difficult to reconstruct for objects at farther distances. Nevertheless, the reconstruction algorithm finds a 2-D picture, which can be used for object detection.

The third and fourth position (Fig. 5.2(g) to 5.2(l)) are closer to the sensor surface (approximately 15 mm). Again, the pairs of electrodes, which are closer to the object, receive a higher capacitance change. The reconstruction algorithm is able to reconstruct the position and size of the approaching object in  $\Omega_{ROI}$ .

The measurements and reconstruction results in Fig. 5.2 show similar performance compared to a common ECT system (see section 4.4 and for example [Wego6; Pen+12]). It has to be mentioned that the image quality of the reconstruction method not only depends on the measurement circuitry and the electrode structure, but also (to a great extent) on the reconstruction algorithm used (see section 4.4). In this thesis the focus lies more on the front end circuitry and electrode structure than



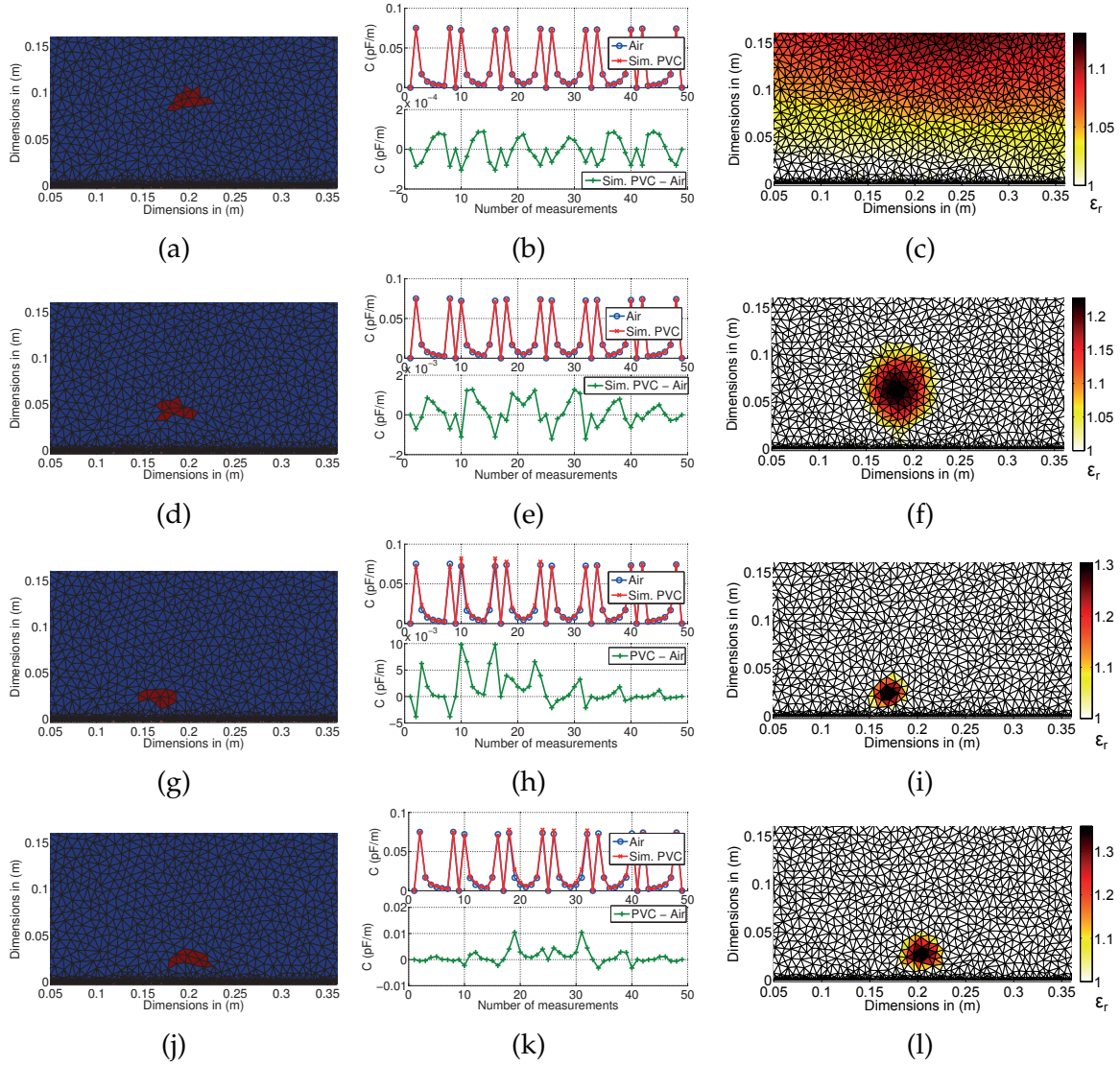


Figure 5.2.: Open environment simulation and reconstruction of a dielectric object at different positions. (a), (d), (g), and (j) show the simulated object and its position in  $\Omega_{ROI}$ . The objects' relative permittivity  $\epsilon_r$  is set to 3.5. (b), (e), (h), and (k) show the simulation results for each position. In (c), (f), (i), and (l) the reconstruction results are shown. For the object farthest away from the sensor surface (shown in (a)) no position or size of the object can be reconstructed. Only the presence of an object can be detected. For closer distances a localization and size estimation is possible. A more detailed explanation of the results is referred to in the text.



the reconstruction algorithm. More information about reconstruction algorithms can be found in [Neu+11] and the literature referenced therein.

The results with the simulated forward problem are validated with real-world measurements shown in Fig. 5.3. All measurements were taken with the measurement circuitry presented in section 4.5. As mentioned above, small dielectric objects with a small capacitance to the world ground induce minor leakage. Thus, the measured transmitting current does not change and is neither simulated nor measured in this measurement setup.

Similar to the simulation results, the PVC object farthest away from the sensor surface by approximately 100 mm shown in Fig. 5.4(d) to (c) cannot be reconstructed. Although the capacitances indicate an object (increase compared to an air filled  $\Omega_{ROI}$ ), the objects position cannot be reconstructed.

A dielectric object closer to the sensor surface as shown in Fig. 5.4(g) does have a higher influence on the measured capacitances. Fig 5.3(e) shows especially neighbouring pairs of electrodes suffer to a great extent from the shielding effect. Thus, the measured capacitance is decreased. Similar to the ECT case, this is not a problem for the reconstruction of the spatial permittivity distribution. Since the shielding effect is a 2-D effect, it also occurs in the simulation of the forward problem (see Fig. 5.2(e)) and thus, can be “handled” by the reconstruction algorithm. The reconstructed picture in Fig. 5.3(f) suffers from high blurring (according to the soft field property of the sensing principle and the measurement noise) but an approaching object can be identified. For closer distances (approximately 10 mm) the objects’ relative permittivity, size and position can be reconstructed to some extent. The measurement results show that at close distances, the shielding effect has only minor influence (see section 4.3.2). Again, the measurement results show the same trends as the simulation results. Thus, with the presented measurement circuitry and electrode structure, open environment sensing is possible for dielectric objects and results in performances similar to ECT.

### Leakage Objects

“Leakage objects” refer to objects which have a good connection (i.e. high capacitance or susceptance  $B$ ) to ground. For solving the forward problem, the presented approach in section 4.3.4 is used. To validate the approach, a small object (size of 1 or 2 finite elements) at different positions is simulated and reconstructed in Fig. 5.4. Since the leakage effect mainly contributes to the transmitting currents, they are also simulated in this measurement setup.

Fig. 5.4(a) shows two finite elements at the centre of  $\Omega_{ROI}$  connected to ground (i.e. a certain value of  $B$  is applied to these two elements). As can be seen in

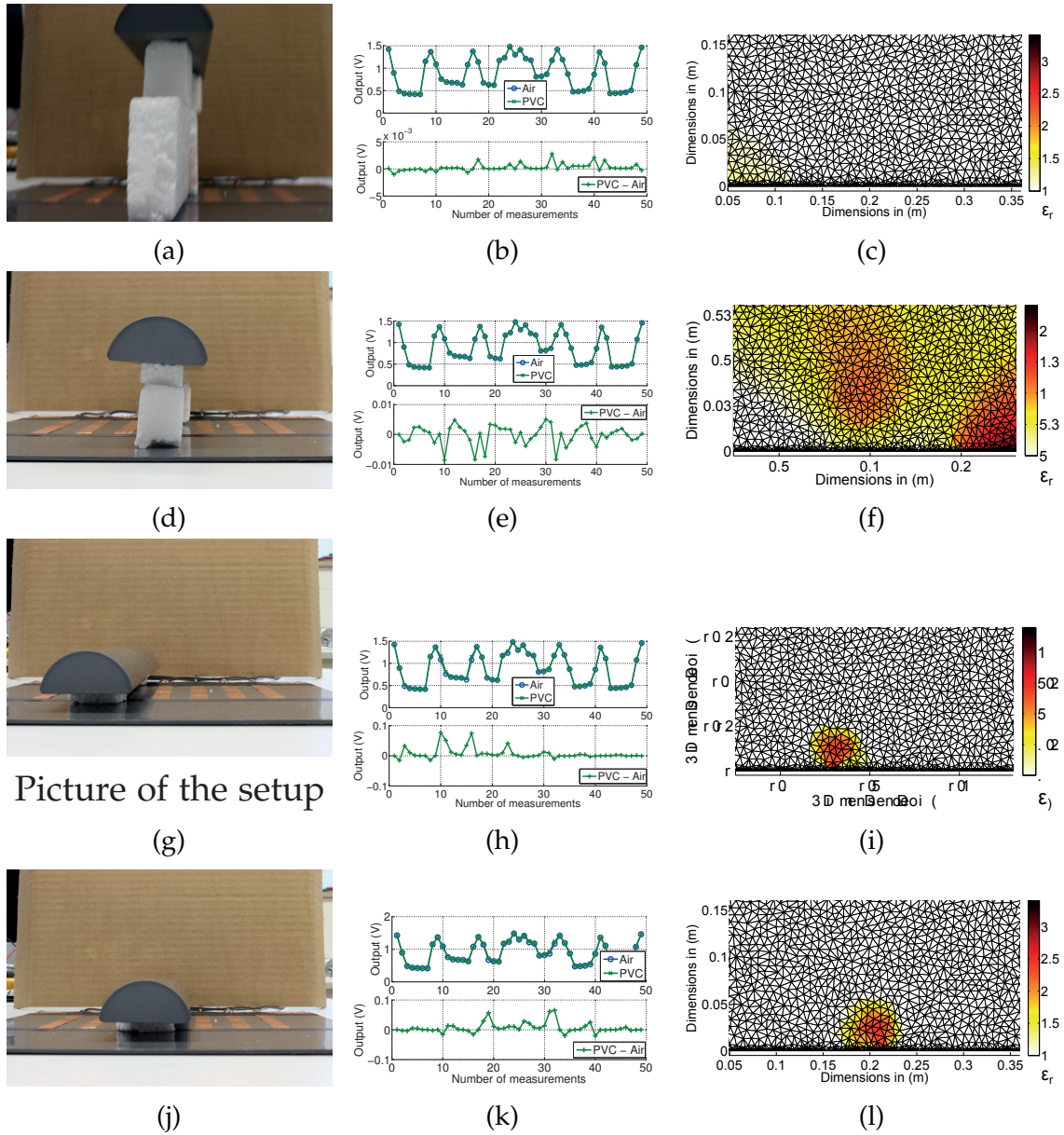


Figure 5.3.: Open environment measurements and reconstruction results for a dielectric object in  $\Omega_{ROI}$ . (a) to (c) The PVC bar ( $\epsilon_r \approx 3$  at a measurement frequency of 1 MHz) cannot be reconstructed due to the distance (approximately 100 mm). (d) to (f) For a closer distance (approx. 35 mm) the measurement signal suffers from the leakage effect, but a blurry spatial permittivity distribution can be reconstructed. (g) to (l) The object of interest can be reconstructed and its position and size can be determined.

Fig. 5.4(b) the transmitting current (i.e. capacitance from one electrode to ground) outweighs all inter electrode capacitances. Since only one forward problem is solved for determining the whole capacitance matrix  $C$ , no active guarding is used. Thus, when measuring the capacitance between one electrode and ground, all other electrodes are set to ground resulting in a high capacitance. Compared to the measurement result without a leakage object (i.e. only air in  $\Omega_{ROI}$ ), all inter electrode capacitances decrease and the electrode-ground capacitance increases. For an object further away, the reconstruction result is shown in Fig. 5.4(c). The result is blurry and thus the size does not fit the true object. However, the object can be identified to be in  $\Omega_{ROI}$  and its connection to ground can also be estimated.

For closer objects (for example shown in Fig. 5.4(d)), the measurement results are similar to the ones for the object further away. The position of the object on the x axis can easily be determined from the electrode-ground capacitances as shown in Fig. 5.4(e). The electrode with the highest increase of transmitting current (i.e. highest capacitance to ground) is closest to the leakage object. The reconstruction result in Fig. 5.4(f) shows a good estimation of the leakage object. It is still blurry but the position and connection to ground can be determined.

Fig. 5.4(g) to (i) show the position, measurement and reconstruction results for a leakage object very close (approx. 10 mm) above one electrode. The electrode-ground capacitance of this electrode is much higher compared to the others and almost no inter electrode capacitances change compared to the measurements without any object. Thus, the reconstruction shows a conductive object very close to the effected electrode, but the size and value for the conduction to ground differ from the true simulated value.

As can be seen from the measurement results in Fig. 5.4, the transmitting currents are much higher compared to the inter electrode capacitances. As will be shown later, this is not the case in real world measurements. In the simulations no active guarding was used. Thus, a high displacement current runs from the transmitting electrode to the grounded shield at the back side. This has no effect on the reconstruction result since only the difference with and without an object in the vicinity of the sensor surface is taken into account.

The simulations and reconstructions above validate the approach presented in section 4.3.4. In the next experiments, the developed measurement hardware is used to take static measurements from “leakage objects” (i.e. with a good connection to ground). Similar to the simulation figures, the measurements of the transmitting current and all inter electrode capacitances are plotted and subtracted from an empty measurement. Afterwards, the reconstruction of the spatial susceptibility distribution in 2D is attempted. The contour plot holds arbitrary units (or procedure-defined units, p.d.u.), which shows the ratio between no connection to

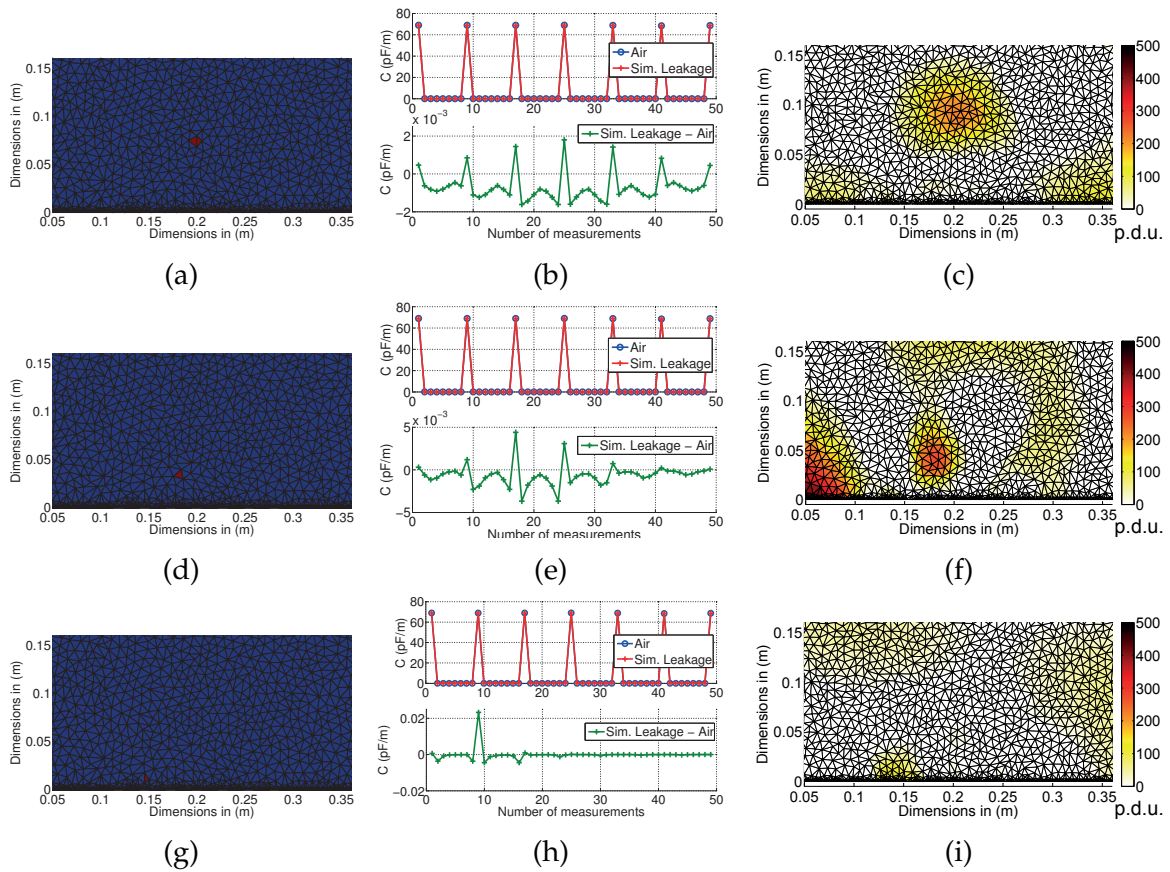


Figure 5.4.: Open environment simulation and reconstruction of a “leakage” (i.e. good connection to ground) object. (a), (d), and (g) show the different position of the small object (one or two finite elements), which are the author attempts to reconstruct. (b), (e), and (h) show the results of the simulated forward problem and followed the approach presented in section 4.3.4. (c), (f), and (i) The reconstruction results show promising performance. Even objects far away (approx. 80 mm) can be reconstructed. It is difficult to reconstruct objects that are very close to one electrode since the inter electrode capacitances get very small and only the relating electrode-ground capacitance increases highly.



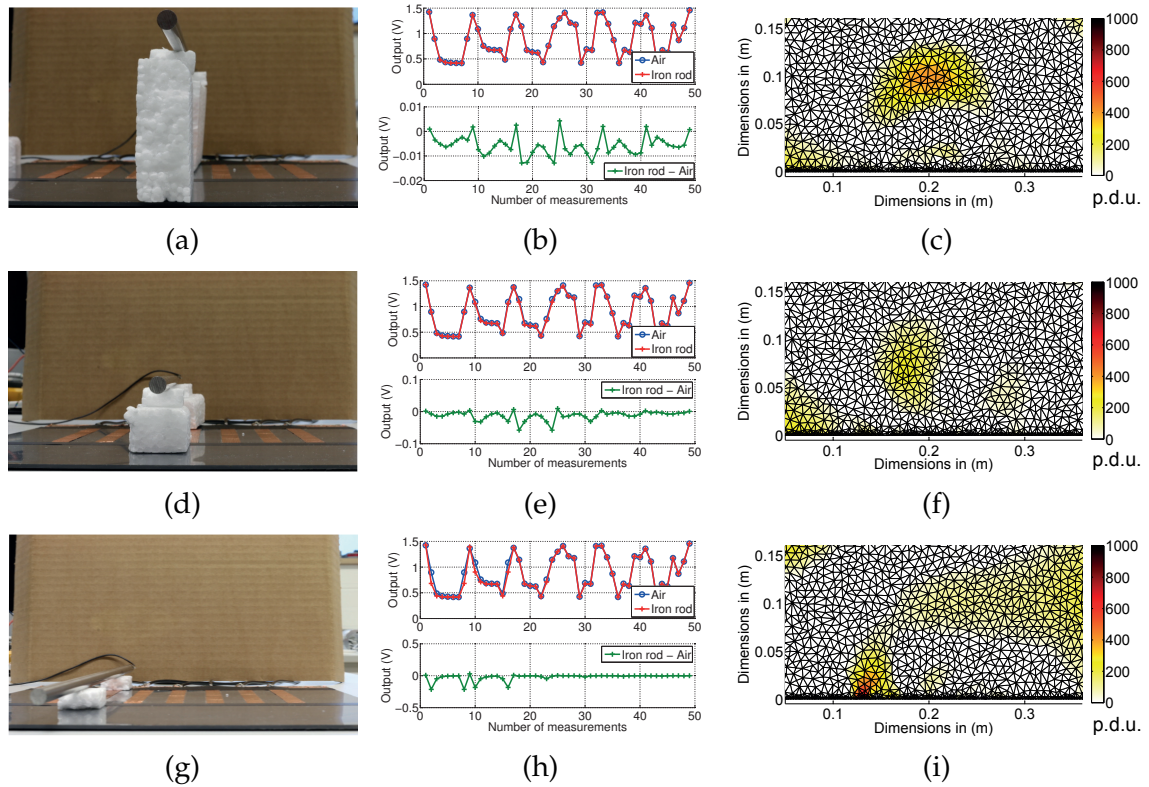


Figure 5.5.: Open environment measurements and reconstruction of a “leakage” iron rod (i.e. iron rod with a good connection to ground). (a), (d), and (g) show the different positions of the iron rod above the sensor surface. (b), (e), and (h) show the measurement results for the iron rod. As can be seen from the differences (lower pictures of the measurement results), the measured capacitance decreases in mutual capacitance mode and increases for the self capacitance mode. (c), (f), and (i) The reconstruction results for an iron rod. Each position can be reconstructed. Although, the reconstructions results get blurrier for farther distances.

ground and a defined connection to ground from the calibration measurements (see section 5.1.1).

The first object is an iron rod connected to ground and placed at three different positions above the sensor surface (see Fig. 5.5(g), 5.5(d), and 5.5(a)). As can be seen from the pictures, the iron rod is placed on Styrofoam ( $\epsilon_r \approx 1$ ) to avoid any influence from other objects in the vicinity. The measurement results obtained are similar to the simulation results for all three positions. The self capacitance measurements show a lower amplitude compared to the simulations. As explained above, active shielding is used in the measurements, which prevents a high capacitance at the backside. Thus, the measurement of transmitting currents was smaller compared to the simulation results. Similar to the simulation results, the reconstructions result is blurry for positions farther away from the sensor surface (see Fig. 5.5(c) and 5.5(f)). For closer distances such as shown in Fig. 5.5(g), the reconstruction algorithm is able to estimate the size and position of the “leakage object”.

The second “leakage object” is a simple electric wire made of copper with a diameter of 0.8 mm connected to ground. Again, Styrofoam is used to place the wire at a certain position above the sensor surface. Although the diameter of the wire is much smaller than the iron rod, similar measurement results were obtained. The reconstruction results also showed similar spatial susceptance distributions. Since copper and iron differ by a factor of approximately 6, the copper wire does have a similar leakage current compared to the bigger iron rod.

The last experiment shows the benefits of the proposed 2.5D reconstruction compared to the usual 2D reconstruction used in ECT applications. In Fig. 5.7, a human hand is shown at two positions above the sensor surface. Styrofoam is used to ensure repeatable measurement setups. Since its relative permittivity is similar to that of air, it does not have any influence on the obtained measurements. As can be seen from Fig. 5.7(b) and 5.7(f), the measurement results show similar trends compared to the measurements with an iron rod and an electric wire. The transmitting capacitances increase and the inter electrode capacitances decrease as the human hand is in the vicinity of the corresponding electrodes. Fig. 5.7(c) and 5.7(g) demonstrate an attempt to reconstruct the spatial permittivity distribution as it is commonly done in ECT applications. Due to the leakage effect no suitable result was obtained. Although the human hand has a relative permittivity higher than that of air, the leakage effect has such a high influence that the obtained capacitances decrease compared to a measurement without any object in  $\Omega_{ROI}$ . The reconstruction of the leakage map is shown in Fig. 5.7(d) and 5.7(h). It is evident that the position and the size can even be estimated for farther distances. Thus, object detection is still possible and collision, for example, could be avoided.

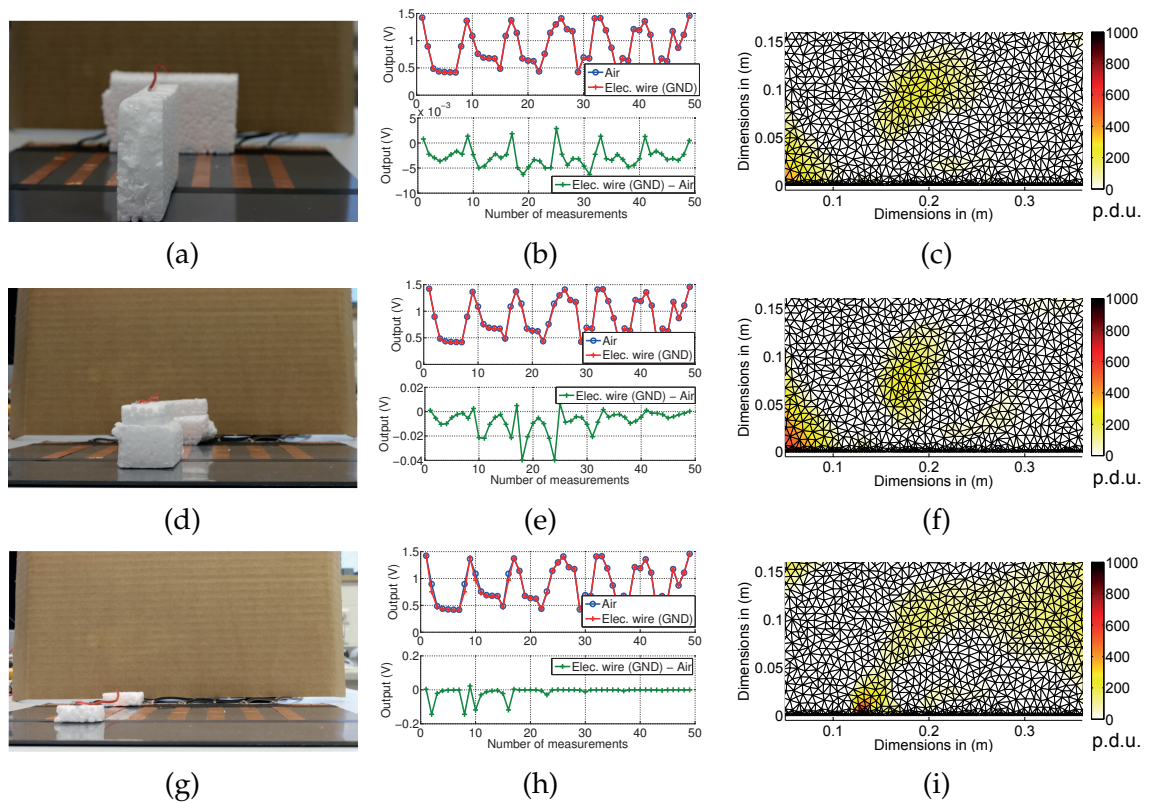


Figure 5.6.: Open environment measurements and reconstruction of a “leakage” electric wire (i.e. electric wire with a good connection to ground, 0.8 mm in diameter). (g), (d), and (a) show the different positions of the iron rod above the sensor surface. (h), (e), and (b) show the measurement results for the electric wire. As can be seen from the differences (lower pictures of the measurement results), the measured capacitance decreases in mutual capacitance mode and increases for self capacitance mode. For very close distances, the position of the electric wire can even be estimated from the measurement results (above the electrodes with the highest difference). (i), (f), and (c) The reconstruction results for an electric wire above the sensor surface. Each position can be reconstructed. However, the reconstructions results get blurrier at farther distances.



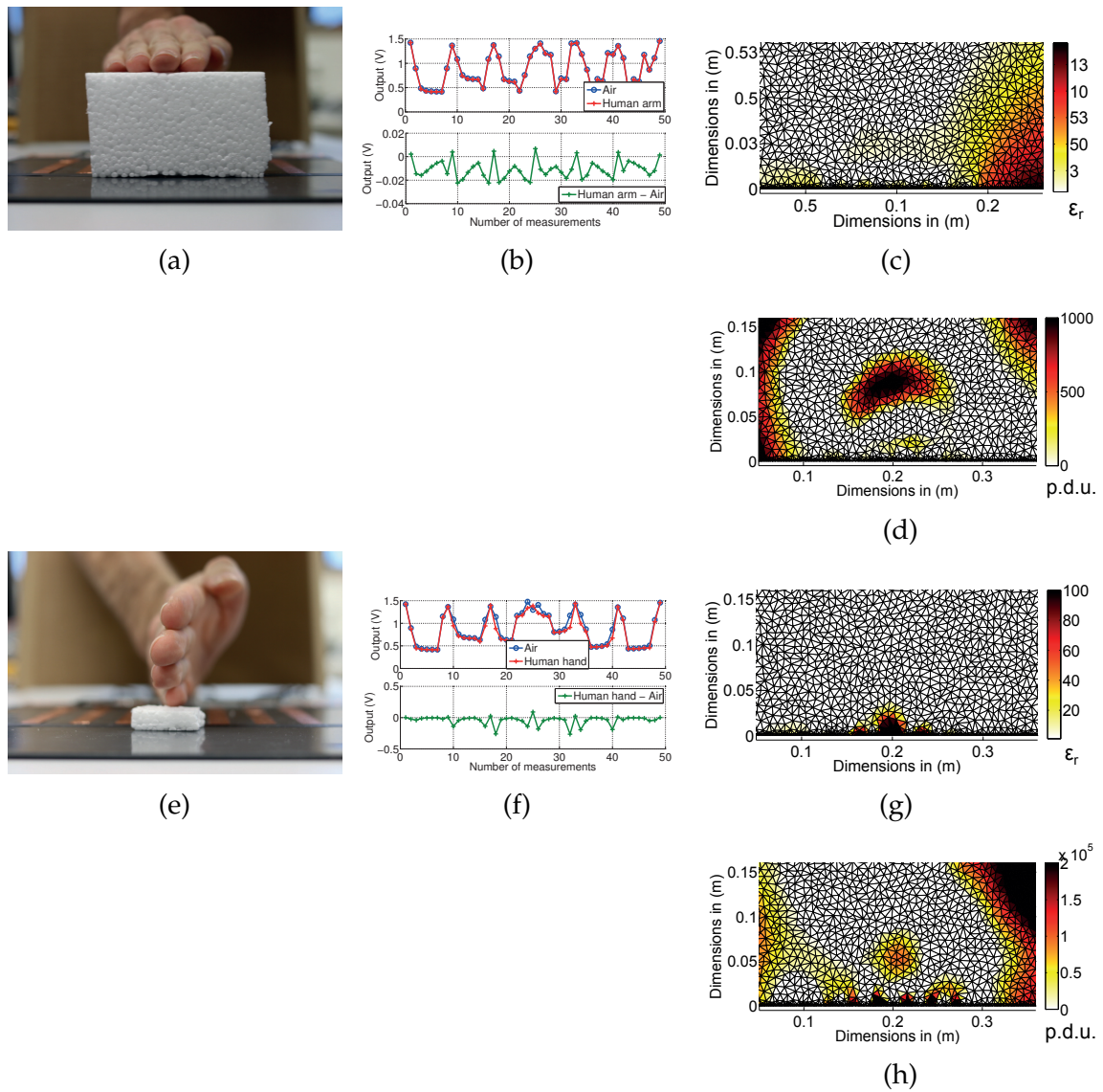


Figure 5.7.: Open environment measurements and reconstruction of a human hand at two positions above the sensor surface. (a) and (e) Pictures of the measurement setup with a human hand at two distances and different orientations above the sensor surface. (b) and (f) Measurement results in mutual and self capacitance mode. The human hand decreases the measured capacitances in mutual capacitance mode and increases the measured value in self capacitance mode. Thus, the human hand can be seen as a leakage object (i.e. object with a good connection to ground). (c) and (g) Results for the reconstruction of the spatial permittivity distribution. (d) and (h) Reconstruction of the leakage map for a human hand.

## 5.2. Realisation Example - Robot Collision Avoidance<sup>1</sup>

As stated in the introduction of this thesis and in [Sch+13b]', special precautions are required to avoid injury when robots and humans share an environment. As shown in section 3.1.1, vision systems play an important part but also suffer from several drawbacks (for example inclusions). Thus, in the following application, a robot arm (Kuka LWR 4) is attached with the presented capacitance measurement system to avoid a human-robot collision. Fig. 5.8 shows a picture of the setup comprising the robot arm and the sensing electrodes.

Although the presented application is particularly suitable to avoid collision with humans, the measurement system is also able to detect other objects, such as conductive or dielectric ones (see section 5.1.2 and the measurement results below).

### 5.2.1. Highly Reactive Robot Motion Generation and Control

The capacitance measurement hardware has already been described in section 4.5. To combine the presented sensor with a robot, measurement data has to be observed from the robot motion control. Below, a short description of the motion generation and control there were used is given. It describes only one out of many options, however, as the intention was to keep the control scheme very simple. The discrete control scheme shown in Fig. 5.9 works on a sampling period of  $T^{cycle}$ . A state of motion at an instant  $T_i$  is represented by the robots position  $\vec{P}_i$ , its velocity  $\vec{V}_i$ , and its acceleration  $\vec{A}_i$ . Taking into account kinematic motion constraints  $\mathbf{B}_i$  that contain maximum values for the velocity, acceleration, and jerk vectors, the online trajectory generation algorithms [Krö10] of the Reflexxes Motion Libraries [Krö11] compute a time-optimal, jerk-limited, and synchronized trajectory that transfers the robot system from its current state  $(\vec{P}_i, \vec{V}_i, \vec{A}_i)$  a desired target position  $\vec{P}_i^{trgt}$  and velocity  $\vec{V}_i^{trgt}$ . These algorithms are executed at every control cycle, so that the system can always react instantaneously in a deterministic way. The output of the algorithms  $(\vec{P}_{i+1}, \vec{V}_{i+1}, \vec{A}_{i+1})$  is forwarded to the underlying robot motion controller.

The underlying controller can be a position controller, a trajectory following controller, an impedance controller, or any other controller that is capable of following a trajectory. As long as no object is detected in the proximity of the virtual whiskers, the task-dependent input values  $\vec{P}_i^{trgt, task}$ ,  $\vec{V}_i^{trgt, task}$ , and  $\mathbf{B}_i^{trgt, task}$  are used. At the moment an object is detected, the value of the switching variable  $\sigma_i$  changes, and a

<sup>1</sup>Parts of this section have been published in [Sch+13a]'

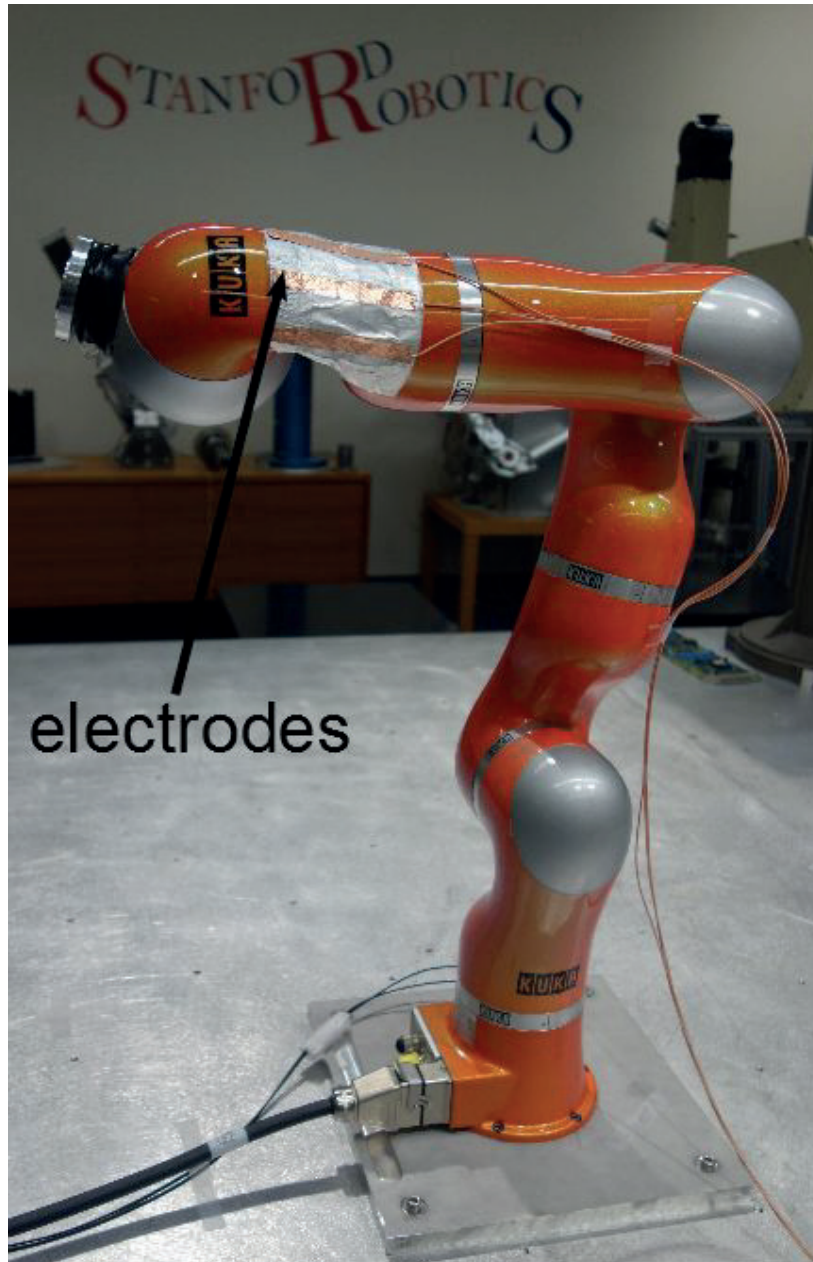


Figure 5.8.: Proposed capacitance measurement system mounted on the 7 doF robot arm (Kuka LWR 4). The sensing electrodes are connected to the electronic circuitry through shielded wires. The electronic circuitry can be placed outside the working range of the robot arm.

different set of input values  $\vec{P}_i^{trgt, react}$ ,  $\vec{V}_i^{trgt, react}$ , and  $\mathbf{B}_i^{trgt, react}$  are used so that the robot can react immediately and try to avoid the potential collision.

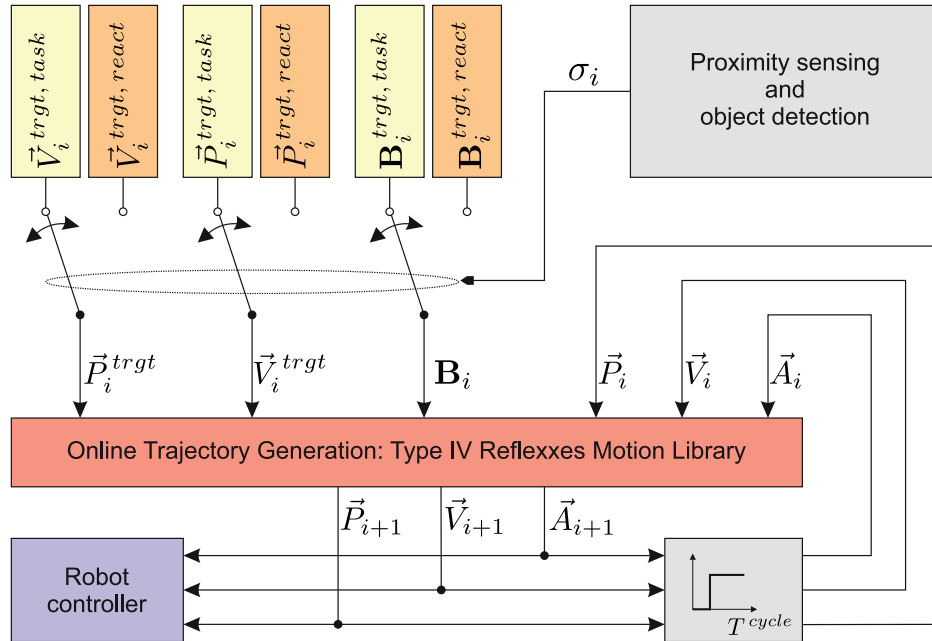


Figure 5.9.: Overview of one of the simplest possible robot motion generation architectures from [Kr11]. The two sets of motion parameters *task* and *react* can be changed from one control cycle to another using the switching signal  $\sigma_i$ . The online trajectory generation algorithms [Kr10] of the Reflexxes Motion Library [Kr11] let robots react to the input signals from the proximity sensor within the same control cycle they occur.

### 5.2.2. Experiments and Results

An experiment and measurement results are shown in Fig. 5.10 and 5.11, respectively. The robot arm is moving in its workspace. As soon as an object (e.g. human hand) is detected by the capacitance measurement system, the robot arm reacts instantaneously to the measurements and tries to avoid contact with the object [Kr10] (shown in Fig. 5.10(a)). Fig. 5.10(b) shows the same scenario with an empty plastic case and the measurement system working in self capacitance mode. It is evident that the object is not detected early enough and thus the robot arm touches the plastic case before it retreats (the touch is detected). Using the mutual capacitance mode shown in Fig. 5.10(c), the object can be detected early enough (i.e. no contact between robot arm and plastic case).

Fig. 5.11 shows the measurements of the proposed measurement system for an approaching human hand and an approaching plastic case (shown in Fig. 5.10(b)).



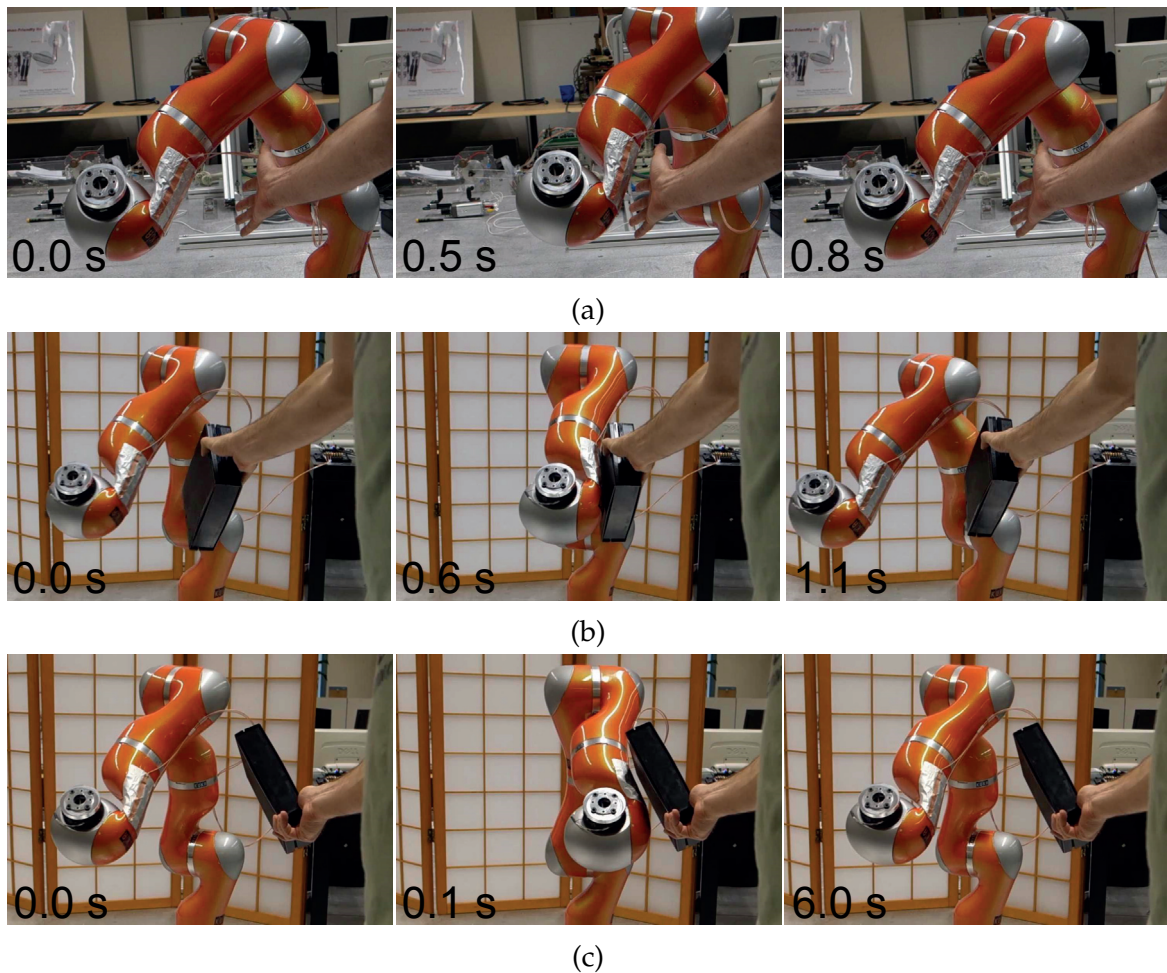


Figure 5.10.: Experiments with the proposed measurement system on a robot arm (KUKA LWR 4) from [Sch+13a]'. (a) A robot arm reacts instantaneously to the measurement data of the presented capacitive sensor. Capacitive sensing allows the robot to avoid collision with a human hand, maintaining a minimum distance of approximately 50 mm. (b) In the self capacitance mode an empty plastic (PVC) box cannot be detected early enough. Thus, the robot arm touches the box before it reacts and the arm retreats. (c) Using the capacitive sensor in the mutual capacitance mode enables the system to detect the empty plastic box early enough and to avoid a collision.

The left column shows the measurement results for the self capacitance mode and the right column for the results using the mutual capacitance mode. Although the SNR is better in the self capacitance mode, there exist situations wherein the mutual capacitance mode outperforms the self capacitance mode by means of signal amplitude for approaching objects (for example in the case of an approaching plastic case shown in Fig. 5.11(b)).

The pictures from Fig. 5.10 are part of a video that was made to show a series of experiments using the KUKA Lightweight Robot IV and the presented capacitance measurement hardware. The experiments include several human-robot collision avoidance scenarios (including using human heads) and the use of several materials while the two different sensing modes are applied. It can be found at:

[http://youtu.be/v7C\\_SHweCxM](http://youtu.be/v7C_SHweCxM)

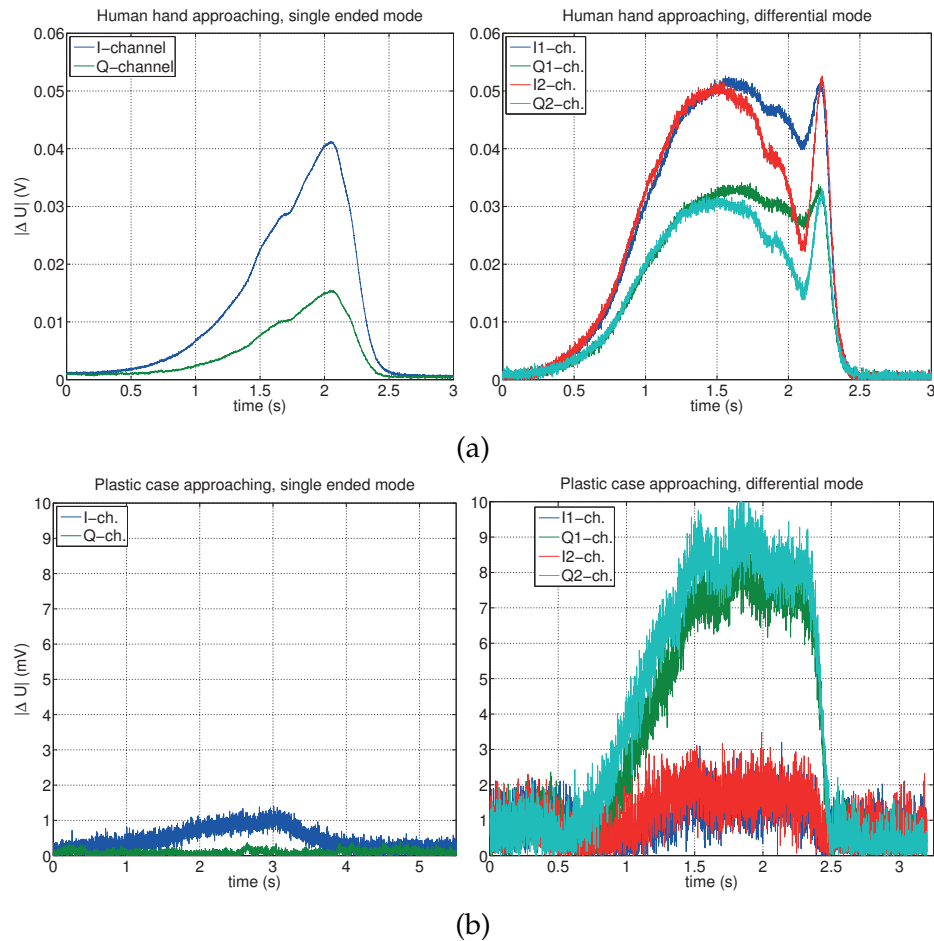


Figure 5.11.: Measurement results with the proposed system on a robot arm (KUKA LWR 4) adopted from [Sch+13a]. (a) Measurement results for an approaching human hand to the sensor surface mounted on the robot arm in the self and mutual capacitance mode. It is apparent that the human hand can be detected in both measurement modes. The described parasitic effects in section 4.3.2 can be observed in mutual capacitance mode. The maximum sensor signal is reached at a distance of approximately 5 mm. (b) Measurement results for an approaching plastic case (compare Fig. 5.10). The plastic can only be detected in mutual capacitance mode and for very close distances (signal maximum at approximately 5 mm).



## 6. Conclusion and Outlook

The aim of this thesis was to develop a measurement system to reduce the high number of injuries to humans caused by their being in areas where they just should not be. Thus, a safety sensor is needed. The term “safety” was investigated based on international standards to define requirements which have to be achieved before a sensor system is allowed to conduct safety-related functions.

According to the requirements (for example: size, weight, power consumption, etc.) for different safety functions, no state-of-the-art sensor technology (for example vision, RFID, time of flight, etc.) was satisfying, which is why capacitance measurement technology was used. Although capacitance measurement is a mature sensor technology suitable for many measurement tasks, it still has a lot of “unused potential” for open environment sensing, as has been shown in this thesis. A review of state-of-the-art capacitance sensor systems showed the performance of actual measurement systems. An investigation of the open environment, resulting parasitic effects, and effects of different approaching objects, resulted among others in two main findings for this thesis:

- Development of an open environment algorithm that uses existing algorithms from ECT and adds a second forward solution for the presented leakage map. This leakage map can provide additional information about the approaching object and prevents the need for a 3D simulation and reconstruction.
- Development of a capacitance measurement hardware that is able to deal first with the high reactive requirements in some applications (for example, in robotics) and second, with the parasitic effects that arise in open environments (for example, the leakage effect).

Simulations and measurement results show the performances of the developed algorithm. It was shown that objects can be distinguished based on their size and connection to ground. The measurement results were obtained with the developed measurement hardware. This hardware was also used for a highly responsive robot collision system, which led to the capacitance measurement system being mounted on a robot arm at the robotics group at Stanford University. The sensor performed well, especially in detecting and avoiding collisions with a human hand.

For a commercial usage of the measurement system including the reconstruction algorithms, some work is still necessary. For example, if the measurement hardware

is intended for safety-related functions, IEC or ISO certification is mandatory. Therefore, the hardware has to be evaluated for its reliability, lifespan, etc. (as was shown in chapter 2). Future research could also examine the real time capabilities of the reconstruction algorithms for the spatial permittivity distribution and the leakage map. Although the reconstruction results showed a promising performance, real time capability was not achieved. Concerning robotic applications, the results showed a high potential for a commercial use. The overall goal has to be whole-robot coverage with capacitive sensing electrodes. If such a robot surface could be created, external sensors (for example, cameras) would no longer be needed. This would enable to a safe human-robot interaction to be realized without any restrictions on spatial boundaries.

Thus, capacitive sensing still has a lot of interesting aspects to be investigated and continues to be an exciting research topic in many fields of application.

# Appendix

## Appendix A.

# Leakage Approach for Quadratic Triangular Shape Functions

The entities of the matrix  $M$  and  $T$  in sections 4.1.2 and 4.3.4, respectively, could easily be calculated analytically (see equations (4.18) and (4.23)) due to the use of linear shape functions [Polo6]. For higher order shape functions, for example quadratic shape functions as shown in equations (A.1), the integrals for  $M_{ij}$ ,  $T_{ij}$ ,  $f_i$ , and  $p_i$  in equations (4.18) can be conveniently solved using numerical methods [Akio5]. Thus, the Gaussian quadrature rule is used to solve these integrals [Polo6].  $M_{ij}$  and  $T_{ij}$  are shown here again for the reader's convenience:

$$M_{ij} = - \iint_{\Omega_e} \left[ \alpha_x \left( \frac{\partial N_i}{\partial x} \right) \left( \frac{\partial N_j}{\partial x} \right) + \alpha_y \left( \frac{\partial N_i}{\partial y} \right) \left( \frac{\partial N_j}{\partial y} \right) \right] dx dy$$
$$T_{ij} = \iint_{\Omega_e} \beta N_i N_j dx dy$$

The following equations (A.1) show the quadratic shape functions for triangular elements [Sch91]:

$$N_1 = (2\zeta + 2\eta - 1)(\zeta + \eta - 1) \quad (\text{A.1a})$$

$$N_2 = \zeta(2\zeta - 1) \quad (\text{A.1b})$$

$$N_3 = \eta(2\eta - 1) \quad (\text{A.1c})$$

$$N_4 = -4\zeta(\zeta + \eta - 1) \quad (\text{A.1d})$$

$$N_5 = 4\zeta\eta \quad (\text{A.1e})$$

$$N_6 = -4\eta(\zeta + \eta - 1) \quad (\text{A.1f})$$

$\zeta$  and  $\eta$  are the natural coordinates of the so-called "master triangle" [Polo6]. Every triangle is mapped to the master triangle which lies on the orthogonal axes defined

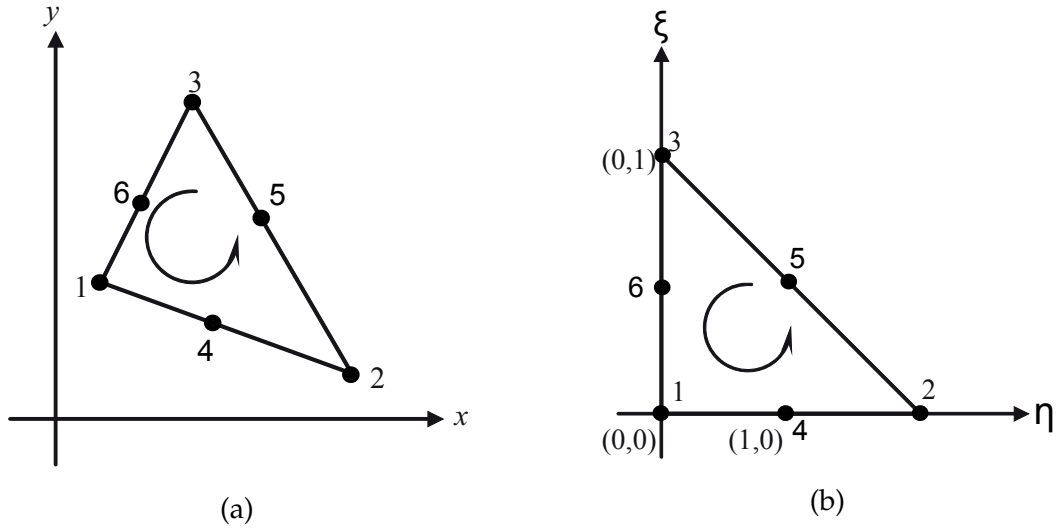


Figure A.1.: Triangle of arbitrary shape mapped in  $xy$  plane in (a) is mapped on the natural coordinates  $\xi\eta$  in (b) (adopted from [Polo6]).

by  $\xi$  and  $\eta$ . Fig. A.1 shows a sketch of an arbitrarily-shaped triangle in the  $xy$  plane which is mapped on the natural coordinates.

Due to the use of the natural coordinate system, every arbitrary triangle can be calculated by following integral:

$$\iint_{\Omega} f(x, y) dx dy = \int_0^1 \int_0^{1-\eta} f(x(\xi, \eta), y(\xi, \eta)) |J| d\xi d\eta, \quad (\text{A.2})$$

where  $|J|$  denotes the determinate of the Jacobian (see (A.3)). With equation (A.2)  $M$  and  $T$  can be solved (by means of the Gaussian quadrature approximation) using the mapping of the partial derivatives of the shape function to the natural coordinates using the Jacobian:

$$\begin{Bmatrix} \frac{\partial N_i}{\partial \xi} \\ \frac{\partial N_i}{\partial \eta} \end{Bmatrix} = J \begin{Bmatrix} \frac{\partial N_i}{\partial x} \\ \frac{\partial N_i}{\partial y} \end{Bmatrix}, \text{ with } J = \begin{bmatrix} \frac{\partial x}{\partial \xi} & \frac{\partial y}{\partial \xi} \\ \frac{\partial x}{\partial \eta} & \frac{\partial y}{\partial \eta} \end{bmatrix}. \quad (\text{A.3})$$

Depending on the number of support points  $n$ , Gauss quadrature approximation can be applied for triangles in the following form [Sch91]:

$$\int_0^1 \int_0^{1-\eta} f(\xi, \eta) d\xi d\eta = \sum_{i=1}^n f(\xi, \eta) \omega_i, \quad (\text{A.4})$$

Table A.1.: Weights and support points for Gaussian quadrature approximation for triangular elements with 3 and 4 support points from [Aki05].

n	$\omega_i$	$\xi_i$	$\eta_i$
3	1/6	1/6	1/6
	1/6	2/3	1/6
	1/6	1/6	2/3
n	$\omega_i$	$\xi_i$	$\eta_i$
4	-9/32	1/3	1/3
	25/96	3/5	1/5
	25/96	1/5	3/5
	25/96	1/5	1/5

where  $\omega_i$  are the Gauss weights and  $\xi_i$  and  $\eta_i$  are the coordinates of the Gauss points.

table A.1 shows the weights and natural coordinates of the support points for triangular elements when using 3 (exact integration for polynomials of second order) or 4 (exact integration for polynomials of third order) support points.

# Appendix B.

## Circuitry

### B.1. Front-End Circuitry

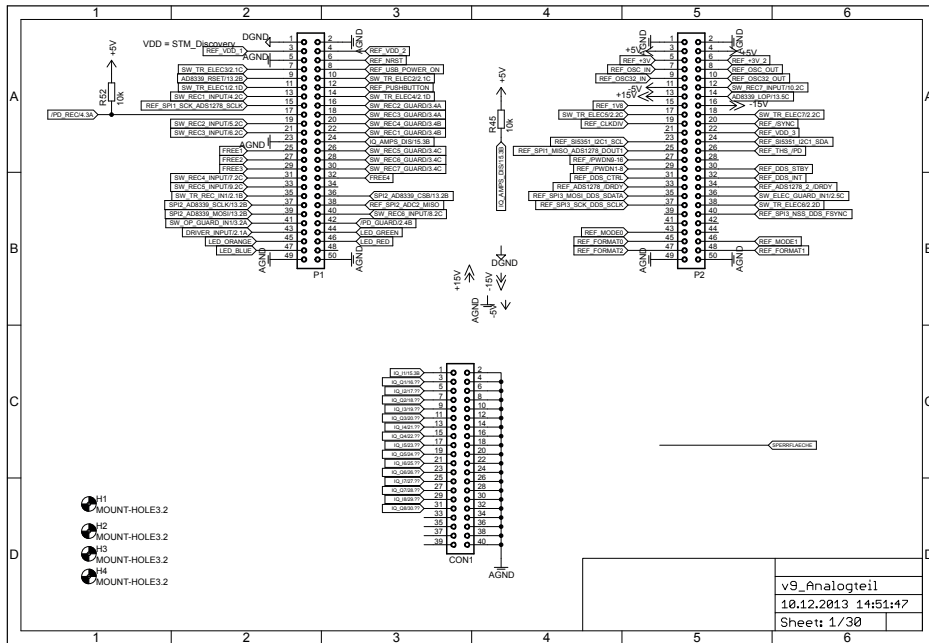


Figure B.1.: Schematic: Connectors and signals of “analog” circuitry board.



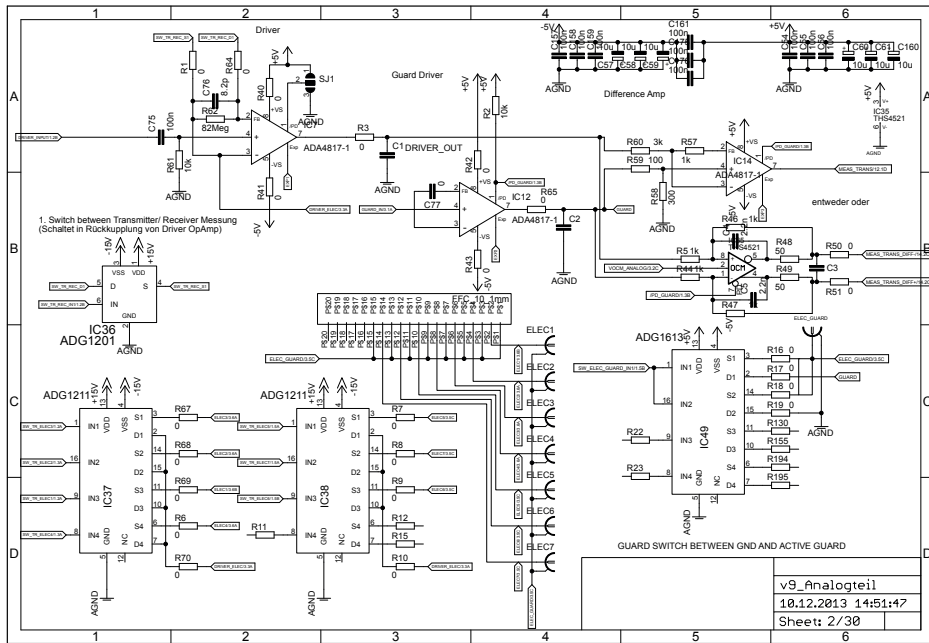


Figure B.2.: Schematic: Transmitter front end circuitry and transmitter switches.

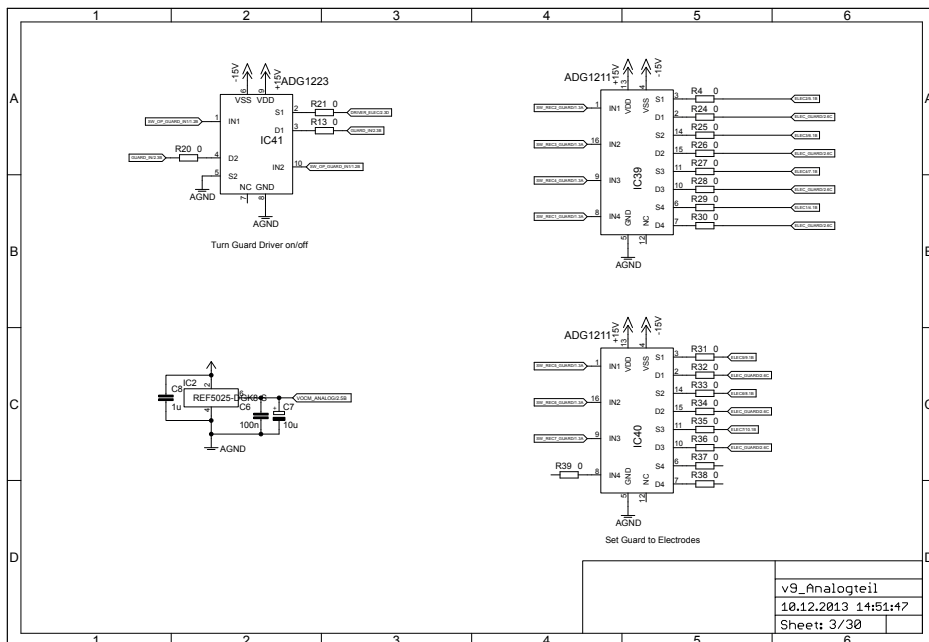


Figure B.3.: Schematic: Switches for guard driver.

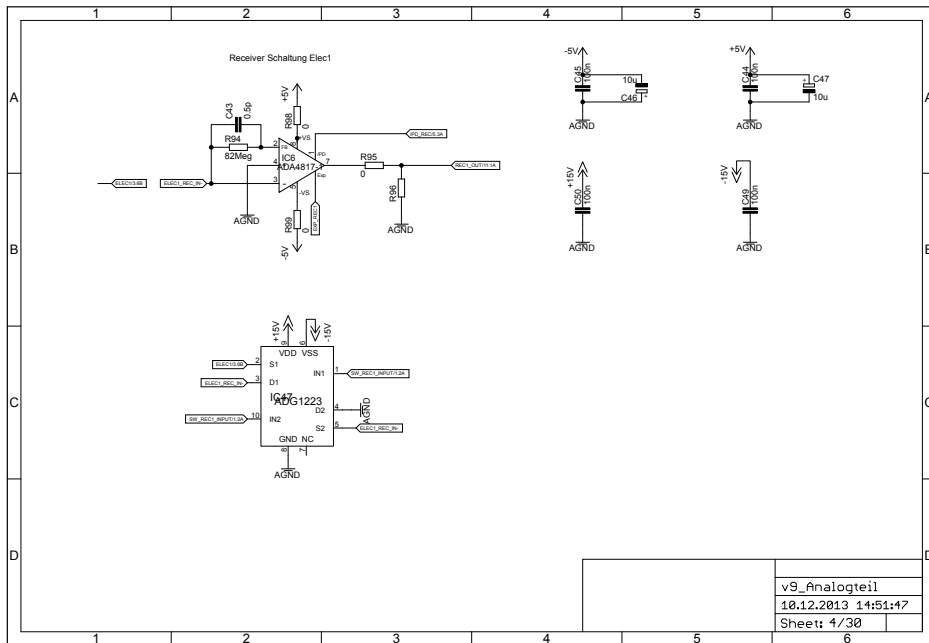


Figure B.4.: Schematic: Representative receiver amplifier circuitry. Six other receiver circuitries are used.

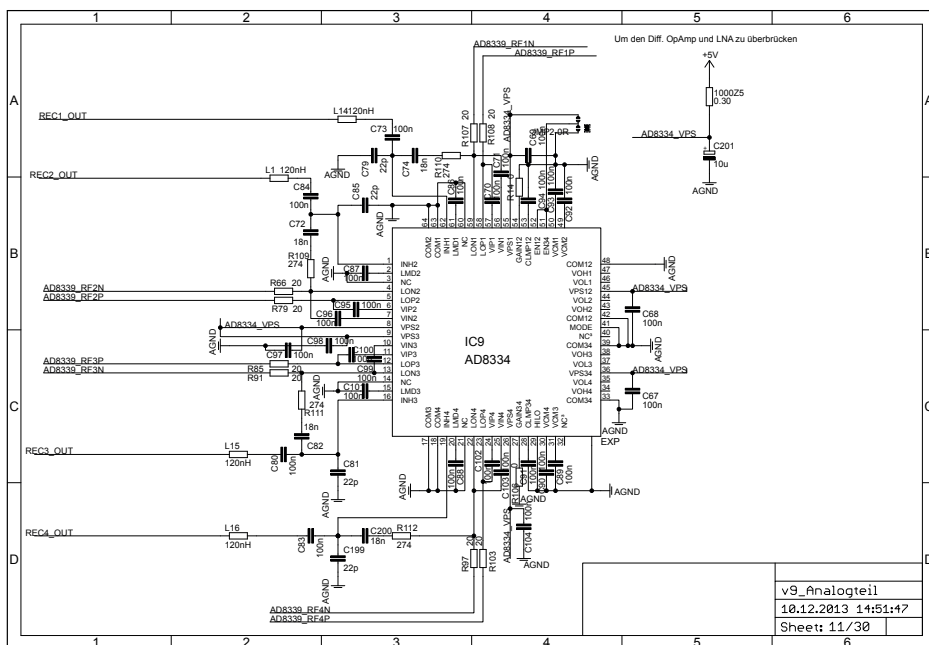


Figure B.5.: Schematic: Low noise amplifier circuitry.

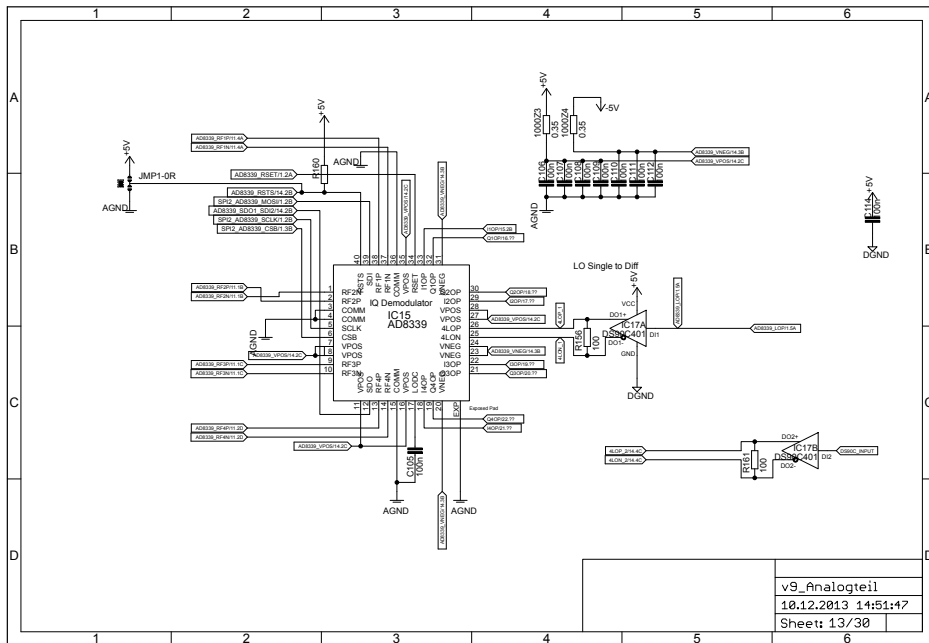


Figure B.6.: Schematic: IQ demodulator circuitry.

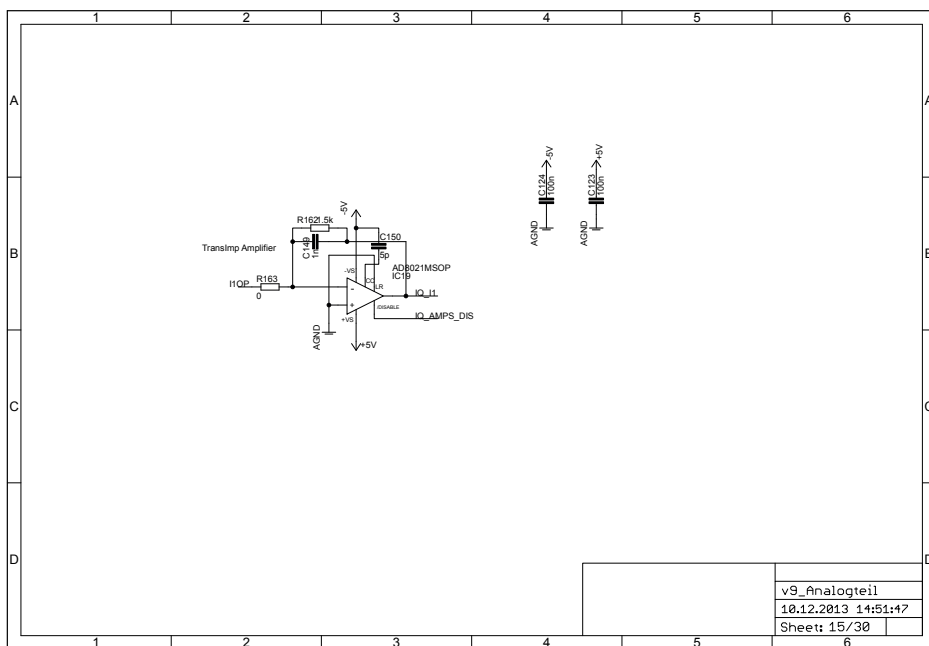


Figure B.7.: Schematic: Representative active low pass filter circuitry. Each output channel of the IQ demodulator needs one filter circuitry.

## B.2. Signal Generation and Data Acquisition Circuitry

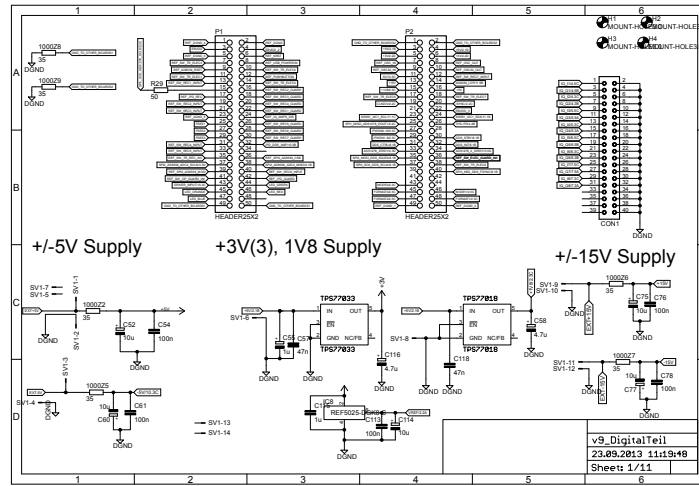


Figure B.8.: Schematic: Connectors and supply of the measurement circuitry.

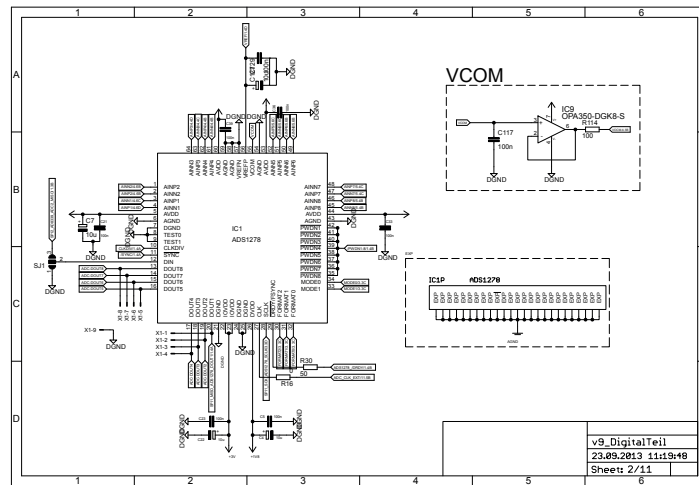


Figure B.9.: Schematic: First ADC circuitry including voltage reference.

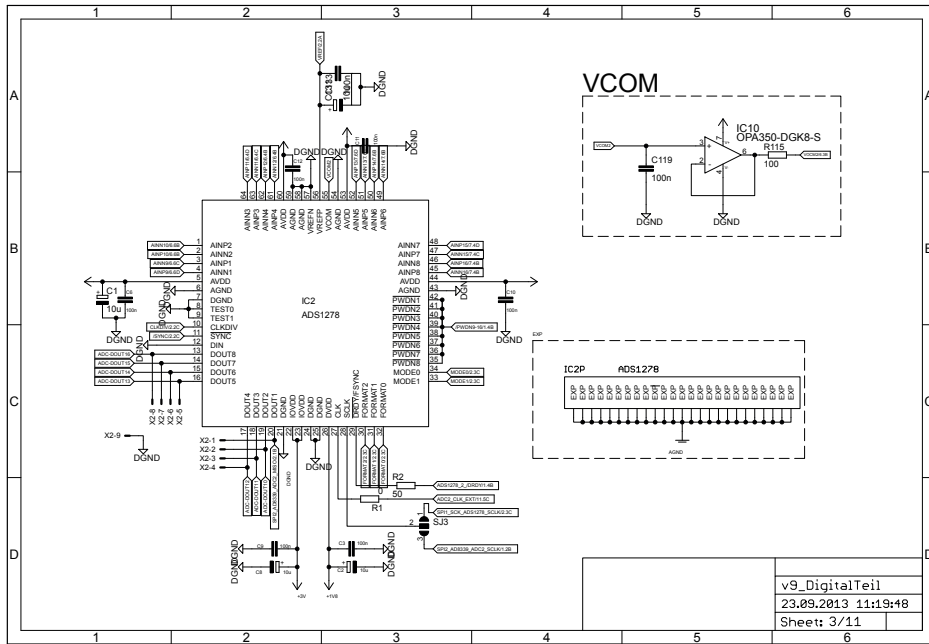


Figure B.10.: Schematic: Second ADC circuitry including voltage reference.

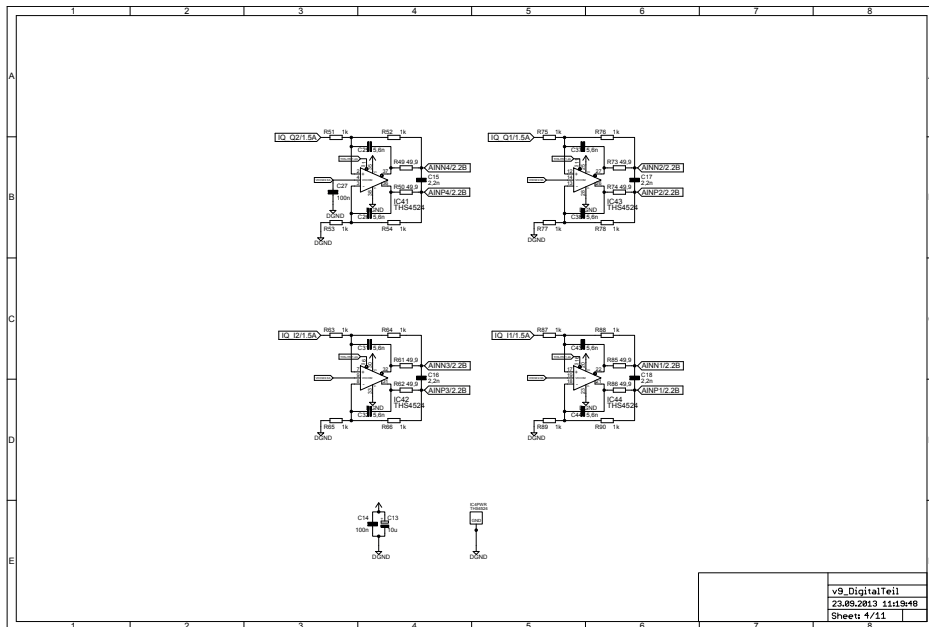


Figure B.11.: Schematic: Single to differential pre amplifier circuitry for ADC (4 of 16 channels).

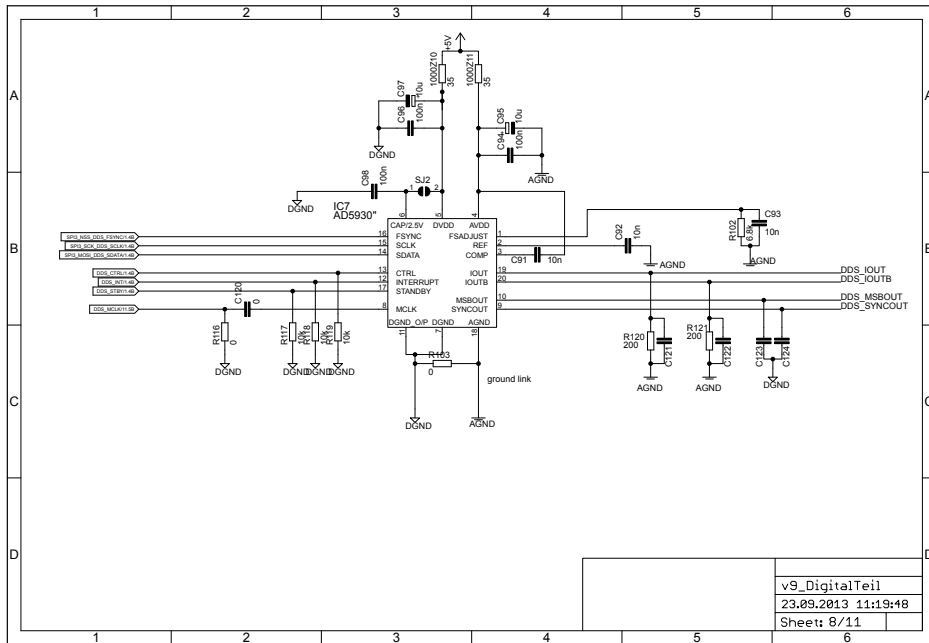


Figure B.12.: Schematic: DDS circuitry.

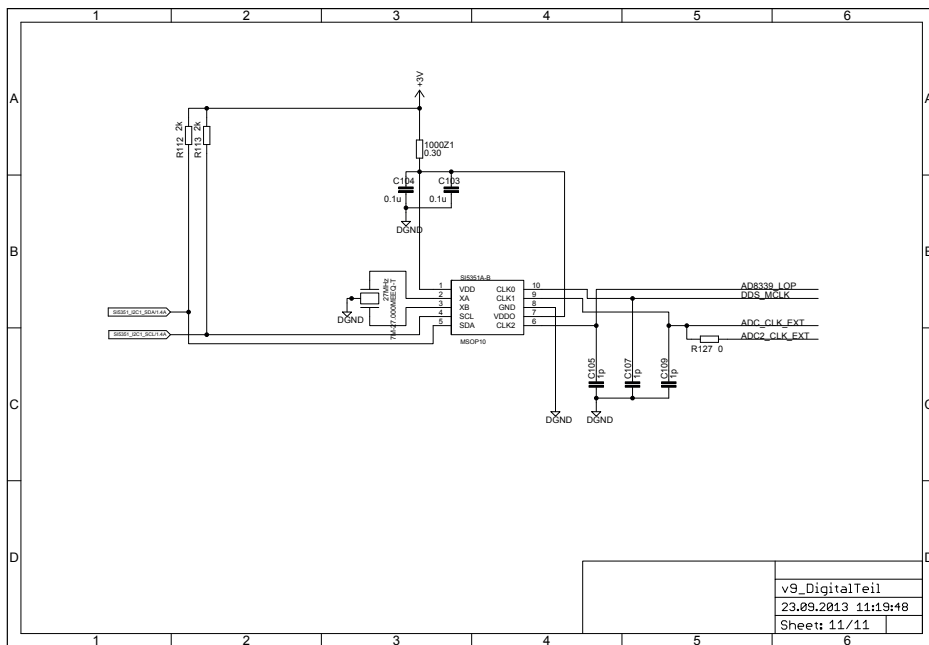


Figure B.13.: Schematic: Clock generator circuitry.

# List of Figures

1.1.	Capacitive collision detection system and simulated results . . . . .	4
1.2.	Overview and common thread of this thesis . . . . .	8
2.1.	Overview of safety standards . . . . .	11
2.2.	Relation of the IEC 61508 standard to industry specific standards . .	12
2.3.	Elements of risk . . . . .	15
2.4.	Safety life cycle . . . . .	18
2.5.	Main parts of IEC 61508 . . . . .	21
2.6.	Example of a safety pattern. . . . .	24
2.7.	1002D architectures . . . . .	26
2.8.	GSN diagram for the safety frequency converter . . . . .	27
2.9.	Initial concept for a SRECS . . . . .	30
2.10.	Subsystems of a SRECS . . . . .	31
3.1.	Publication statistics . . . . .	34
3.2.	Vision sensor system for human safety in workcell . . . . .	36
3.3.	Vision sensor system on mobile robots . . . . .	38
3.4.	Sensor using the seashell effect . . . . .	40
3.5.	Magnetic sensing results . . . . .	40
3.6.	Sensor fusion system on car bumper . . . . .	43
3.7.	Photo of capacitive ice sensor . . . . .	44
3.8.	Block diagram of power line contact system . . . . .	45
3.9.	Capacitive safety system on a chainsaw . . . . .	46
3.10.	Capacitive pretouch sensor on robotic hand . . . . .	48
3.11.	Sensor fusion system on a robot grasper . . . . .	50
4.1.	Electric field produced by a Mormyridae . . . . .	54
4.2.	Capacitance measurement results for different objects. . . . .	60
4.3.	Schematic of a state-of-the-art ECT system . . . . .	61
4.4.	ECT example and reconstruction result . . . . .	62
4.5.	Sketch of occurring parasitic effects with capacitive sensing . . . . .	64
4.6.	Sketch of the shielding and coupling effect . . . . .	66
4.7.	Pictorial description of the leakage effect . . . . .	67
4.8.	Profiles of a 2D and 3D simulation setup. . . . .	68



---

4.9. Simulation setup in 2D and 3D . . . . .	69
4.10. Simulation results for validation of the leakage effect . . . . .	72
4.11. Simulation setup to validate leakage effect . . . . .	72
4.12. Simulation results for a 2D, a 3D, and a 2D leakage simulation. . . . .	73
4.13. Pictorial representation of a leakage map . . . . .	74
4.14. Sketch of possible leakage suppressing methods . . . . .	76
4.15. Block diagram of measurement hardware for leakage suppression . . . . .	77
4.16. Experimental measurement results for leakage suppression . . . . .	78
4.17. Sketch and measurement of both measurement modes . . . . .	80
4.18. Experimental test setup for investigation of curvature effects . . . . .	82
4.19. Simulation setup and results for bending electrode structures . . . . .	83
4.20. ECT measurement system . . . . .	85
4.21. Experimental results from an ECT system . . . . .	87
4.22. ECT simulation and reconstruction results for a PVC bar . . . . .	89
4.23. ECT measurement and reconstruction for a PVC bar . . . . .	90
4.24. ECT simulation of the leakage effect . . . . .	91
4.25. ECT measurements and reconstruction results for a leakage object . . . . .	92
4.26. ECT to capacitive sensing approach . . . . .	93
4.27. Electrode structure and $\Omega_{ROI}$ . . . . .	94
4.28. Capacitance evaluation circuitry . . . . .	98
4.29. Sample objects to test capacitance measurement hardware . . . . .	100
4.30. Measurement results with proposed measurement system . . . . .	101
5.1. Calibration schemes and measurement results for the leakage effect . . . . .	103
5.2. Open environment simulation of a dielectric object. . . . .	105
5.3. Open environment measurements of a dielectric object. . . . .	107
5.4. Open environment simulation of a “leakage” object. . . . .	109
5.5. Open environment results of a “leakage” iron rod. . . . .	110
5.6. Open environment results of a “leakage” electric wire. . . . .	112
5.7. Open environment results of a human hand. . . . .	113
5.8. Proposed measurement system on a robot arm . . . . .	115
5.9. Overview of a trajectory generation controller . . . . .	116
5.10. Experiments on a robot arm . . . . .	117
5.11. Measurement results on a robot arm . . . . .	119
A.1. Triangle of arbitrary shape mapped on the natural coordinate . . . . .	124
B.1. Schematic: Connectors and signals of “analog” circuitry board . . . . .	126
B.2. Schematic: Transmitter front end circuitry and transmitter switches . . . . .	127
B.3. Schematic: Switches for guard driver . . . . .	127
B.4. Schematic: Representative receiver amplifier circuitry . . . . .	128
B.5. Schematic: Low noise amplifier circuitry . . . . .	128

---

B.6. Schematic: IQ demodulator circuitry . . . . .	129
B.7. Schematic: Representative active low pass filter circuitry . . . . .	129
B.8. Schematic: Connectors and supply of the measurement circuitry . .	130
B.9. Schematic: First ADC circuitry including voltage reference . . . . .	130
B.10. Schematic: Second ADC circuitry including voltage reference . . . .	131
B.11. Schematic: Single to differential pre amplifier circuitry for ADC . . .	131
B.12. Schematic: DDS circuitry . . . . .	132
B.13. Schematic: Clock generator circuitry . . . . .	132

# List of Tables

2.1.	Probability of everyday risk of death . . . . .	13
2.2.	Terms and definitions in safety standards . . . . .	14
2.3.	Definition of Safety Integrity Levels . . . . .	17
2.4.	Minimum independence of the assessor . . . . .	20
2.5.	Link between safety tactics and IEC 61508 . . . . .	25
2.6.	Estimation of the severity parameter . . . . .	29
2.7.	Frequency and probability of occurrence . . . . .	29
2.8.	Probability of avoiding or limiting harm . . . . .	29
2.9.	Estimating the necessary SIL . . . . .	30
2.10.	Probability of dangerous failure per hour for a given SIL target . . . . .	32
2.11.	Hardware fault tolerance for a given safe failure fraction . . . . .	32
3.1.	Material classification results . . . . .	47
3.2.	Comparison of exteroceptive sensors and capacitance sensors . . . . .	52
4.1.	Simulation results of the leakage effects . . . . .	70
4.2.	Change of space charge according to object length . . . . .	71
4.3.	Comparison of capacitive sensor front-end circuitry . . . . .	96
4.4.	Comparison of capacitive measurement systems . . . . .	99
A.1.	Weights and support points for Gaussian quadrature approximation . . . . .	125

# Acronyms

$\Omega_{ROI}$  region of interest.

**ADC** analog digital converter.

**ALARP** as low as reasonably practicable.

**BEM** boundary element method.

**DDS** direct digital synthesizer.

**ECT** electrical capacitance tomography.

**EMC** electromagnetic compatibility.

**FEM** finite element method.

**GMR** Giant magnetoresistance.

**GSN** Goal Structuring Notation.

**IEC** International Electrotechnical Commission.

**ISO** International Organization for Standardization.

**MLE** maximum likelihood estimator.

**PCB** printed circuit board.

**PEHD** polyethylene high-density.

**PTFE** polytetrafluorethylen.

**PUR** polyurethane.

**PVC** polyvinylchlorid.

**RFID** Radio-frequency identification.

**SIL** safety integrity level.

**SILCL** safety integrity level claim limit.

**SLAM** simultaneous localization and mapping.

**SNR** signal-to-noise ratio.

**SRCF** safety-related control function.

**SRECS** safety-related electronic control system.

# Bibliography

- [AIS77] C. Alexander, S. Ishikawa, and M. Silverstein. *A Pattern Language: Towns, Buildings, Construction (Center for Environmental Structure Series)*. Oxford University Press, Aug. 17, 1977. ISBN: 0195019199 (cit. on p. 22).
- [Aki05] J.E. Akin. *Finite Element Analysis with Error Estimators*. 2005. ISBN: 978-0-7506-6722-7 (cit. on pp. 123, 125).
- [Ana14] Analog Devices. *Capacitance to Digital Converters*. Apr. 2014. URL: <http://www.analog.com/en/analog-to-digital-converters/capacitance-to-digital-converters/products/index.html> (cit. on pp. 43, 81, 99, 100).
- [Bax97] L.K. Baxter. *Capacitive Sensors, Design and Applications*. IEEE Press, 1997 (cit. on pp. 54, 55, 67, 82, 87, 95).
- [BHW03] B. Brandstätter, G. Holler, and D. Watzenig. "Reconstruction of inhomogeneities in fluids by means of capacitance tomography." In: *COMPEL: The International Journal for Computation and Mathematics in Electrical and Electronic Engineering* 22.3 (2003), pp. 508–519 (cit. on p. 60).
- [BLBo8] A. Blais, M. Lacroix, and L. Brouillette. "Hydro quebecs de-icing system: Automated overhead line monitoring and de-icing system." In: *Cigre Session*. Vol. B2-211. Paris, France, Aug. 2008, pp. 1–7 (cit. on p. 44).
- [BM07] J. Berthing and T. Maier. "A Taxonomy for Modelling Safety Related Architectures in Compliance with Functional Safety Requirements." In: *Computer Safety, Reliability, and Security*. Ed. by Francesca Saglietti and Norbert Oster. Vol. 4680. Lecture Notes in Computer Science. Springer Berlin Heidelberg, 2007, pp. 505–517. ISBN: 978-3-540-75100-7. DOI: 10.1007/978-3-540-75101-4\_47 (cit. on pp. 25, 26).
- [BPCo8] A. Bicchi, M.A. Peshkin, and J.E. Colgate. "Safety for Physical Human-Robot Interaction." In: *Springer Handbook of Robotics*. Ed. by B. Siciliano and O. Khatib. first. Berlin, Heidelberg, Germany: Springer, 2008. Chap. 4, pp. 1335–1348 (cit. on pp. 35, 42).

- [Bra+05] W. Bracke, P. Merken, R. Puers, and C. Van Hoof. "On the optimization of ultra low power front-end interfaces for capacitive sensors." In: *Sensors and Actuators A: Physical* 117.2 (2005), pp. 273–285. ISSN: 0924-4247. DOI: 10.1016/j.sna.2004.06.011 (cit. on p. 63).
- [Bra03] G. Brasseur. "Design rules for robust capacitive sensors." In: *IEEE Transactions on Instrumentation and Measurement* 52 (4 Aug. 2003), pp. 1261–1265 (cit. on pp. 3, 64, 99).
- [Bra97] K. Brauner. *Elektrische Fische*. Schoolbook. 1997 (cit. on p. 54).
- [CFm14] CFmathematics. *Sense of Touch can be determined by a Virtual Whisker Probe*. May 14, 2014. URL: <http://cfmathematics.com.au/2012/05/14/sense-of-touch-can-be-determined-by-a-virtual-whiskers-probe/> (cit. on p. 42).
- [CHo8] H.I. Christensen and G.D. Hager. "Sensing and Estimation." In: *Springer Handbook of Robotics*. Ed. by B. Siciliano and O. Khatib. first. Berlin, Heidelberg, Germany: Springer, 2008. Chap. 4, pp. 87–108 (cit. on p. 35).
- [Cho+11] B.-S. Choi, J.-W. Lee, J.-J. Lee, and K.-T. Park. "A Hierarchical Algorithm for Indoor Mobile Robot Localization Using RFID Sensor Fusion." In: *Industrial Electronics, IEEE Transactions on* 58.6 (2011), pp. 2226–2235. ISSN: 0278-0046. DOI: 10.1109/TIE.2011.2109330 (cit. on p. 38).
- [Cho+13] B. Choi, C. Mericli, J. Biswas, and M. Veloso. "Fast human detection for indoor mobile robots using depth images." In: *Robotics and Automation (ICRA), 2013 IEEE International Conference on*. May 2013, pp. 1108–1113. DOI: 10.1109/ICRA.2013.6630711 (cit. on pp. 36–38, 52).
- [CHPo8] M.R. Cutkosky, R.D. Howe, and W.R. Provancher. "Force and Tactile Sensors." In: *Springer Handbook of Robotics*. Ed. by B. Siciliano and O. Khatib. first. Berlin, Heidelberg, Germany: Springer, 2008. Chap. 4, pp. 1253–1281 (cit. on p. 41).
- [Cui+11] Z. Cui, H. Wang, Z. Chen, Y. Xu, and W. Yang. "A high-performance digital system for electrical capacitance tomography." In: *Measurement Science and Technology* 22 (2011) (cit. on p. 95).
- [DEo8] K. Daniilidis and J.-O. Eklundh. "3-D Vision and Recognition." In: *Springer Handbook of Robotics*. Ed. by B. Siciliano and O. Khatib. first. Berlin, Heidelberg, Germany: Springer, 2008. Chap. 4, pp. 543–562 (cit. on pp. 35, 36, 39).
- [DHo8] H. Durrant-Whyte and T.C. Henderson. "Multisensor Data Fusion." In: *Springer Handbook of Robotics*. Ed. by B. Siciliano and O. Khatib. first. Berlin, Heidelberg, Germany: Springer, 2008. Chap. 4, pp. 1253–1281 (cit. on p. 38).

- [Di +04] M. Di Santo, A. Vaccaro, D. Villacci, and Eugenio Zimeo. "A distributed architecture for online power systems security analysis." In: *Industrial Electronics, IEEE Transactions on* 51.6 (2004), pp. 1238–1248. ISSN: 0278-0046. DOI: 10.1109/TIE.2004.837862 (cit. on p. 44).
- [Dye04] S.A. Dyer. *Wiley Survey of Instrumentation and Measurement*. Wiley, 2004 (cit. on p. 55).
- [Eur13] Eurostat. *Accidents at work (ESAW)*. Nov. 29, 2013. URL: <http://epp.eurostat.ec.europa.eu/portal/page/portal/eurostat/home> (visited on 01/26/2014) (cit. on p. 1).
- [FKo8] R.B. Fisher and K. Konolige. "Range Sensors." In: *Springer Handbook of Robotics*. Ed. by B. Siciliano and O. Khatib. first. Berlin, Heidelberg, Germany: Springer, 2008. Chap. 4, pp. 1253–1281 (cit. on pp. 38, 52).
- [Fla+12] F. Flacco, T. Kroger, A. De Luca, and O. Khatib. "A depth space approach to human-robot collision avoidance." In: *Robotics and Automation (ICRA), 2012 IEEE International Conference on*. 2012, pp. 338–345. DOI: 10.1109/ICRA.2012.6225245 (cit. on p. 37).
- [FN94] J.T. Feddema and J.L. Novak. "Whole arm obstacle avoidance for teleoperated robots." In: *Robotics and Automation, 1994. Proceedings., 1994 IEEE International Conference on*. May 1994, 3303–3309 vol.4. DOI: 10.1109/ROBOT.1994.351062 (cit. on p. 47).
- [Fos+12] A. Fossati, J. Gall, H. Grabner, X. Ren, and K. Konolige. *Consumer Depth Cameras for Computer Vision: Research Topics and Applications*. Springer, 2012. ISBN: 9781447146391 (cit. on p. 36).
- [Fuk11] A. Fukada. "The latest updates on international standardization activities to realize the safe and reliable human environment." In: *SICE Annual Conference (SICE), 2011 Proceedings of*. 2011, pp. 2048–2053 (cit. on pp. 10, 11).
- [Geo+09] B. George, H. Zangl, T. Bretterkieber, and G. Brasseur. "Seat Occupancy Detection Based on Capacitive Sensing." In: *Instrumentation and Measurement, IEEE Transactions on* 58.5 (May 2009), pp. 1487–1494. ISSN: 0018-9456. DOI: 10.1109/TIM.2009.2009411 (cit. on p. 66).
- [Gou+90] J.D. Gould, S.L. Greene, S.J. Boies, A. Meluson, and M. Rasamny. "Using a touchscreen for simple tasks." In: *Interacting with Computers* 2.1 (1990), pp. 59–74. ISSN: 0953-5438. DOI: 10.1016/0953-5438(90)90014-9 (cit. on p. 54).
- [GSN11] GSN working group. *GSN Community Standard Version 1*. 2011. URL: [http://www.goalstructuringnotation.info/documents/GSN\\_Standard.pdf](http://www.goalstructuringnotation.info/documents/GSN_Standard.pdf) (visited on 20/09/2013) (cit. on p. 23).



- [GZBo8] B. George, H. Zangl, and Th. Bretterkieber. "A Warning System for Chainsaw Personal Safety based on Capacitive Sensing." In: *IEEE International Conference on Sensors*. Lecce, Italy, Oct. 2008, pp. 419–422 (cit. on pp. 46, 52).
- [Had+12] S. Haddadin, S. Haddadin, A. Khoury, T. Rokahr, S. Parusel, R. Burgkart, A. Bicchi, and A. Albu-Schaffer. "A truly safely moving robot has to know what injury it may cause." In: *Intelligent Robots and Systems (IROS), 2012 IEEE/RSJ International Conference on*. 2012, pp. 5406–5413. DOI: 10.1109/IROS.2012.6386163 (cit. on pp. 34, 42, 52).
- [HC89] R.D. Howe and M.R. Cutkosky. "Sensing skin acceleration for slip and texture perception." In: *Robotics and Automation, 1989. Proceedings., 1989 IEEE International Conference on*. 1989, 145–150 vol.1. DOI: 10.1109/ROBOT.1989.99981 (cit. on p. 41).
- [HC93] R.D. Howe and M.R. Cutkosky. "Dynamic tactile sensing: perception of fine surface features with stress rate sensing." In: *Robotics and Automation, IEEE Transactions on* 9.2 (1993), pp. 140–151. ISSN: 1042-296X. DOI: 10.1109/70.238278 (cit. on p. 41).
- [Hey10] C. Heyer. "Human-robot interaction and future industrial robotics applications." In: *Intelligent Robots and Systems (IROS), 2010 IEEE/RSJ International Conference on*. 2010, pp. 4749–4754. DOI: 10.1109/IROS.2010.5651294 (cit. on p. 35).
- [HM13] H.A. Haus and J.R. Melcher. *Electromagnetic Fields and Energy*. Massachusetts Institute of Technology: MIT OpenCourseWare. Dec. 1, 2013. URL: <http://ocw.mit.edu>. Also available from Prentice-Hall: Englewood Cliffs, NJ, 1989. ISBN: 9780132490207 (cit. on pp. 54, 55).
- [IECo5] IEC/EN 62061. *Safety of machinery, Functional safety of safety-related electrical, electronic and programmable electronic control systems*. Dec. 31, 2005 (cit. on pp. 27, 29–32).
- [IEC10a] IEC. *IEC Guide 104 Ed. 4.0, The preparation of safety publications and the use of basic safety publications and group safety publications*. International Electrotechnical Commission, Aug. 30, 2010 (cit. on p. 10).
- [IEC10b] IEC/TC65/SC65A/MT61508 IEC 61508 ed2.0. *Functional safety of electrical/electronic/programmable electronic safety-related systems - all parts*. International Electrotechnical Commission, Apr. 30, 2010 (cit. on pp. 9, 11, 16, 17, 20, 26–28, 32, 33).
- [IEC13a] IEC. *IEC History*. International Electrotechnical Commission. Aug. 25, 2013. URL: <http://www.iec.ch/about/history/> (cit. on p. 9).

- [IEC13b] IEC 60204-SER ed1.0. *Safety of machinery - Electrical equipment of machines - all parts*. International Electrotechnical Commission, Apr. 23, 2013 (cit. on p. 13).
- [Isa96] O. Isaksen. "A Review of Reconstruction Techniques for Capacitance Tomography." In: *Measurement Science and Technology* 7 (1996), pp. 325–337 (cit. on p. 60).
- [ISOo1] ISO/IEC. *ISO/IEC Guide 71:2001, Guidelines for standards developers to address the needs of older persons and persons with disabilities*. International Organization for Standardization / International Electrotechnical Commission, 2001 (cit. on p. 11).
- [ISOo2] ISO/IEC. *ISO/IEC Guide 50:2002, Safety aspects - Guidelines for child safety*. International Organization for Standardization / International Electrotechnical Commission, 2002 (cit. on p. 11).
- [ISO10] ISO/TC 199 ISO 12100. *Safety of machinery - General principles for design - Risk assessment and risk reduction*. International Organization for Standardization, Oct. 20, 2010 (cit. on p. 13).
- [ISO12a] ISO. *ISO Guide 78:2012, Safety of machinery Rules for drafting and presentation of safety standards*. International Organization for Standardization, Dec. 4, 2012 (cit. on p. 10).
- [ISO12b] ISO/TC COPOLCO / SC IEC/Advisory committee on safety. *ISO Guide 51, Safety aspects - Guidelines for their inclusion in standards*. International Organization for Standardization, Oct. 1, 2012 (cit. on pp. 10, 13–15).
- [ISO13a] ISO. *The ISO story*. Aug. 25, 2013. URL: [http://www.iso.org/iso/home/about/the\\_iso\\_story.htm](http://www.iso.org/iso/home/about/the_iso_story.htm) (cit. on p. 10).
- [ISO13b] ISO/TC 243 ISO 10377. *Consumer product safety - Guidelines for suppliers*. International Organization for Standardization, Apr. 15, 2013 (cit. on p. 14).
- [Jano8] C.A. Janicak. "Occupational fatalities due to electrocutions in the construction industry." In: *Journal of Safety Research* 39.6 (2008), pp. 617–621. ISSN: 0022-4375. DOI: 10.1016/j.jsr.2008.10.007 (cit. on p. 45).
- [JS12a] L.-T. Jiang and J.R. Smith. "Pretouch Sensing for Pretouch Sensing for Manipulation." In: *Robotics: Science and Systems (RSS) Workshop: Alternative Sensing Techniques for Robotic Perception*. July 2012 (cit. on pp. 48, 52).
- [JS12b] L.-T. Jiang and J.R. Smith. "Seashell effect pretouch sensing for robotic grasping." In: *Robotics and Automation (ICRA), 2012 IEEE International Conference on*. May 2012, pp. 2851–2858. DOI: 10.1109/ICRA.2012.6224985 (cit. on pp. 39, 52).

- [JS13] L.-T. Jiang and J.R. Smith. "A unified framework for grasping and shape acquisition via pretouch sensing." In: *Robotics and Automation (ICRA), 2013 IEEE International Conference on*. May 2013, pp. 999–1005. DOI: 10.1109/ICRA.2013.6630695 (cit. on p. 40).
- [Kam+04] K. Kamiyama, H. Kajimoto, N. Kawakami, and S. Tachi. "Evaluation of a vision-based tactile sensor." In: *Robotics and Automation, 2004. Proceedings. ICRA '04. 2004 IEEE International Conference on*. Vol. 2. 2004, 1542–1547 Vol.2. DOI: 10.1109/ROBOT.2004.1308043 (cit. on p. 41).
- [Kir+08] N. Kirchner, D. Hordern, D. Liu, and G. Dissanayake. "Capacitive sensor for object ranging and material type identification." In: *Sensors and Actuators A: Physical* 148.1 (2008), pp. 96–104. ISSN: 0924-4247. DOI: 10.1016/j.sna.2008.07.027 (cit. on pp. 47, 52, 99).
- [KK08] L. Kleeman and R. Kuc. "Sonar Sensing." In: *Springer Handbook of Robotics*. Ed. by B. Siciliano and O. Khatib. first. Berlin, Heidelberg, Germany: Springer, 2008. Chap. 4, pp. 1253–1281 (cit. on p. 38).
- [KLY11] H.-K. Kim, S. Lee, and K.-S. Yun. "Capacitive tactile sensor array for touch screen application." In: *Sensors and Actuators A: Physical* 165.1 (2011), pp. 2–7. ISSN: 0924-4247. DOI: 10.1016/j.sna.2009.12.031 (cit. on p. 54).
- [Kor06] B. Kortschak. "Level Set and Boundary Element Method for Reconstruction of Phase Boundaries in Capacitance Tomography." PhD thesis. Graz University of Technology, 2006 (cit. on p. 62).
- [Krö10] T. Kröger. *On-Line Trajectory Generation in Robotic Systems*. first. Vol. 58. Springer Tracts in Advanced Robotics. Berlin, Heidelberg, Germany: Springer, Jan. 2010. ISBN: 978-3-642-05174-6 (cit. on pp. 114, 116).
- [Krö11] T. Kröger. "Opening the door to new sensor-based robot applications - The Reflexxes Motion Libraries." In: *Robotics and Automation (ICRA), 2011 IEEE International Conference on*. 2011, pp. 1–4. DOI: 10.1109/ICRA.2011.5980578 (cit. on pp. 114, 116).
- [LCY09] H.-K. Lee, S.-I. Chang, and E. Yoon. "Dual-Mode Capacitive Proximity Sensor for Robot Application: Implementation of Tactile and Proximity Sensing Capability on a Single Polymer Platform Using Shared Electrodes." In: *Sensors Journal, IEEE* 9.12 (2009), pp. 1748–1755. ISSN: 1530-437X. DOI: 10.1109/JSEN.2009.2030660 (cit. on p. 48).
- [Liu+04] S. Liu, L. Fu, W.Q. Yang, H.G. Wang, and F. Jiang. "Prior-online iteration for image reconstruction with electrical capacitance tomography." In: *Science, Measurement and Technology, IEE Proceedings - 151.3* (May 2004), pp. 195–200. ISSN: 1350-2344. DOI: 10.1049/ip-smt:20040246 (cit. on p. 60).

- [Ltd12] Schneider Electric Ltd. *Safe Machinery Handbook*. 2012 (cit. on pp. 27, 28, 30, 32).
- [LV12] T. Lens and O. Von Stryk. "Investigation of safety in human-robot-interaction for a series elastic, tendon-driven robot arm." In: *Intelligent Robots and Systems (IROS), 2012 IEEE/RSJ International Conference on*. 2012, pp. 4309–4314. DOI: 10.1109/IROS.2012.6386236 (cit. on p. 35).
- [M V+07] M. Soleimani and M. Vauhkonen, W. Yang, A. Peyton, B.S. Kim, and X. Ma. "Dynamic imaging in electrical capacitance tomography and electromagnetic induction tomography using a Kalman filter." In: *Measurement Science and Technology* 18 (11 Nov. 2007), pp. 3287–3294 (cit. on p. 60).
- [Mar06] Q. Marashdeh. "Advances in Electrical Capacitance Tomography." PhD thesis. Graduate School of The Ohio State University, 2006 (cit. on p. 104).
- [MLS10] B. Mayton, L. LeGrand, and J.R. Smith. "An Electric Field Pretouch system for grasping and co-manipulation." In: *Robotics and Automation (ICRA), 2010 IEEE International Conference on*. 2010, pp. 831–838. DOI: 10.1109/ROBOT.2010.5509658 (cit. on pp. 48, 52).
- [Mos+09] M.J. Moser, H. Zangl, Th. Bretterkieber, and G. Brasseur. "An Autonomous Sensor System for Monitoring of High Voltage Overhead Power Supply Lines." In: *e&i Elektrotechnik und Informationstechnik* 126 (2009), pp. 214–219 (cit. on p. 44).
- [Mos+10] M.J. Moser, T. Bretterkieber, H. Zangl, and G. Brasseur. "Capacitive icing measurement in a 220 kV overhead power line environment." In: *Sensors, 2010 IEEE*. Nov. 2010, pp. 1754–1758. DOI: 10.1109/ICSENS.2010.5689885 (cit. on p. 44).
- [Mos+11] M.J. Moser, T. Bretterkieber, H. Zangl, and G. Brasseur. "Strong and Weak Electric Field Interfering: Capacitive Icing Detection and Capacitive Energy Harvesting on a 220-kV High-Voltage Overhead Power Line." In: *Industrial Electronics, IEEE Transactions on* 58.7 (July 2011), pp. 2597–2604. ISSN: 0278-0046. DOI: 10.1109/TIE.2010.2098362 (cit. on pp. 44, 52).
- [NBB95] A.Y. Nooralahiyan, B.S. Boyle, and J. Bailey. "Performance of neural network in image reconstruction and interpretation for electrical capacitance tomography." In: *IEE Colloquium on Innovations in Instrumentation for Electrical Tomography*. May 1995, pp. 5/1–5/3 (cit. on p. 60).

- [Neu+11] M. Neumayer, H. Zangl, D. Watzenig, and A. Fuchs. "New Developments and Applications in Sensing Technology." In: ed. by S.C. Mukhopadhyay, A. Lay-Ekuakille, and A.s Fuchs. Vol. 83. Lecture Notes in Electrical Engineering. Springer, 2011. Chap. Current Reconstruction Algorithms in Electrical Capacitance Tomography, p. 337 (cit. on pp. 60, 86, 88, 102, 106).
- [Neu11] M. Neumayer. "Accelerated Bayesian Inversion and Calibration for Electrical Tomography." PhD thesis. Austria: Graz University of Technology, 2011 (cit. on p. 87).
- [NF92] J.L. Novak and J.T. Feddema. "A capacitance-based proximity sensor for whole arm obstacle avoidance." In: *Robotics and Automation, 1992. Proceedings., 1992 IEEE International Conference on.* 1992, 1307–1314 vol.2. DOI: 10.1109/ROBOT.1992.220068 (cit. on p. 47).
- [NLH12] S. Norouzzadeh, T. Lorenz, and S. Hirche. "Towards safe physical human-robot interaction: An online optimal control scheme." In: *ROMAN, 2012 IEEE.* 2012, pp. 503–508. DOI: 10.1109/ROMAN.2012.6343801 (cit. on p. 35).
- [NS07] M. Norgia and C. Svelto. "RF-Capacitive Proximity Sensor for Safety Applications." In: *Instrumentation and Measurement Technology Conference Proceedings, 2007. IMTC 2007. IEEE.* 2007, pp. 1–4. DOI: 10.1109/IMTC.2007.379178 (cit. on pp. 46, 52).
- [NSW12] M. Neumayer, G. Steiner, and D. Watzenig. "Electrical Capacitance Tomography: Current sensors/algorithms and future advances." In: *Instrumentation and Measurement Technology Conference (I2MTC), 2012 IEEE International.* May 2012, pp. 929–934. DOI: 10.1109/I2MTC.2012.6229569 (cit. on p. 60).
- [NW91] J.L. Novak and J.J. Wiczner. "A high-resolution capacitive imaging sensor for manufacturing applications." In: *Robotics and Automation, 1991. Proceedings., 1991 IEEE International Conference on.* 1991, 2071–2078 vol.3. DOI: 10.1109/ROBOT.1991.131932 (cit. on p. 47).
- [OYF12] K.S. Ong, Y.H.H., and L.C. Fu. "Sensor fusion based human detection and tracking system for human-robot interaction." In: *Intelligent Robots and Systems (IROS), 2012 IEEE/RSJ International Conference on.* 2012, pp. 4835–4840. DOI: 10.1109/IROS.2012.6386222 (cit. on p. 35).
- [Pen+12] L. Peng, J. Ye, G. Lu, and W. Yang. "Evaluation of Effect of Number of Electrodes in ECT Sensors on Image Quality." In: *Sensors Journal, IEEE* 12.5 (May 2012), pp. 1554–1565. ISSN: 1530-437X. DOI: 10.1109/JSEN.2011.2174438 (cit. on p. 104).



- [Pha+11] S. Phan, Z.F. Quek, P. Shah, D. Shin, Z. Ahmed, O. Khatib, and M. Cutkosky. "Capacitive skin sensors for robot impact monitoring." In: *Intelligent Robots and Systems (IROS), 2011 IEEE/RSJ International Conference on*. 2011, pp. 2992–2997. DOI: 10.1109/IROS.2011.6095083 (cit. on pp. 41, 52).
- [PKo8] E. Prassler and K. Kosuge. "Domestic Robotics." In: *Springer Handbook of Robotics*. Ed. by B. Siciliano and O. Khatib. first. Berlin, Heidelberg, Germany: Springer, 2008. Chap. 4, pp. 1253–1281 (cit. on pp. 38, 52).
- [PKK13a] C. Preschern, N. Kajtazovic, and C. Kreiner. "Applying and Evaluating Architectural IEC 61508 Safety Patterns." In: *Lecture notes on Software Engineering*. IACSIT Press, 2013 (cit. on pp. 23, 25–27).
- [PKK13b] C. Preschern, N. Kajtazovic, and C. Kreiner. "Architectural Pattern System for Functional Safety." In: *European Conference on Pattern Language of Programs (EuroPLoP)*. 2013 (cit. on pp. 23, 24).
- [PKK13c] C. Preschern, N. Kajtazovic, and C. Kreiner. "Catalog of Safety Tactics in the light of the IEC 61508 Safety Lifecycle." In: *VikingPLoP*. 2013 (cit. on p. 23).
- [Polo6] A.C. Polycarpou. *Introduction to the Finite Element Method in Electromagnetics*. 2006. DOI: 10.2200/S00019ED1V01Y200604CEM004 (cit. on pp. 55, 58, 75, 123, 124).
- [Pue93] R. Puers. "Capacitive sensors: When and how to use them." In: *Sensors and Actuators A: Physical* 37 - 38 (1993), pp. 93–105. ISSN: 0924-4247. DOI: 10.1016/0924-4247(93)80019-D (cit. on p. 54).
- [RB+11] Towal R.B., Quist B.W., Gopal V., Solomon J.H., and Hartmann M.J.Z. "The Morphology of the Rat Vibrissal Array: A Model for Quantifying Spatiotemporal Patterns of Whisker-Object Contact." In: *PLoS Comput Biol*. (2011). DOI: 10.1371/journal.pcbi.1001120 (cit. on pp. 41, 52).
- [Ren+10] W. Renhart, M. Bellina, C. Magele, and A. Köstinger. "Hidden metallic object localization by using Giant Magnetic Resistor sensors." In: *14th IGTE Symposium*. 2010 (cit. on p. 39).
- [Ryb+12] P. Rybski, P. Anderson-Sprecher, D. Huber, C. Niessl, and R. Simmons. "Sensor fusion for human safety in industrial workcells." In: *Intelligent Robots and Systems (IROS), 2012 IEEE/RSJ International Conference on*. 2012, pp. 3612–3619. DOI: 10.1109/IROS.2012.6386034 (cit. on pp. 34, 36, 37, 52).
- [Sal10] C. Salter. *Entangled: Technology and the Transformation of Performance*. The MIT Press, 2010 (cit. on p. 54).

- [Sat+13] S. Satake, T. Kanda, D.F. Glas, M. Imai, H. Ishiguro, and N. Hagita. "A Robot that Approaches Pedestrians." In: *Robotics, IEEE Transactions on* 29.2 (2013), pp. 508–524. ISSN: 1552-3098. DOI: 10.1109/TR0.2012.2226387 (cit. on p. 39).
- [SBZ11] T. Schlegl, T. Bretterkieber, and H. Zangl. "Curvature Effects on Elongated Capacitive Proximity Sensors." In: *Sensor+Test Conference*. June 7–9, 2011 (cit. on pp. 6, 81).
- [Sch+10] T. Schlegl, T. Bretterkieber, M. Neumayer, and H. Zangl. "A novel sensor fusion concept for distance measurement in automotive applications." In: *IEEE Sensors*. 2010, pp. 775–778. DOI: 10.1109/ICSENS.2010.5690781 (cit. on pp. 6, 43).
- [Sch+11] T. Schlegl, T. Bretterkieber, M. Neumayer, and H. Zangl. "Combined Capacitive and Ultrasonic Distance Measurement for Automotive Applications." In: *Sensors Journal, IEEE* 11.11 (Nov. 2011), pp. 2636–2642. ISSN: 1530-437X. DOI: 10.1109/JSEN.2011.2155056 (cit. on pp. 6, 43, 52, 59, 60, 64).
- [Sch+12] T. Schlegl, S. Mühlbacher-Karrer, M. Neumayer, and H. Zangl. "A GMR based magnetic pretouch sensing system for a robot grasper." In: *Instrumentation and Measurement Technology Conference (I2MTC), 2012 IEEE International*. May 2012, pp. 1506–1510. DOI: 10.1109/I2MTC.2012.6229681 (cit. on pp. 6, 49).
- [Sch+13a] T. Schlegl, T. Kröger, A. Gaschler, O. Khatib, and H. Zangl. "Virtual whiskers - Highly responsive robot collision avoidance." In: *Intelligent Robots and Systems (IROS), 2013 IEEE/RSJ International Conference on*. 2013, pp. 5373–5379. DOI: 10.1109/IROS.2013.6697134 (cit. on pp. 6, 41, 42, 73, 97, 99–101, 114, 117, 119).
- [Sch+13b] T. Schlegl, M. Neumayer, S. Mühlbacher-Karrer, and H. Zangl. "A Pretouch Sensing System for a Robot Grasper Using Magnetic and Capacitive Sensors." In: *Instrumentation and Measurement, IEEE Transactions on* 62.5 (2013), pp. 1299–1307. ISSN: 0018-9456. DOI: 10.1109/TIM.2013.2238034 (cit. on pp. 6, 39, 40, 47, 49, 52, 93, 114).
- [Sch10] T. Schlegl. "A Sensor Fusion Concept for Object Detection in Automotive Applications." Masterthesis. Graz University of Technology, 2010 (cit. on p. 59).
- [Sch91] H.R. Schwarz. *Methode der finiten Elemente: Eine Einführung unter besonderer Berücksichtigung der Rechnpraxis*. 1991. ISBN: 3-519-22349-X (cit. on pp. 56, 123, 124).



- [Shi+04] M. Shimojo, A. Namiki, M. Ishikawa, R. Makino, and K. Mabuchi. "A tactile sensor sheet using pressure conductive rubber with electrical-wires stitched method." In: *Sensors Journal, IEEE* 4.5 (2004), pp. 589–596. ISSN: 1530-437X. DOI: 10.1109/JSEN.2004.833152 (cit. on p. 41).
- [Shi+11] D. Shin, Z.F. Quek, S. Phan, M. Cutkosky, and O. Khatib. "Instantaneous stiffness effects on impact forces in human-friendly robots." In: *Intelligent Robots and Systems (IROS), 2011 IEEE/RSJ International Conference on*. 2011, pp. 2998–3003. DOI: 10.1109/IROS.2011.6094675 (cit. on p. 42).
- [SKo8] T. Sanpechuda and L. Kovavisaruch. "A review of RFID localization: Applications and techniques." In: *Electrical Engineering/Electronics, Computer, Telecommunications and Information Technology, 2008. ECTI-CON 2008. 5th International Conference on*. Vol. 2. 2008, pp. 769–772. DOI: 10.1109/ECTICON.2008.4600544 (cit. on p. 38).
- [SLo5] M. Soleimani and W.R. Lionheart. "Nonlinear Image Reconstruction for Electrical Capacitance Tomography Using Experimental Data." In: *Measurement Science and Technology* 16 (10 Oct. 2005), pp. 1987–1996 (cit. on p. 60).
- [Smi99] J. Smith. "Electric Field Imaging." PhD thesis. Massachusetts Institute of Technology, 1999 (cit. on p. 53).
- [SMZ12] T. Schlegl, M.J. Moser, and H. Zangl. "Directional human approach and touch detection for nets based on capacitive measurement." In: *Instrumentation and Measurement Technology Conference (I2MTC), 2012 IEEE International*. 2012, pp. 81–85. DOI: 10.1109/I2MTC.2012.6229473 (cit. on p. 6).
- [SMZ13] T. Schlegl, M.J. Moser, and H. Zangl. "Vorrichtung zur Erkennung eines Naheverhältnisses und Erfassung von Eigenschaften von Objekten." AT 512878 (A1). 2013 (cit. on p. 6).
- [SNZ12] T. Schlegl, M. Neumayer, and H. Zangl. "A Mobile and Wireless Measurement System for Electrical Capacitance Tomography." In: *Mikroelektroniktagung ME12*. Apr. 2012 (cit. on pp. 6, 84, 85).
- [SS11] D.J. Smith and K.G.L. Simpson. *Safety Critical Systems Handbook. A Straightforward Guide to Functional Safety: IEC 61508 (2010 Edition) and Related Standards*. Elsevier Ltd., 2011. ISBN: 978-0-08-096781-3 (cit. on pp. 10–13, 15–19, 21, 30, 33).
- [SS91] A. Sears and B. Shneiderman. "High precision touchscreens: design strategies and comparisons with a mouse." In: *International Journal of Man-Machine Studies* 34.4 (1991), pp. 593–613. ISSN: 0020-7373. DOI: 10.1016/0020-7373(91)90037-8 (cit. on p. 54).

- [SSTo8] O. Schlappal, A. Schwarzkopf, and J. Trautmann. *Elektrische Fische: Signalerzeugung und Rezeption. Funktion, Aufbau und Einsatz elektrischer Organe*. Schriftliche Ausarbeitung. Biotechnik-Zentrum, TU Darmstadt, July 31, 2008 (cit. on p. 53).
- [Sta97] International Organization for Standardization. *Friendship Among Equals. Recollections from Iso's first fifty years*. 1997. ISBN: 92-67-10260-5. URL: [http://www.iso.org/iso/2012\\_friendship\\_among\\_equals.pdf](http://www.iso.org/iso/2012_friendship_among_equals.pdf) (visited on 08/25/2013) (cit. on p. 10).
- [SZ11] T. Schlegl and H. Zangl. "Simulation and Verification of a Capacitive Proximity Sensor." In: *COMSOL Conference*. Oct. 26–28, 2011 (cit. on pp. 6, 65).
- [SZ13] T. Schlegl and H. Zangl. "Sensor Interface for Multimodal Evaluation of Capacitive Sensors." In: *Journal of Physics: Conference Series*. June 26, 2013. DOI: 10.1088/1742-6596/450/1/012018 (cit. on pp. 6, 97).
- [SZ14] T. Schlegl and H. Zangl. *Capacitive Sensing for Safety Applications*. In: *Technologies for Smart Sensors and Sensor Fusion*. Ed. by Kevin Yallup. Ed. by Krzysztof (Kris) Iniewski. 2014. ISBN: 9781466595507 (cit. on pp. 63, 93, 95, 97).
- [TGA04] F.C. Trigo, R. Gonzalez-Lima, and M.B.P. Amato. "Electrical impedance tomography using the extended Kalman filter." In: *Biomedical Engineering, IEEE Transactions on* 51.1 (Jan. 2004), pp. 72–81. ISSN: 0018-9294. DOI: 10.1109/TBME.2003.820389 (cit. on p. 60).
- [TRL12] M.I. Tiwana, S.J. Redmond, and N.H. Lovell. "A review of tactile sensing technologies with applications in biomedical engineering." In: *Sensors and Actuators A: Physical* 179 (2012), pp. 17–31. ISSN: 0924-4247. DOI: 10.1016/j.sna.2012.02.051 (cit. on p. 54).
- [VB13] M. Vasic and A. Billard. "Safety issues in human-robot interactions." In: *Robotics and Automation (ICRA), 2013 IEEE International Conference on*. May 2013, pp. 197–204. DOI: 10.1109/ICRA.2013.6630576 (cit. on p. 35).
- [Weg+05] H. Wegleiter, A. Fuchs, G. Holler, and B. Kortschak. "Analysis of hardware concepts for electrical capacitance tomography applications." In: *Sensors, 2005 IEEE*. 2005, pages. DOI: 10.1109/ICSENS.2005.1597792 (cit. on pp. 60, 95).
- [Weg06] H. Wegleiter. "Low-Z Carrier Frequency Front-End for Electrical Capacitance Tomography." PhD Thesis. Graz University of Technology, July 2006 (cit. on p. 104).

- [WF09] D. Watzenig and C. Fox. "A review of statistical modelling and inference for electrical capacitance tomography." In: *Measurement Science and Technology* 20.5 (2009), pp. 052002+. DOI: 10.1088/0957-0233/20/5/052002 (cit. on p. 60).
- [WSB07] D. Watzenig, G. Steiner, and M. Brandner. "A particle filter approach for tomographic imaging based on different state-space representations." In: *Measurement Science and Technology* 18 (1 2007), pp. 30–40 (cit. on p. 60).
- [Yah13] Yahoo! *Yahoo! Design Pattern Library*. Sept. 18, 2013. URL: <http://developer.yahoo.com/ypatterns/> (cit. on p. 22).
- [Yan10] W. Yang. "Design of electrical capacitance tomography sensors." In: *Measurement Science and Technology* 21.10 (2010). DOI: 10.1088/0957-0233/21/4/042001 (cit. on p. 84).
- [YP03] W.Q. Yang and L. Peng. "Image reconstruction algorithms for electrical capacitance tomography." In: *Measurement Science and Technology* 14.1 (2003), R1–R13 (cit. on p. 60).
- [Zan+06] L. Zang, H.X. Wang, M. Ma, and X.Z. Jin. "Image reconstruction algorithm for electrical capacitance tomography based on radial basis functions neural network." In: *Proceedings of the Fourth International Conference on Machine Learning and Cybernetics*. Guangzhou, China, Aug. 2006, pp. 4149–4152 (cit. on p. 60).
- [Zan+07] H. Zangl, D. Watzenig, G. Steiner, A. Fuchs, and H. Wegleiter. "Non-Iterative Reconstruction for Electrical Tomography using Optimal First and Second Order Approximations." In: *Proceedings of the 5th World Congress on Industrial Process Tomography*. Bergen, Norway, Sept. 2007, pp. 216–223 (cit. on pp. 58, 60).
- [Zan05] H. Zangl. "Design Paradigms for Robust Capacitive Sensors." PhD thesis. Graz, Austria: Graz University of Technology, May 2005 (cit. on pp. 3, 63, 64, 96).
- [Zan09] H. Zangl. "SafeTom: Safety by Electrical Capacitance Tomography." Research proposal. 2009 (cit. on pp. 67, 73, 74, 76).
- [ZN10] H. Zangl and M. Neumayer. "Fast Gain Invariant Reconstruction Method for Electrical Tomography." In: *Proceedings of the 14th International IGTE Symposium*. 2010 (cit. on p. 64).
- [ZPN10] S. Zeng, J.R. Powers, and B.H. Newbraugh. "Effectiveness of a worker-worn electric-field sensor to detect power-line proximity and electrical-contact." In: *Journal of Safety Research* 41.3 (2010), pp. 229–239. DOI: 10.1016/j.jsr.2010.02.011 (cit. on pp. 45, 52).

- 
- [ZTZoo] O.C. Zienkiewicz, R.L. Taylor, and J.Z. Zhuf. *The Finite Element Methode*. 6th. Elsevier Butterworth-Heinemann, 2000. ISBN: 978-0-7506-6431-8 (cit. on p. 75).